DYNAMICS OF COMPLEX FLOW NETWORKS

DISSERTATION
(Cumulative Thesis)
to acquire the doctoral degree in mathematics and natural science
"Doctor rerum naturalium"
at the Georg-August-Universität Göttingen

within the doctoral degree program IMPRS-PBCS
of the Georg-August University School of Science (GAUSS)

submitted by
DEBSANKHA MANIK
from Purba Medinipur, India

Göttingen, 2017

I hereby declare that I have written this thesis independently and with no other sources and aids than quoted.

Göttingen, November 2017

Place, Date   Debsankha Manik

LIST OF PUBLICATIONS

†[**1**] Debsankha Manik et al. "Supply networks: Instabilities without overload." In: *The European Physical Journal Special Topics* 223.12 (2014), pp. 2527–2547 (for preprint, see Chapter 4).

[**2**] Debsankha Manik et al. "Network susceptibilities: Theory and applications." In: *Physical Review E* 95.1 (2017), p. 012319.

[**3**] Henrik Ronellenfitsch, Debsankha Manik, Jonas Horsch, Tom Brown, and Dirk Witthaut. "Dual theory of transmission line outages." In: *IEEE Transactions on Power Systems* (2017).

†[**4**] Debsankha Manik, Marc Timme, and Dirk Witthaut. "Cycle flows and multistability in oscillatory networks." In: *Chaos: An Interdisciplinary Journal of Nonlinear Science* 27.8 (2017), p. 083123 (for reprint, see Chapter 5).

[**5**] Andreas Sorge, Debsankha Manik, Stephan Herminghaus, and Marc Timme. "Towards a unifying framework for demand- driven directed transport (D3T)." In: *Proceedings of the 2015 Winter Simulation Conference*. IEEE Press. 2015, pp. 2800–2811.

† Manuscripts included in this cumulative thesis. Declarations of own contributions are given in the beginnings of the corresponding Chapters 4–5.

CONTENTS

INTRODUCTION

Flow networks consist of individual units called *nodes* connected by edges transporting *flows* of some quantity – such as electricity, water or cars. Each of us encounters more than one flow network every day. They form the backbone of much of our technical infrastructure, such as road networks and the electrical power grid. They also enable many biological transport processes, such as venation networks in plant leaves and trachea networks in animal lungs. To perform well, such networks need to be *stable* - i.e. the flows must return to some *steady values* following a reasonably small perturbation. They should also be *resilient* - i.e. damaging small parts of the network should not render the whole network dysfunctional. At the same time they should also be *economical*. Since adding or strengthening edges costs money, nutrients or some other resource, economy in most flow networks means having as few or as weak edges as possible. The goal of this thesis is to understand how, and to which extent, the *topological properties* of such networks influence their *flows*.

1.1 PRELIMINARIES

1.1.1 *Importance of topology in complex networks*

Topology of a network refers to the connectivity pattern between its nodes. Topology becomes important for studying a flow network, when the collective dynamics of the whole network cannot be explained from understanding the dynamics of each single node. In many networks, flow network or otherwise, dynamics of each node is governed by quite simple rules – for example that of harmonic oscillators – but nevertheless the system as a whole displays rich collective dynamics. One common example is the so-called *spontaneous synchrony* in phase oscillator networks [1, 2]: Sinusoidally coupled harmonic oscillators with various natural frequencies oscillate with a common frequency, if the coupling is sufficiently strong. Similarly, groups of birds in flight manage to fly in flocks [3] by maintaining cohesion with their immediate few neighbours.

Some insights into the dynamics of complex networks can be gained ignoring topology. For example, one can use mean field techniques to derive the "critical coupling" at which phase oscillators synchronize [4, 2], for infinite *and* all-to-all coupled networks. In this approach, one treats each node's dynamics to be effectively decoupled from all other nodes, by assuming each node to be coupled to a common global vari-

able called the "mean field". Another example is the calculation of the global magnetization of an Ising spin lattice at a fixed temperature using the canonical ensemble technique of statistical physics.

Such approaches by construction ignore the fact that connectivity patterns may differ between nodes, limiting their applicability outside completely (all-to-all) connected or regular networks (i.e. each node having identical degree, e.g. a square lattice). Certain dynamical properties derived using these techniques often hold true in general topologies (typically with some restrictions), but many dynamical properties do not. One example is the phase transition in oscillator networks from disordered (nodes oscillating with different frequencies) to ordered phase (every node oscillating with a common frequency). Regardless of the topology, such transitions occur upon increasing the coupling strength, but the *order* of the transition depends on topology [5]. We find another example of a universal dynamical property across different topologies in the context of bond percolation in 2-D; where cluster sizes follow scale free distributions with the same exponent independent of network topology [6]; on the other hand the *percolation threshold* does depend on the topology [7].

1.1.2 *Role of Graph theory*

The mathematical discipline of graph theory aims to establish relationships between different topological properties of a graph, ignoring dynamical aspects by construction. Nevertheless, graph theoretic results often provide valuable insights into the dynamics of networks. For example, the max-flow-min-cut theorem [8, p. 127] tells us the maximum current that can possibly flow through a network with a single source and a single sink, no matter which dynamics governs the flows. Although the network dynamics must still be taken into account to understand how a specific flow network behaves, graph theory provides a strict upper bound.

In addition, graph theory provides many of the common tools in a network scientists' repertoire. Various graph theoretic concepts help us to categorize networks in a quantitative way; e.g. centrality (how often a node falls in a shortest path between two other nodes), clustering coefficient (how likely two neighbours of a node are to be connected to each other) and connectivity (if each node can be reached from every other node. Graph theory also provides us with many algorithms to numerically compute various graph properties, e.g. Dijkstra's shortest path finding algorithm [9] and Borůvka's minimal spanning tree finding algorithm [10].

1.1.3   *Dynamics of complex flow networks*

In flow networks, each node either generates or consumes a certain resource, which *flows* via the edges from generators to consumers. We call this resource "input": positive for generator nodes and negative for consumer nodes. Two parameters specify the topology of a flow network: first, the edges connecting the nodes; second, the distribution of inputs among the nodes (we define flow networks in detail in Section 2.2).

To design more efficient flow networks and to identify weak points in existing ones, we need to understand how these two topological factors influence the flow dynamics. Research on this topic has only gathered steam in the last few decades. One reason behind that is the computational complexity of simulating dynamical processes in large networks. The second reason is the difficulty in obtaining real world network topology data. Rapid increase in computing power in recent decades has helped alleviate the first concern. Discovery of random graph models such as the Watts-Strogatz model [11] and the Barabási–Albert model [12] emulating real world networks in various topological properties, as well as availability of detailed datasets on real-world flow networks [13, 14] have helped with the second.

In this thesis, we have focused on two flow networks. The first one is a network of phase oscillators called *Kuramoto oscillators* that is used to model electrical AC power transmission grids, as well as systems as diverse as firing of fireflies [4], coupled Josephson junctions [15], neuronal networks [16] and chemical oscillators [17], to name a few. The second type of networks we studied is the linear flow network that can be used to model venation networks in plant leaves [14], as well as DC power grids [18].

1.2   MOTIVATION OF THE THESIS

1.2.1   *When do steady flows exist in AC power transmission networks?*

It is expensive to increase the capacity of transmission lines in power grids. Therefore, it is important to know which network topologies can reliably transmit power with the least edge capacities. This question has been studied widely in recent years using a model of AC transmission grid [19] based on the popular Kuramoto model (defined in detail in Section 2.2.1).

Steady flows in power grid systems translate to *phase locking* or *frequency synchrony* in Kuramoto model. Stability (or lack thereof) of Kuramoto networks is well understood in all-to-all coupled systems in the infinite system limit: no steady flows exist below a certain *critical coupling* and above this critical coupling precisely one steady flow exists. This critical coupling can be easily derived from the statistical distribution of the power inputs. Unfortunately, power grids are far

from all-to-all coupled: they are almost planar and have very few long distance edges due to high cost [20, 21]. Necessary and sufficient conditions for steady flows to exist in realistic topologies are still not known, although various connections between topological features and stability have been discovered for power grid models.

For example, Barabási-Albert networks have been shown numerically to synchronize at higher critical coupling than those with uniform randomly chosen edges (i.e. Erdős-Rényi networks) [22], although *partial synchrony* emerges at lower coupling strengths for Barabási-Albert networks. Similar numerical studies in Watts-Strogatz networks showed that a small amount of rewiring drastically reduces critical coupling [23]. High *clustering* has been shown to promote partial synchrony but at the same time inhibit full synchrony [24].

The topological property of input distribution has also proved to be an important factor for the existence of steady flows. Correlations between degree and inputs have been shown to cause explosive synchronization [5], i.e. discontinuous transition from disordered to ordered phase. Spatially distributed [25, 26] positioning of generator (i.e. positive input) and consumer (i.e. negative input) nodes, as well as the existence of rerouting pathways [27] have been shown to make the grid more robust against topological perturbations. However, the following remains an open question: For power transmission networks with arbitrary topology and arbitrary power input distribution, if a steady flow exists, and which topological features help in steady flows emerging. Our work on this question constitutes Chapter 4 of this thesis.

1.2.2   *Multistability in oscillator networks*

In flow networks like power grids, the existence of a *unique and globally attracting* steady flow is a desirable property. Otherwise, flows across the edges may switch to different values following a temporary perturbation; such as shutting down a transmission line for repairs and reconnecting it afterwards. For Kuramoto like phase oscillator networks used to model power grids, steady states are indeed guaranteed to be unique, in the *densest* (i.e. all-to-all coupled) and the *sparsest* (i.e. tree) topologies. Such guarantees do not hold for intermediately dense topologies, which real world power grids happen to have. A widely cited article [28] presented an analytical argument that one can always find a sufficiently high coupling strength guaranteeing unique steady flows in any topology. Puzzlingly, it has been also reported that more than one steady flows can occur [29, 30, 31] in Kuramoto networks with ring topology. In Chapter 5, we provide a solution to this puzzle by demonstrating the uniqueness claim in [28] to be flawed. We also establish how three topological features lead to more steady flows: length of fundamental cycles, coupling strength of the edges, and spatial homogeneity of generators.

1.2.3 *Braess' paradox in flow networks*

When a flow network needs to support more flow than it is currently capable of, adding more edges or increasing existing edge capacities is a common solution. In 1968, traffic engineer D. Braess introduced a curious phenomenon, later termed Braess' paradox [32]: In a road network, where each driver drives his/her car so that his/her own travel time is minimized, opening a new road can lead to the travel time *increasing for everyone*. This phenomenon has been widely studied in transport research [33, 34, 35] and also recently in general flow networks [36, 37, 38]. It is not known to this date, which edges in a given flow network exhibit Braess' paradox, and which topological features *cause* them to exhibit it. In Chapter 6, we derive an exact mapping from this question to a familiar problem in electrostatics; that of calculating electric potential due to a single dipole source. We define a topological feature called "flow alignment" and demonstrate that edges that are flow aligned to the maximally loaded edge are more likely to cause Braess' paradox. Moreover, we demonstrate that Braess' paradox has a *beneficial effect*: Braessian edges can be *intentionally damaged* to mitigate overload caused by damage at another edge.

To summarize, this thesis is motivated by this broad question: "How does the topology influence the flows in a network"? We have studied three aspects of this question: namely, topological conditions determining the stability of steady flows, topological conditions causing multi-stability of steady flows, and topological features causing certain edges to exhibit Braess paradox.

1.3 ORGANIZATION OF THIS THESIS

In this Chapter, we have outlined the importance of topology in studying dynamics of complex flow networks and described the open problems in the field motivating this thesis. In Chapter 2 we will describe the tools and concepts from graph theory and network science we utilize in this thesis. The results of this thesis will be presented in Chapters 4, 5 and 6: in the form of two published articles and one unpublished manuscript. In this introduction, we intentionally did not delve into the technical details of our approaches, in order to avoid invoking technical concepts before defining them. Therefore, before the result chapters begin, in Chapter 3, we will provide an in-depth outline of our approaches for arriving at our results. Finally, we will summarize those results and point out scope of further research in Chapter 7.

THEORETICAL BACKGROUND

In this section we will introduce some concepts of graph theory that will be used in the rest of the thesis. More detailed treatments on these topics can be found in many graph theory textbooks; in particular [8, 39].

Definition 2.1.1 (Graph). *A graph is a collection of* nodes, *and* edges *that each connect exactly two nodes. In a mathematically precise way, a graph G is a tuple $(\mathbb{V}, \mathbb{E})$ satisfying $\mathbb{E} \subseteq [\mathbb{V}]^2$. Its nodes are $v_i \in \mathbb{V}$ and edges are 2-element subsets of $\mathbb{V}$. We will assume throughout this thesis that $\mathbb{V}$ and $\mathbb{E}$ are both finite.*

Example 2.1.1. *The 3-element cycle graph*

$$G(\mathbb{V} = \{1, 2, 3\}, \mathbb{E} = \{\{1, 2\}, \{2, 3\}, \{3, 1\}\}).$$

Definition 2.1.2 (Directed graphs). *A directed graph (or digraph) has edges with* directionality, *i.e. they have a start node or "head" and an end node or "tail". Mathematically speaking, a digraph is a tuple $(\mathbb{V}, \mathbb{E})$ satisfying $\mathbb{E} \subseteq \mathbb{V} \times \mathbb{V}$.*

Example 2.1.2. *The 3-element directed cycle graph*

$$G(\mathbb{V} = \{1, 2, 3\}, \mathbb{E} = \{(1, 2), (2, 3), (3, 1)\}).$$

Remark 2.1.1. *Often the edges of undirected graphs are denoted as tuples e.g. $(2, 3)$, although $\{2, 3\}$ would be the correct choice. It is implicitly assumed that $(2, 3)$ and $(3, 2)$ denote the same edge. Following conventions in existing literature, we often use this notation in this thesis. Since we do not study directed graphs in this thesis at all, we hope this sloppiness of notation will not lead to any confusion.*

Normally graphs are illustrated by drawing a dot denoting each node and a line connecting every pair of nodes between which an edge exists. The same graph can generally be drawn in many different ways. We illustrate the distinction between a graph and a drawing of a graph in Figure 2.1.

Definition 2.1.3 (Drawing of a graph). *Given a graph $G(\mathbb{V}, \mathbb{E})$, a drawing of it is another graph $G_d(\mathbb{V}_d, \mathbb{E}_d)$ with the following properties:*

    1. Nodes of G_d are points in $\mathbb{R}^2$: $\mathbb{V}_d \subset \mathbb{R}^2$.

$G = (\mathbb{V}, \mathbb{E})$
$\mathbb{V} = \{1, 2, 3, 4, 5, 6, 7\}$
$\mathbb{E} = \{\{1, 2\}, \{2, 3\}, \{3, 4\}, \{4, 5\},$
$\quad \{5, 6\}, \{6, 7\}, \{2, 6\}, \{3, 7\},$
$\quad \{5, 7\}, \{4, 5\}\}$
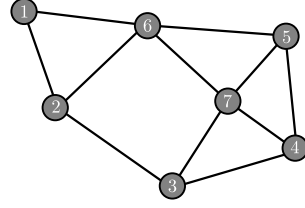
Figure 2.1: (left) A graph with 7 nodes and 10 edges. (right) One possible drawing of the same graph.

2. Edges of G_d are straight line segments, whose endpoints are distinct elements of $\mathbb{V}_d$.

Definition 2.1.4 (Degree of a node). *Given a graph $G(\mathbb{V}, \mathbb{E})$, the degree $Deg(j)$ of a node j is defined as the number of edges containing j.*

$$Deg(j) = \sum_{e \in \mathbb{E}, j \in e} 1.$$

Definition 2.1.5 (Cut, cutset). *Given a graph $G(\mathbb{V}, \mathbb{E})$, a cut (or a 2-partition) is a tuple $(\mathbb{V}_1, \mathbb{V}_2)$ satisfying*

$$\mathbb{V}_1 \cup \mathbb{V}_2 = \mathbb{V}$$
$$\mathbb{V}_1 \cap \mathbb{V}_2 = \{\}.$$

The cutset associated with this cut is the set of edges having two endpoints in two different partitions,

$$\{\{u, v\} \in \mathbb{E} \quad | u \in \mathbb{V}_1, v \in \mathbb{V}_2\}.$$
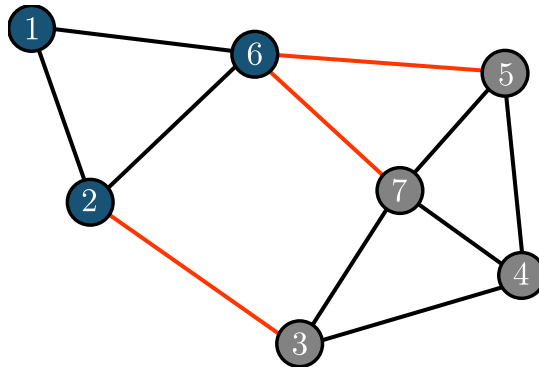
Figure 2.2: A cut $(\mathbb{V}_1, \mathbb{V}_2)$ of a graph. Nodes in $\mathbb{V}_1$ coloured blue, nodes in $\mathbb{V}_2$ coloured grey. The edges in the cutset are coloured red.

Definition 2.1.6 (Planar graph). *A graph that can be drawn on $\mathbb{R}^2$ without any of its edges meeting any other edge apart from at an endpoint is called a planar graph.*
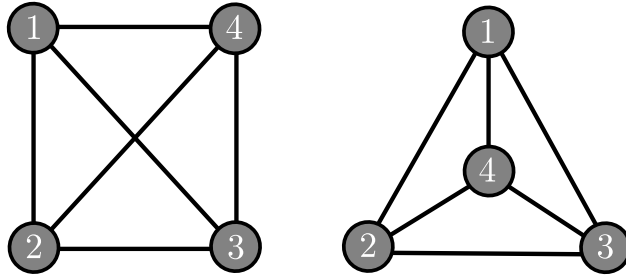
Figure 2.3: A 4-node planar graph with two different drawings. In the drawing on the left, two edges intersect, but not in the drawing on the right.

Remark 2.1.2. *A graph can have intersecting edges in a specific drawing and still be planar. One example is the complete 4-node graph illustrated in Figure 2.3.*
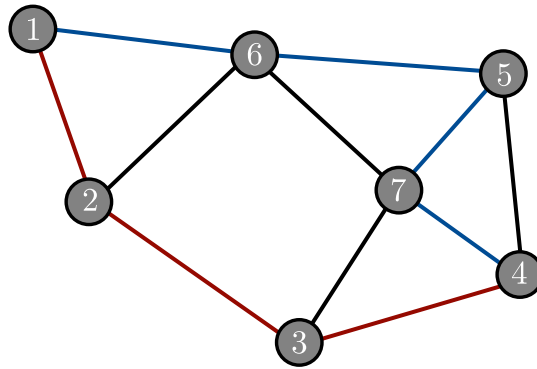
Figure 2.4: A length 3 path $\mathcal{P}_1 = (1, 2, 3, 4)$ and a length 4 path $\mathcal{P}_2 = (1, 6, 5, 7, 4)$ between nodes 1 and 4 in a graph. $\mathcal{P}_1$ is a shortest path.

Definition 2.1.7 (Path, path length, shortest path). *In a graph $G(\mathbb{V}, \mathbb{E})$, a sequence of distinct nodes $\mathcal{P} = (u_1, u_2, \cdots, u_n)$ is called a path between the nodes u_1 and u_n if there exists an edge between each successive pair of nodes in the sequence,*

$$\text{for all } 1 \leq j \leq n-1, \{u_j, u_{j+1}\} \in \mathbb{E}, \tag{2.1}$$

$$\text{for all } 1 \leq i < j \leq n, u_i \neq u_j. \tag{2.2}$$

The Length *of a path $\mathcal{P}$ is defined as the length of the sequence $\mathcal{P}$. A path $\mathcal{P} = (u_1, u_2, \cdots, u_n)$ is called a* shortest path *between u_1 and u_n if the length of $\mathcal{P}$ is smaller than or equal to the lengths of all other paths between u_1 and u_n. This is illustrated in Figure 2.4.*

Remark 2.1.3. *Often in graph theory literature, a sequence of nodes not satisfying the distinctness condition Eq. (2.2) (i.e. where a node appears more than once) is also called a path, and a "simple path" refers to what we call path.*

Definition 2.1.8 (Connected graph). *A graph G is called connected if there exists at least one path between any two pair of distinct nodes in the graph. This is illustrated in Figure 2.5.*
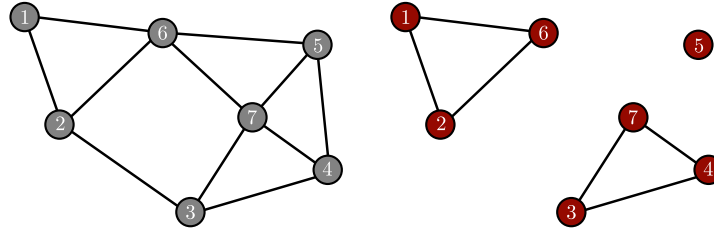
Figure 2.5: (left) A connected graph, (right) a non connected graph.

Definition 2.1.9 (Cycle). *Given a graph $G(\mathbb{V}, \mathbb{E})$, a sequence of distinct nodes $(u_1, u_2, \cdots, u_n)$ is called a cycle C if there exists an edge between every successive pair of nodes in the sequence and also between the first and last node,*

$$\text{for all } 1 \le j \le n-1, u_j, u_{j+1} \in \mathbb{E}, \quad \{u_n, u_1\} \in \mathbb{E},$$
$$\text{for all } 1 \le i < j \le n, u_i \ne u_j.$$

This is illustrated in Figure 2.6.
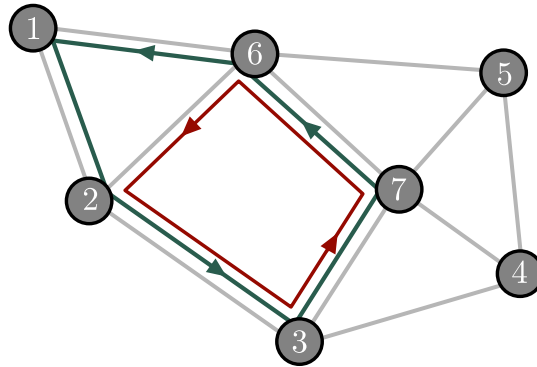
Figure 2.6: A graph and two cycles: $C_1 = (1, 2, 3, 7, 6)$ (green) and $C_2 = (2, 3, 7, 6)$ (red).

Remark 2.1.4 (Simple cycle). *As with paths, often cycles are defined in a way so that one (or more) nodes appearing more than once is permitted. Then a "simple cycle" is defined as what we call cycle.*

Remark 2.1.5. *A cycle $C = (u_1, u_2, \cdots, u_n)$ and all its cyclic permutations such as $(u_k, u_{k+1}, \cdots, u_n, u_1, u_2, \cdots, u_{k-1})$ are considered to be the same cycle.*

A cycle $C = (u_1, u_2, \cdots, u_n)$ and its reversal $(u_n, u_{n-1}, \cdots, u_2, u_1)$ are also considered to be the same cycle.

Remark 2.1.6 (Edges in a cycle). *A cycle* $C = (u_1, u_2, \cdots, c_n)$ *contains* n *edges* $(\{u_1, u_2\}, \{u_2, u_3\}, \cdots, \{u_{n-1}, u_n\}, \{u_n, u_1\})$. *We also refer to its edge set by the term "cycle".*

Remark 2.1.7 (Symmetric difference between cycles). *Given two cycles* C_1 *and* C_2 *of a graph, the symmetric difference of their edge sets* $C_1 \setminus C_2$ *is also a cycle. This is demonstrated in Figure 2.7.*
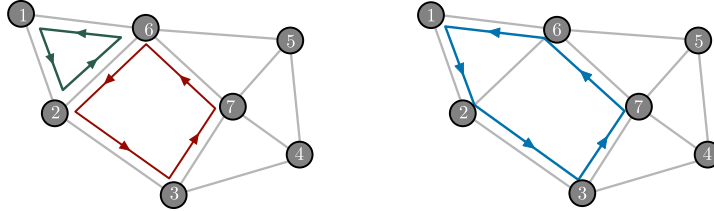
Figure 2.7: Symmetric difference between two cycles (green and red) is also a cycle (blue).

Definition 2.1.10 (Cycle space, cycle basis). *Given a graph* $G(\mathbb{V}, \mathbb{E})$, *the set of all cycles of the graph* $\mathcal{C}$ *defines a vector space over the* two element finite field $\mathbb{Z}_2$. *The* **vector addition** *between two cycles is the symmetric difference. The* **scalar multiplication** *is defined as*

$$\text{for all } C \in \mathcal{C}, \quad C \cdot 0 = \{\}$$
$$C \cdot 1 = C.$$

A basis of this cycle space is called a cycle basis B_C *of the graph. We illustrate a graph and* two cycle bases in Figure 2.8.
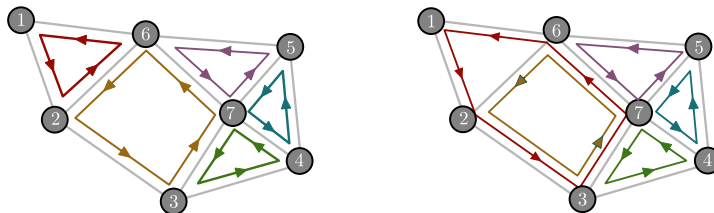
Figure 2.8: Two different cycle basis of a graph.

Definition 2.1.11 (Graph incidence matrix). *Given a graph* $G(\mathbb{V}, \mathbb{E})$, *an incidence matrix* I *for that graph is a* $|\mathbb{V}| \times |\mathbb{E}|$ *matrix containing information about which edge connects which pair of nodes. In order to construct such a matrix, we first impose an arbitrary order on* $\mathbb{V}$ *and* $\mathbb{E}$. *Furthermore, for each edge* (i, j) *we arbitrarily assign an "orienta-*

tion" by choosing either i or j to be its "head" and the other one to be its "tail". Then I is constructed as follows:

$$
I_{j,e} = \begin{cases} +1 & \text{if node } j \text{ is the head of } e \mathrel{\widehat{=}} \{j, \ell\}, \\ -1 & \text{if node } j \text{ is the tail of } e \mathrel{\widehat{=}} \{j, \ell\}, \\ 0 & \text{otherwise.} \end{cases}
\tag{2.3}
$$

Nodes	Edges					
	1	2	3	4	5	6
1	1	1	0	0	0	0
2	-1	0	1	1	0	0
3	0	0	0	-1	1	0
4	0	0	0	0	-1	1
5	0	-1	-1	0	0	-1
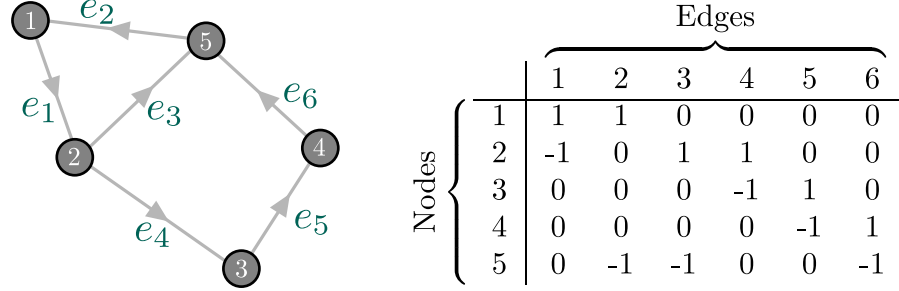
Figure 2.9: (left) a graph and (right) one of the many possible incidence matrices describing the graph. The arrowheads on each edge do *not* mean the edge is directed: it just shows the arbitrarily chosen *orientation* for constructing the incidence matrix.

Remark 2.1.8 (Weighted incidence matrix). *For an weighted graph with edge weights $\{K_{ij} \mid \{i, j\} \in \mathbb{E}\}$, the weighted incidence matrix I^w is constructed identically to the unweighted incidence matrix, but the nonzero entries are $\pm K_{ij}$ instead of ± 1,*

$$
I^w_{j,e} = \begin{cases} K_{ij} & \text{if node } j \text{ is the head of } e \mathrel{\widehat{=}} \{j, \ell\}, \\ -K_{ij} & \text{if node } j \text{ is the tail of } e \mathrel{\widehat{=}} \{j, \ell\}, \\ 0 & \text{otherwise.} \end{cases}
\tag{2.4}
$$

Definition 2.1.12 (Laplacian matrix). *Given a graph $G(\mathbb{V}, \mathbb{E})$, its Laplacian matrix L is a $\mathbb{V} \times \mathbb{V}$ matrix. To construct it, we first need to impose an arbitrarily chosen order on $\mathbb{V}$, just as in definition 2.1.11. Then L is defined as*

$$
L_{i,j} = \begin{cases} Deg(i) & \text{if } i = j, \\ -1 & \text{if } i \neq j \text{ and } (i, j) \in \mathbb{E}, \\ 0 & \text{otherwise.} \end{cases}
\tag{2.5}
$$

Remark 2.1.9 (Weighed Laplacian matrix). *For an weighted graph with edge weights $\{K_{ij} \mid \{i, j\} \in \mathbb{E}\}$, the weighted incidence matrix L^w is defined as*

$$
L_{i,j} = \begin{cases} \displaystyle\sum_{k \in \mathbb{V}, \{i,k\} \in \mathbb{E}} K_{ik} & \text{if } i = j, \\ -K_{ij} & \text{if } i \neq j \text{ and } (i, j) \in \mathbb{E}, \\ 0 & \text{otherwise.} \end{cases}
\tag{2.6}
$$

2.2   FLOW NETWORKS

Definition 2.2.1 (Flow). *Given a graph* $G(\mathbb{V}, \mathbb{E})$, *a flow* $\mathcal{F}$ *on it is defined as a mapping, that associates to each vertex pair* (i, j) *connected by an edge* e *a real number* F_{ij} *denoting a "flow" from* j *to* i.

$$
\begin{aligned}
\mathcal{F} : \{(i, j) \quad | \{i, j\} \in \mathbb{E}\} &\to \mathbb{R} \\
: (i, j) &\mapsto F_{ij}.
\end{aligned}
\tag{2.7}
$$

Definition 2.2.2 (Flow network). *Given a graph* G *and a flow* $\mathcal{F}$ *across its edges, the tuple* $(G, \mathcal{F})$ *is called a* flow network.

Remark 2.2.1 (Directionality of flows). *We implicitly assume* $F_{ij} = -F_{ji}$. *This is consistent with the intuitive notion of flows being directed quantities: flow from a to b must be opposite in sign and equal in magnitude to the flow from b to a.*

Remark 2.2.2 (Flow vector). *Often it is useful to treat a flow as a* $|\mathbb{E}|$ *element vector* $\mathbf{F}$. *Such a vector contains the same information as the mapping* $\mathcal{F}$ *itself and is constructed as follows.*

Consider a specific ordering of the edge set $\mathbb{E} = \{e_1, e_2, \cdots, e_{|\mathbb{E}|}\}$ *and a specific* orientation *of the edges (see definition 2.1.11) of* G. *Then the flow vector is*

$$
\mathbf{F} = (F_1, F_2, \cdots, F_{|\mathbb{E}|})
\tag{2.8}
$$

$$
F_k = \begin{cases} F_{ij} & \text{if } i \text{ is the head of } e_k \\ -F_{ij} & \text{if } j \text{ is the head of } e_k. \end{cases}
\tag{2.9}
$$

Definition 2.2.3 (Conservative flow). *If a flow from* i *to* j *is a* monotonically increasing, continuous and differentiable *function of the difference between certain vertex property* across the edge $\{i, j\}$,

$$
\begin{aligned}
F_{ij} &= K_{ij} f(\varphi_j - \varphi_i) & \text{(2.10)} \\
\Phi &: \mathbb{V} \to \mathbb{R}^{\mathbb{V}} & \text{(2.11)} \\
&: v_j \mapsto \varphi_j & \text{(2.12)} \\
f &: \mathbb{R} \to \mathbb{R} & \text{(2.13)} \\
f(y) &> f(x) \Leftrightarrow y > x, & \text{(2.14)}
\end{aligned}
$$

then it is called a conservative flow.

Remark 2.2.3. *To satisfy the flow directionality condition (see remark 2.2.1),* f *must be an odd function*

$$
f(-x) = -f(x).
$$

Remark 2.2.4 (Flow continuity/Kirchoff's law). *Often, flows are quantities that* enter *or* exit *a graph at certain nodes and their total*

quantity follows a certain conservation law *called Kirchoff's law. Defining a vertex property called* input $I_j \in \mathbb{R}$ *for all nodes j, this law states*

$$I_j + \sum_{(j,l) \in \mathbb{E}} F_{jl} = 0. \tag{2.15}$$

Definition 2.2.4 (Conservative flow network). *Let G be a graph with inputs I_j at each node j. Let $\mathcal{F}$ be a conservative flow satisfying the flow continuity condition Eq.* (2.15). *Then the tuple* $(G, \mathbf{I}, \mathcal{F})$ *is called a* conservative flow network.

Now we will give two examples of conservative flow networks: first, Kuramoto oscillator networks, and second, linear flow networks.

2.2.1   *Kuramoto networks*

Kuramoto model [1] describes phase oscillators coupled to each other by sinusoidal couplings. This model has been used to study the collective dynamics of coupled Josephson junctions [15], neuronal networks [16], chemical oscillators [17], and a variety of other synchronization phenomena [4, 2, 40, 41].

This system is described by an undirected graph G with N nodes and M edges. Each node is a phase oscillator with natural frequencies $\theta_j, j \in \{1, 2, \cdots, N\}$. Each edge $\{i, j\}$ has an associated *coupling strength* $K_{ij} > 0$. The phase variables in this system are the phase angles of each node $\theta_j, j \in \{1, 2, \cdots, N\}$, and the equations of motion are given by

$$\frac{d\theta_j}{dt} = \omega_j + \sum_{(i,j) \in \mathbb{E}} K_{ij} \sin\left(\theta_i - \theta_j\right), \tag{2.16}$$

for all $1 \leq j \leq N$. By construction, $K_{ji} = K_{ij}$.

Kuramoto model as a flow network

The steady state of a Kuramoto network is defined by phase angles $\{\theta_1^*, \theta_2^*, \cdots, \theta_N^*\}$ satisfying

$$\omega_j + \sum_{\{i,j\} \in \mathbb{E}} K_{ij} \sin\left(\theta_i - \theta_j\right) = 0, \text{ for all } 1 \leq j \leq N. \tag{2.17}$$

Such a steady state describes a flow (see definition 2.2.1),

$$\mathcal{F}^{\text{kuram}} : \{(i,j) \quad | \{i,j\} \in \mathbb{E}\} \quad \to \mathbb{R} \tag{2.18}$$

$$: (i,j) \qquad\qquad\qquad \mapsto K_{ij} \sin\left(\theta_i - \theta_j\right). \tag{2.19}$$

We see from Eq. (2.17) that $\mathcal{F}^{\text{kuram}}$ satisfies the flow conservation condition Eq. (2.15). Thus a steady state of Kuramoto oscillator networks defines a conservative flow network $\left(G, \boldsymbol{\omega}, \mathcal{F}^{\text{kuram}}\right)$.

2.2.2   *Linear flow networks*

If in a flow network, the flows across each edge is proportional to certain *potential* difference across each edge, then it is called a *linear flow network*. Such networks are encountered in various systems such as incompressible fluid flow in pipes [42, 43], DC flow in resistor networks [44] as well as flow of sap in plant leaves [14].

Such networks consist of *inputs* I_j at each node $i \in \mathbb{V}$. Each edge is defined to have a certain *conductivity* K_{ij} and the flows in such networks are given by

$$
\begin{aligned}
\mathcal{F}^{\text{linear}} : \{(i,j) \quad | \{i,j\} \in \mathbb{E}\} \quad &\to \mathbb{R} & (2.20) \\
: (i,j) \quad &\mapsto K_{ij}\left(\varphi_i - \varphi_j\right), & (2.21)
\end{aligned}
$$

satisfying the flow continuity condition Eq. (2.15)

$$
I_j + \sum_{\{i,j\} \in \mathbb{E}} K_{ij}\left(\varphi_i - \varphi_j\right) = 0.
$$

Thus $\left(G, \mathbf{I}, \mathcal{F}^{\text{linear}}\right)$ defines a conservative flow network.

CONNECTING THE DOTS

In Chapter 1, we motivated the topic of this thesis: "dynamics of complex flow networks". In Chapter 2, we introduced the tools and concepts we will be using. Here we will connect the dots between the different open problems motivating this thesis, put them in the context of existing research and explain in detail our approaches in solving these problems.

3.1 TOPOLOGY DEPENDENCE OF STEADY FLOWS AND THEIR STABILITY

For proper functioning of a flow network, often it is desirable that the flows across the edges are *stationary* (i.e. they do not change with time, barring external perturbations). For instance, in AC power grids, the loss of such stationary (or steady) states results in a power outage. Therefore, it is of paramount importance to understand under which conditions such steady states exist, under which conditions they are stable, and which topological features help to achieve these steady states.

In the context of Kuramoto networks, it was reported by Kuramoto himself [1] that for *all-to-all coupled* networks in the limit of *infinitel* system size, the answer to this question is simple: if the coupling strength is below some critical coupling K_c, there exists no steady state, and otherwise there exists a unique globally attracting steady state (Here we emphasize again that by the term "steady state" we refer to a globally phase locked state where all oscillators rotate with the same frequency. We do not distinguish between the "partially phase locked" and the "unsynchronized" state as they are often called in classic Kuramoto literature because none of them have steady flows and hence are equally "unsynchronized" from the flow dynamics perspective). This critical coupling is easily obtained from the distribution of natural frequencies of the oscillators (or power injections in the analogous AC power grid model): if the frequencies are all very close the average value, critical coupling is low; but if they have a "wider" distribution, critical coupling is high. Unfortunately, such necessary and sufficient conditions for steady states in general topology Kuramoto networks have not been found to date.

We know that the critical coupling strength can no longer be computed from the statistical distribution of oscillator frequencies alone, since the topological distribution of the oscillators (i.e. of their natural frequencies) matter, as do the connectivity pattern of individual nodes. Therefore, graph theoretic notions such as node degree distri-

bution [22], clustering coefficient [24] and global graph partitions [45] have been invoked to determine the critical coupling.

Lozano et. al. showed [45] that the critical coupling in any topology must be greater than the sum of all power injections P_j in any 2-way partition or *cut* into subgraphs with disjoint vertex sets $\mathbb{V}_1$ and $\mathbb{V}_2$ (defined in 2.1.5), divided by the total strength of all inter-partition edges,

$$K_c \geq \max_{\substack{\mathbb{V}_1 \cup \mathbb{V}_2 = \mathbb{V} \\ \mathbb{V}_1 \cap \mathbb{V}_2 = \{\}}} \frac{\sum_{j \in \mathbb{V}_1} P_j}{\sum_{\substack{(i,j) \in \mathbb{E} \\ i \in \mathbb{V}_1, j \in \mathbb{V}_2}} 1}. \tag{3.1}$$

While this result suggests that dense networks should need less coupling strength to have a steady state; this is not generally true, since adding a link can also *increase* [37] critical coupling, a phenomenon known as Braess' paradox that is studied in detail in the Chapter 6 of this Thesis.

The spectrum of graph Laplacians (defined in 2.1.12) has been shown again and again [46, 47, 48, 49] to have deep connections with the existence and stability of the steady states. It has been shown [50] that critical coupling is lowered when the natural frequencies of the network are arranged as close as possible to the most dominant Laplacian eigenvector.

Determining necessary and sufficient conditions for a Kuramoto oscillator network with general topologies to have a fully phase locked state nevertheless remains an open question. This is the problem we study in Chapter 4, for a modified version of Kuramoto model called the "swing equation model" for electric AC power grids. We first prove that the steady states and their bifurcation properties of Kuramoto networks (described by first order differential equations) are identical with those for swing equation model (described by second order differential equations). We connect the fact that the Jacobian for linear stability for Kuramoto systems can be interpreted as a graph Laplacian [51], to the fact from graph theory that multiplicity of the zero eigenvalue of a graph Laplacian is equal to its number of connected components [52, p. 156]. Thus we conclude that stability is lost in such systems, precisely when there exists a cut in the graph, such that all the edges in the cutset are maximally loaded. This has striking parallels with the results obtained using purely topological arguments in [45], but is a stronger statement.

Intriguingly, we find when phase differences along some edges exceed $\frac{\pi}{2}$, instability can occur without a single line being overloaded. This phenomenon shows that relying on load to predict whether an edge is vulnerable or not has its limitations, a topic that was subsequently studied by Witthaut et. al. in [27].

3.2 MULTISTABILITY AND TOPOLOGY

We noted in Section 3.1 that all-to-all coupled Kuramoto networks have either one or no steady states in the infinite system size limit. For power grid operation, this is a very desirable property: given a fixed distribution of power injections at the nodes, each edge is guaranteed to carry a fixed amount of flow, independent of initial conditions or temporary perturbations in the grid. The problem is, power grids are almost never all-to-all coupled. In fact, they tend to be planar or almost planer [20, 21]. Taylor [29] showed that uniqueness of steady states holds also in non all-to-all coupled systems as long as the network is denser than a certain limit. It has been claimed in a highly cited article [28] that for any Kuramoto network there always exists a certain coupling strength, above which uniqueness of steady states is guaranteed.

However, this claim contradicts results demonstrating multistability [30, 53] in Kuramoto systems. As one core contribution of this thesis, we identified a flaw the proof in [28], at an application of Banach's contraction principle. As a consequence, high coupling strength happens to *increase* the number of steady state, rather that decreasing it to one.

It had already been shown [30] that in ring topologies the number of steady state scales linearly with ring size. Such states, containing *twisted* phase angles, were postulated [53] to have basin volumes decreasing with the amount of "twist" quantified in a so-called winding number. Interestingly, it is known that a unique steady state exists for both the sparsest (i.e. tree) and densest (i.e. all-to-all connected) topologies [54], but not for intermediately dense ones. Research conducted parally and independently from our thesis work showed [55] in 2016 that the number of steady states increase with loop lengths of the network in plane embedded Kuramoto networks with identical frequencies. However, counting the number of steady states in Kuramoto networks with general topologies and general natural frequency distribution is still an unsolved problem.

In Chapter 5, we demonstrate that the number of coexisting steady flow in planar Kuramoto networks increase with *coupling strengths* of the edges, *length of fundamental cycles* as well as the *spatial homogeneity* of the natural frequencies. For large network size and large coupling strength, we derive a scaling law for the number of steady states. We numerically show that the said scaling matches very well with reality (for cycle lengths as low as 50), as opposed to previously known upper bounds, which were much higher than the actual numbers.

3.3 TOPOLOGICAL PERTURBATIONS AND STEADY FLOWS

Flow networks are often subjected to topological perturbations, both planned and unplanned. Examples include shutdown of power lines due to a storm or scheduled maintenance; or leaf veins being eaten

through by bugs. *Resilience* against such perturbations is therefore a very desirable property for flow networks. Indeed, electrical power grids are supposed to fulfill the "$n-1$ criteria" mandating that there should be no blackout due to the shutdown of any *one* power line at a time.

Nevertheless, topological perturbations sometimes cause other lines to fail, resulting in collective failures of big parts of the grid [56, 57]. Indeed, in 2006 shutdown of a single power line in the Ems river in northern Germany, done intentionally in order to let a ship pass, resulted in a continent wide blackout reaching up to Spain [57].

As a result, understanding, predicting and preventing such failures is an important issue that has been approached from various different directions in the past. Attempts to establish correlation between vulnerability of edges and their topological properties indicate that decentral power grids [26] are more robust against topological damages. Nodes with higher degrees seem to be crucial for stable operation, as a result scale free networks have been numerically shown [58] to be vulnerable to deliberate sabotage targeting their hubs. Intentionally *cutting* transmission lines have been demonstrated [59] to be sometimes effective in preventing cascading failures. In a different context, leaf venation networks with more cycles were shown [14] to be robust against topological perturbation compared to leaves with less cycles.

How steady flows are affected by damage or removal of an edge in a flow network is still not well understood. We will now describe a specific aspect of this issue that we studied in this thesis: the so called "Braess' paradox".

3.3.0.1   *Braess' paradox*
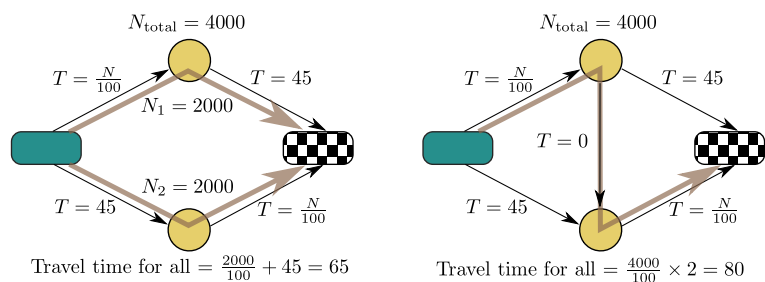
Figure 3.1: Braess' paradox as reported by D. Braess. (Left) A four edge network has two edges with travel time proportional to the number of cars in it. In the other two edges, travel time is constant. Each car chooses the shortest path selfishly. With total **4000** cars in the network, each takes **65** minutes to reach its destination. (Right) Opening a new zero travel time edge causes all cars to take **80** minutes to reach their destinations.

In the context of traffic networks, a curious phenomenon was reported in 1968 (illustrated in Figure 3.1), where opening a new street led to

increased travel time for every car [32]. Later, the same phenomenon, termed *Braess' paradox*, has been observed in the context of other flow networks like AC and DC power grids [36, 37, 38]. Braess' paradox can cause undesirable flow patterns and potentially instabilities in flow networks if not properly accounted for, because adding new edges or strengthening existing ones is a very common strategy to compensate for increased load in flow networks. Despite extensive research [60, 35, 61] on the topic, the question of which edges in a flow network will exhibit Braess' paradox, remains unanswered to date.

In Chapter 6, we systematically study the phenomenon of Braess' paradox in a class of continuous flow networks we call *conservative flow networks* (defined in 2.2.4), which includes both Kuramoto networks and leaf venation networks in plants, among other systems. We take a differential view to Braess' paradox: We define an edge to be Braessian if infinitesimal increase in its strength results in the *maximum* flow in the network *increasing*. We first derive an exact mapping from the problem of detecting Braessian edges to computing steady state flows in a modified "meta graph" of residual capacities with only one dipole source. This boils down to solving Laplace equation with a single dipole source in a weighted graph (continuum variant of which is very familiar from electrostatics). Guided by this insight, we define an intuitive notion of *flow alignment*, and demonstrate that edges with flows aligned to the maximally loaded edge are more likely to be Braessian. We build and test three classifiers to detect Braessian edges. The first one, based on edge distances, is applicable to any graph and computationally fast; but error prone. The second one is based on distances in dual graphs, and consequently applicable only to plane graphs; but with significantly more accurate than the first one. We propose a third classifier based on rerouting pathways in the graph, that performs as well as the second one, and at the same time applicable to non-planar graphs as well. The only disadvantage of this classifier is high computational complexity. Last, we demonstrate that Braess' paradox has a very *beneficial effect:* Braessian edges can be *intentionally damaged* to mitigate overload caused by damage at another edge.

3.4 SUMMARY

In this thesis, we studied three aspects of the general question: how does network topology influence the dynamics of flow networks? In Chapter 4, we derive equivalence of steady states (and their bifurcations) between Kuramoto oscillators and the swing equation model of AC power grid. We map loss of stability in these two systems to graph theoretic notion of connectedness. In Chapter 5, we demonstrate how the number of steady states in the same system increases with three topological properties – namely number of fundamental cycles, coupling strength at the edges and spatial homogeneity of natural frequencies.

In Chapter 6, we demonstrate that we can predict Braessian edges in a conservative flow network from topological features of the edges, and show that Braess' paradox can be put to good use to mitigate overload in a flow network. In Chapter 7, we summarize our results and identify future research directions.

4

ARTICLE – SUPPLY NETWORKS: INSTABILITIES WITHOUT OVERLOAD

Debsankha Manik[1,4], Dirk Witthaut [a1,4], Benjamin Schäfer[1,3], Moritz Matthiae[1], Andreas Sorge[1], Martin Rohden[1], Eleni Katifori[1,2], Marc Timme[1,2]

[1] Network Dynamics, Max Planck Institute for Dynamics and Self-Organization (MPI DS), 37077 Göttingen, Germany

[2] Faculty of Physics, University of Göttingen, 37077 Göttingen, Germany

[3] Otto-von-Guericke-Universität Magdeburg, 39106 Magdeburg, Germany

[4] These authors contributed equally to this work.

Original contribution:
I carried out most of the analytical calculations behind the results, contributing almost all the results in Sec 3 and 5, as well as interpretation and analytical calculations for results in Sec 6.1 and 6.2. I wrote significant parts of all the text sections, except Sec 4. I revised the manuscript during revision process, updating texts and figures as per referee reports.

a *Current address*: Forschungszentrum Jülich, Institute for Energy and Climate Research (IEK-STE), 52425 Jülich, Germany; e-mail: **witthaut@nld.ds.mpg.de**

Abstract. Supply and transport networks support much of our technical infrastructure as well as many biological processes. Their reliable function is thus essential for all aspects of life. Transport processes involving quantities beyond the pure loads exhibit alternative collective dynamical options compared to processes exclusively characterized by loads. Here we analyze the stability and bifurcations in oscillator models describing electric power grids and demonstrate that these networks exhibit instabilities without overloads. This phenomenon may well emerge also in other sufficiently complex supply or transport networks, including biological transport processes.

4.1   INTRODUCTION

Today's society depends on the reliable supply of electric power. The Energy transition to renewable energy (*Energiewende*) impairs the conventional power distribution system and poses great challenges for the security of the energy supply [62, 63]. It has been shown by Pesch et al. [64] that the grid might become more heavily loaded in the future as electric power generation varies over time and has to be transported over large distances. For instance, current planning assigns new large-distance distribution lines from off-shore wind parks to the inner land – making the grid more susceptible to perturbations. Moreover, wind turbines and photovoltaic arrays are strongly intermittent; their power output fluctuates on all timescales from years to below seconds [65, 66, 67]. To ensure continued stable operation of power grids, it is advisable to understand how the network structure of the power grid determines its *dynamic* stability and how instabilities generally emerge.

4.2   AN OSCILLATOR MODEL FOR POWER GRID OPERATION

In this article we analyze network models of power grids consisting of rotating machines representing electric generators and motors. These models describe the *phase dynamics* of the machines and thus capture important problems of synchronization and dynamical stability of complex power grids [68, 69, 19, 70] and have recently attracted considerable interest in physics and mathematics [26, 36, 71, 49, 72, 73]. Notably, these models are mathematically very similar to the celebrated Kuramoto model describing the dynamics of coupled limit cycle oscillators [1, 4, 2].

Variations of these models are widely used in power engineering [68, 69, 74, 70, 75, 76]. In many of the applications, however, passive loads are considered instead of motors which can be eliminated via a Kron reduction [77]. The resulting model is mathematical equivalent to the one analyzed here, but its dimension is typically significantly smaller *after this reduction* (see Section 4.2.2 for details).

4.2.1 *The oscillator model*

We model the power grid as a network of N rotating machines representing, for instance, wind turbines or electric motors [19, 26]. Let the machines be denoted by a natural number $j \in Z_N$ where $Z_N = \{1, 2, \cdots, N\}$. Each machine j is characterized by the mechanical power P_j^{mech} it generates ($P_j^{\text{mech}} > 0$) or consumes ($P_j^{\text{mech}} < 0$). The state of each rotating machine is determined by its mechanical phase angle $\phi_j(t)$ and its velocity $d\phi_j/dt$. During the regular operation, generators as well as consumers within the grid run with the same frequency $\Omega = 2\pi \times 50\text{Hz}$ (Europe) or $\Omega = 2\pi \times 60\text{Hz}$ (USA). The phase of each element j is then written as

$$\phi_j(t) = \Omega t + \theta_j(t), \tag{4.1}$$

where θ_j denotes the phase difference to the reference value Ωt.

The equations of motion for all θ_j can now be obtained from the energy conservation law, i.e. the generated energy P_j^{mech} of each single element must equal the accumulated and dissipated mechanical energy of this machine plus the electric energy P_j^{el} transmitted to the rest of the grid. We also have

$$P_j^{\text{diss}} = D_j(\dot{\phi}_j)^2 \tag{4.2}$$

$$P_j^{\text{acc}} = \frac{1}{2} I_j \frac{d}{dt}(\dot{\phi}_j)^2, \tag{4.3}$$

where I_j is the moment of inertia and D_j is the damping torque. The energy conservation law reads

$$P_j^{\text{mech}} = P_j^{\text{diss}} + P_j^{\text{acc}} + P_j^{\text{el}}. \tag{4.4}$$

We will now insert equation (4.1) in the formula for the accumulated and dissipated mechanical energy to derive the equations of motion. In the vicinity of the regular operation of the grid, phase changes are small compared to the reference frequency [19] $|\dot{\theta}_j| \ll \Omega$ and we can write the equations of motion for θ_j as

$$\forall j \in Z_N, \quad I_j \Omega \ddot{\theta}_j = P_j^{\text{mech}} - D_j \Omega^2 - 2D_j \Omega \dot{\theta}_j - P_j^{\text{el}}. \tag{4.5}$$

The electric power is determined as follows. In a synchronous machine with p_f number of poles, the phase ϕ_j of the AC electric voltage and the mechanical phase ϕ_j^{mech} have a fixed ratio [74, p. 47]

$$\phi_j = \frac{p_f}{2}\phi_j^{\text{mech}}.$$

We here consider common two-pole machines where this ratio is unity, i.e. $\phi_j(t) = \phi_j^{\text{mech}}(t)$.

In an AC circuit, where the current between two nodes I_{ij} and voltage at jth node V_j vary sinusoidally with a relative phase difference δ, the power transmitted from node j to node i is

$$P_{ij}(t) = V_j(t)I_{ij}(t) \tag{4.6}$$

$$= \left(V_{j,\text{rms}}\sqrt{2}\right)\sin\left(\Omega t\right)\left(I_{ij,\text{rms}}\sqrt{2}\right)\sin\left(\Omega t + \delta\right) \tag{4.7}$$

$$= \underbrace{V_{j,\text{rms}}I_{ij,\text{rms}}\cos\delta}_{P_{ij,\text{real}}} - V_{j,\text{rms}}I_{ij,\text{rms}}\cos\left(2\Omega t + \delta\right). \tag{4.8}$$

The second term oscillates between positive and negative values such that the direction of power flow changes direction. The net flow due to this term, when integrated over a full period of the AC cycle, is zero. Since here we consider dynamics on time scales much larger than a time period of the AC cycle $(1/\Omega)$, we ignore this second term. The first term constitutes the *real power* flow from generator to consumers. It is convenient to adopt complex notation at this point:

$$\widetilde{V}_j = V_{j,\text{rms}}e^{i\Omega t} \quad , \quad \widetilde{I}_{ij} = I_{ij,\text{rms}}e^{i(\Omega t + \delta)}, \tag{4.9}$$

such that the apparent and the real power reads

$$S_{ij} = \widetilde{V}_j\widetilde{I}_{ij}^* \quad , \quad P_{ij,\text{real}} = \Re(S_{ij}). \tag{4.10}$$

The net electric power at node j: P_j^{el} in (4.5) is basically the total P_{real} transmitted to all neighbouring nodes:

$$P_j^{\text{el}} = \sum_{k=1}^{N} P_{kj,\text{real}} \tag{4.11}$$

$$= \Re\left[\widetilde{V}_j\sum_{k=1}^{N}\widetilde{I}_{kj}^*\right] \tag{4.12}$$

$$\widetilde{I}_{kj} = Y_{kj}(\widetilde{V}_k - \widetilde{V}_j). \tag{4.13}$$

For simplicity we here neglect ohmic losses in the grid such that the admittance is purely imaginary, $Y_{jk} = iB_{jk}$. Furthermore, we assume that the magnitude of the voltage is constant throughout the grid, $|\widetilde{V}_j| = V_0$ for all nodes $j \in Z_N$. Then P_j^{el} simplifies to

$$P_j^{\text{el}} = \Re\left[\sum_{k=1}^{N}V_0^2 B_{jk}\left\{\sin(\theta_j - \theta_k) + i\left(\cos(\theta_j - \theta_k) - 1\right)\right\}\right] \tag{4.14}$$

$$= \sum_{k=1}^{N}V_0^2 B_{jk}\sin(\theta_j - \theta_k). \tag{4.15}$$

Substituting this result into equation (4.5) thus yields the equations of motion

$$I_j\Omega\frac{d^2\theta_j}{dt^2} + D_j\frac{d\theta_j}{dt} = P_j^{\text{mech}} - D_j\Omega^2 + \sum_{k=1}^{N}V_0^2 B_{jk}\sin(\theta_k - \theta_j). \tag{4.16}$$

The same equations of motions constitute the so-called structure-preserving model in power engineering [68], which is derived under slightly different assumptions.

For the sake of simplicity we introduce the abbreviations

$$P_j = \frac{P_j^{\mathrm{mech}} - D_j \Omega^2}{I_j \Omega} \tag{4.17}$$

$$\alpha_j = \frac{D_j}{I_j \Omega} \tag{4.18}$$

$$K_{jk} = \frac{V_0^2 B_{jk}}{I_j \Omega} \tag{4.19}$$

such that the equations of motion read

$$\forall j \in Z_N, \quad \frac{d^2 \theta_j}{dt^2} = P_j - \alpha_j \frac{d\theta_j}{dt} + \sum_k K_{jk} \sin(\theta_k - \theta_j). \tag{4.20}$$

In this formulation the regular operation of the grid corresponds to a stable fixed point with $d\theta_j/dt = 0$ for all nodes j.

Throughout this paper we assume that the network defined by the coupling matrix is globally connected. Otherwise we can simply consider each connected component separately. We take symmetric transmission capacities

$$K_{jk} = K_{kj} \tag{4.21}$$

for all j, k as appropriate for (electric) supply networks and $K_{jj} = 0$. Furthermore, we assume that the power in the grid is balanced, i.e. $\sum_j P_j = 0$. This is appropriate since we focus on the short-time dynamics of the grid and the stability of steady states. On longer time-scales, the power balance is maintained by the grid operators by adapting the generation.

4.2.2 *Ohmic loads and the classical model*

The oscillator model introduced above assumes that all nodes of the network represent synchronous machines. In contrast, the so-called classical model widely studied in power engineering [70] includes a set of synchronous generators as above, but considers only ohmic loads. The load nodes of the network can then be eliminated which yields a much lower dimensional dynamical system. The resulting equations of motion are mathematically equivalent such that all our results equally well apply to the classical model. However, the network topology is no longer obvious in this model as the effective coupling matrix of the generator nodes is generally non-zero everywhere. Bergen and Hill [68] rectified this issue by introducing the *structure preserving model*, which also gives rise to equations of motion formally identical to the oscillator model. We thus focus on the oscillator model in the rest of the paper.

In the following we briefly summarize the derivation of the classical model [77] to show how to deal with ohmic loads in this framework. We divide the nodes of the networks into active and passive nodes, where the passive ones represent ohmic loads. For the sake of simplicity

we label the nodes such that $j = 1, \ldots, L$ are the active nodes and $k = L+1, \ldots, N$ are the passive nodes. The passive nodes have a fixed power consumption

$$S_j = \widetilde{V}_j \underbrace{\sum_{k=1}^{N} \widetilde{I}_{kj}^*}_{=: \widetilde{I}_j^*}. \tag{4.22}$$

Even more, one assumes that both factors $\widetilde{V}_j$ and $\widetilde{I}_j$ are fixed independently. One can then eliminate these nodes via a Kron reduction as follows.

One starts with Kirchhoff's equations in the form (cf. equation 4.13)

$$\widetilde{I}_j = \sum_{k=1}^{N} \widetilde{I}_{jk} = \sum_k Y_{jk}(\widetilde{V}_k - \widetilde{V}_j) = \sum_k Q_{jk}\widetilde{V}_k, \tag{4.23}$$

where

$$Q_{jk} = Y_{jk} - \delta_{jk} \sum_{\ell} Y_{j\ell} \tag{4.24}$$

is called *the nodal admittance matrix*. These equations are recast into matrix form

$$\begin{pmatrix} \boldsymbol{I}_a \\ \boldsymbol{I}_p \end{pmatrix} = \begin{pmatrix} Q_{aa} & Q_{ap} \\ Q_{pa} & Q_{pp} \end{pmatrix} \begin{pmatrix} \boldsymbol{V}_a \\ \boldsymbol{V}_p \end{pmatrix}, \tag{4.25}$$

where the vectors $\boldsymbol{I}_a$ and $\boldsymbol{I}_p$ collect the currents at the active and the passive nodes, respectively. These equations are solved for the currents

$$\boldsymbol{I}_a = \underbrace{(Q_{ap}Q_{pp}^{-1})}_{=: Q^{\mathrm{ac}}} \boldsymbol{I}_p + \underbrace{(Q_{aa} - Q_{ap}Q_{pp}^{-1}Q_{pa})}_{=: Q^{\mathrm{red}}} \boldsymbol{V}_a \tag{4.26}$$

at the active nodes. The net electric power at one of the active nodes then reads

$$S_j = \widetilde{V}_j \sum_{\ell=1}^{L} Q_{j\ell}^{\mathrm{red}*}\widetilde{V}_\ell^* + \widetilde{V}_j \sum_{\ell=L+1}^{N} Q_{j\ell}^{\mathrm{ac}*}\widetilde{I}_\ell^*. \tag{4.27}$$

The second term is fixed by assumption, such that it can be transfered to the effective mechanical power of the respective node,

$$P_j^{\mathrm{eff}} = P_j^{\mathrm{mech}} - \Re\left[\widetilde{V}_j \sum_{\ell=L+1}^{N} Q_{j\ell}^{\mathrm{ac}*}\widetilde{I}_\ell^*\right]. \tag{4.28}$$

Assuming again that the lines are lossless such that

$$Y_{jk} = iB_{jk} \qquad \text{and} \qquad Q_{j\ell}^{\mathrm{red}*} = iB_{j\ell}^{\mathrm{red}}, \tag{4.29}$$

the equations of motion for the active nodes are then derived from the energy conservation equation (4.4)

$$I_j\Omega\frac{d^2\theta_j}{dt^2} + D_j\frac{d\theta_j}{dt} = P_j^{\text{eff}} - D_j\Omega^2 + \sum_{\ell=1}^{L} V_0^2 B_{j\ell}^{\text{red}} \sin(\theta_\ell - \theta_j). \quad (4.30)$$

This is fully equivalent to the equations of motion for the oscillator model (4.16) such that all mathematical results obtained in the present article can thus be directly applied to the classical model as well.

4.2.3 *Further generalisations*

Both the oscillator and the classical model describe only the phase dynamics of the synchronous machines, assuming a constant voltage throughout the grid. Several important aspects of the voltage dynamics in a complex power grid are described by the so-called third-order model [70]. A recent theoretical study of voltage instabilities can be found in [78]. Still, all these models neglect Ohmic losses of the transmission lines. If Ohmic losses are included, the equations of motion become significantly more complex [70].

4.3   THE NATURE AND BIFURCATIONS OF STEADY STATES

During steady operation of a power grid all nodes run with the grid's reference frequency Ω and fixed phase differences. A stable fixed point (i.e. equilibrium/steady state) of the equations of motion (4.20) describes the steady operation of the power grid. The loss of such a fixed point or a dynamical instability induce a desynchronization of the grid. Therefore, it is essential to understand the properties of the fixed points of the oscillator model, in particular their bifurcations and dynamical stability.

The fixed points of the equations of motion (4.20) are determined by the nonlinear algebraic equations

$$\forall j \in Z_N, \quad P_j + \sum_k K_{jk}\sin(\theta_k^* - \theta_j^*) = 0. \quad (4.31)$$

In the following, we present several results on the existence, stability and bifurcations of these fixed points, some aspects of which have been published for related systems in [79]. Fixed points are marked by an asterisk and the vector $\boldsymbol{\theta} = (\theta_1, \ldots, \theta_N)^T \in S^N$ collects the phases of all machines, where $S = \{x \,|\, 0 \le x \le 2\pi\}$. The local frequencies are referred to by $v_j = d\theta_j/dt$ or $\boldsymbol{v} = d\boldsymbol{\theta}/dt$, respectively.

Lemma 4.3.1. *The network dynamics of the system defined by* (4.20) *and* (4.21) *for* $\alpha_j = 0$ *(zero damping) is a Hamiltonian system of the form*

$$\dot{\theta}_j = \frac{\partial\mathcal{H}}{\partial v_j}, \qquad \dot{v}_j = -\frac{\partial\mathcal{H}}{\partial\theta_j}, \quad (4.32)$$

where the phase θ_j and the phase velocity

$$v_j = d\theta_j/dt \tag{4.33}$$

are canonically conjugate variables for all $j \in \mathbb{Z}_N$. The Hamiltonian function has the natural form

$$\mathcal{H}(v, \theta) = T(v) + V(\theta) \tag{4.34}$$

with the kinetic and potential energies

$$T(v) = \frac{1}{2}\sum_j v_j^2 \tag{4.35}$$

$$V(\theta) = -\sum_j P_j \theta_j - \frac{1}{2}\sum_{i,j} K_{ij}\cos(\theta_i - \theta_j). \tag{4.36}$$

Proof. Let $\mathcal{H}(v, \theta) = T(v) + V(\theta)$ be a Hamiltonian function defined by (4.34), (4.35) and (4.36). Then $\mathcal{H}$ is continuously differentiable on any open star-shaped subset of the phase space with

$$\partial \mathcal{H}/\partial v_j = v_j = \dot{\theta}_j \tag{4.37}$$

and

$$\begin{aligned}\frac{\partial \mathcal{H}}{\partial \theta_j} &= -P_j - \frac{1}{2}\sum_k\sum_l K_{kl}\frac{\partial}{\partial \theta_j}\cos(\theta_k - \theta_l) \tag{4.38}\\ &= -P_j - \sum_k K_{jk}\sin(\theta_k - \theta_j). \tag{4.39}\end{aligned}$$

Where the last equality follows from symmetry (4.21). Substituting (4.33), (4.37) and (4.39) into the Hamilton equations (4.32), the claim follows. □

Corollary 4.3.1. *The set of all fixed points of the oscillator equation (4.20) and (4.21) for arbitrary $\alpha_j \in \mathbb{R}$, $j \in \mathbb{Z}_N$, is identical to the set of fixed points of the Hamiltonian system (4.32) with (4.34) and (4.33). The fixed points are local extrema/saddle points of the potential function $V(\theta)$ (cf. also [80]).*

Proof. The set of fixed points of (4.32) is given by

$$P_{\text{Hamilton}} = \left\{ (\theta^*, v^*) \,\middle|\, \forall j \in \mathbb{Z}_N, \quad \frac{\partial \mathcal{H}}{\partial v_j} = 0 \wedge -\frac{\partial \mathcal{H}}{\partial \theta_j} = 0 \right\} \tag{4.40}$$

The set of fixed points of the oscillator equations (4.20) is given by

$$P_{\text{osc}} = \left\{ (\theta^*, v^*) = (\theta^*, 0) \,\middle|\, \forall j \in \mathbb{Z}_N, P_j + \sum_{k=1}^N K_{jk}\sin(\theta_k^* - \theta_j^*) = 0 \right\}, \tag{4.41}$$

independent of all α_j. If the transmission capacities are symmetric (4.21), the Hamiltonian and the original oscillator dynamics in the $\alpha_j = 0$ case are equivalent (have identical trajectories) as ensured by Lemma 4.3.1. Thus in particular their fixed points are identical. And since the fixed points of the oscillator model don't depend on α_j as per (4.41), the fixed points of the oscillator model for arbitrary α_j are also, by extension, identical to those of the Hamiltonian system.

As $T(\boldsymbol{v})$ is independent of all θ_j we have at each fixed point $(\boldsymbol{\theta}^*, \boldsymbol{v}^*)$ that

$$\left.\frac{\partial \mathcal{H}(\boldsymbol{v}, \boldsymbol{\theta})}{\partial \theta_j}\right|_{\boldsymbol{\theta}^*} = \left.\frac{\partial V(\boldsymbol{\theta})}{\partial \theta_j}\right|_{\boldsymbol{\theta}^*} = 0 \tag{4.42}$$

for all j such that the fixed points are located at local extreme/saddle points of V, demonstrating the second claim. $\qquad\square$

Because of this correspondence, the theory of (damped) Hamiltonian dynamical systems (see [81] and references therein) helps us in characterizing the fixed points of the oscillator model and their bifurcations. We note that one has to be careful about the domain of $\mathcal{H}$. In principle, the phases are only defined modulo 2π but $\mathcal{H}$ is not 2π-periodic. This fact is not a major problem for our purpose, but it prohibits a definition of Gibbsian ensembles in statistical mechanics [80, 2].

As shown in Corollary 4.3.1, the location of the fixed points $\boldsymbol{\theta}^* = (\theta_1^*, \ldots, \theta_N^*)$ is independent of the damping coefficients α_j. Furthermore, the location of the fixed point is the same for the celebrated Kuramoto [1, 4, 2] model such that our results may be adapted for this important model system. The question naturally arises: how do the stability properties of the fixed points change when α_j are varied or when we go from the oscillator model to Kuramoto model? We will answer this question subsequently, in Lemma 4.3.2 and Theorem 4.3.1.

The linear or spectral stability of a fixed point is obtained by linearizing the equations of motion. Writing

$$\boldsymbol{\xi} = \boldsymbol{\theta} - \boldsymbol{\theta}^* \tag{4.43}$$

the linearized equations of motion are given by

$$\frac{d}{dt}\begin{pmatrix}\dot{\boldsymbol{\xi}} \\ \boldsymbol{\xi}\end{pmatrix} = J\begin{pmatrix}\dot{\boldsymbol{\xi}} \\ \boldsymbol{\xi}\end{pmatrix}. \tag{4.44}$$

For the given damped oscillator system with equations of motion (4.20), the Jacobian is given by

$$J = \left(\begin{array}{c|c} -A_{N \times N} & -M_{N \times N} \\ \hline \mathbb{I}_{N \times N} & \mathbf{0}_{N \times N} \end{array}\right), \tag{4.45}$$

where

$$A = \begin{pmatrix} \alpha_1 & 0 & \cdots \\ 0 & \alpha_2 & \cdots \\ \vdots & \vdots & \ddots \end{pmatrix} \tag{4.46}$$

is a diagonal matrix specifying the damping coeeficient at each node and M is the Hesse matrix of the potential function $V(\boldsymbol{\theta})$ with elements

$$M_{ij} = \frac{\partial^2 V}{\partial \theta_i \partial \theta_j} \tag{4.47}$$

$$M = \begin{pmatrix} \sum_{l=1}^{N} K_{1l} \cos(\theta_1^* - \theta_l^*) & -K_{12} \cos(\theta_1^* - \theta_2^*) & \cdots \\ -K_{21} \cos(\theta_2^* - \theta_1^*) & \sum_{l=1}^{N} K_{2l} \cos(\theta_2^* - \theta_l^*) & \cdots \\ \vdots & \vdots & \ddots \end{pmatrix}. \tag{4.48}$$

This can be verified by a straightforward calculation.

Let λ_j be the eigenvalues of the Jacobian matrix J:

$$\forall j \in \{1, 2, \ldots, 2N\}, \quad J\boldsymbol{v_j} = \lambda_j \boldsymbol{v_j} \tag{4.49}$$

and let μ_k be the eigenvalues of the Hesse matrix M:

$$\forall k \in \{1, 2, \ldots, N\}, \quad M\boldsymbol{u_k} = \mu_k \boldsymbol{u_k}, \tag{4.50}$$

then we find the results stated below.

Lemma 4.3.2. *If $\mu_k \geq 0$ for all $k \in \mathbb{Z}_N$, then $\Re(\lambda_j) \leq 0$ for all $j \in \{1, 2, \ldots, 2N\}$. Moreover, for each $\boldsymbol{v_j}$ such that $J\boldsymbol{v_j} = \boldsymbol{0}_{2N}$, there exists one and only one $\boldsymbol{u_k}$ such that*

$$M\boldsymbol{u_k} = \boldsymbol{0}_N \tag{4.51}$$

$$\boldsymbol{v_j} = (\underbrace{0, 0, \cdots, 0}_{\boldsymbol{0}_N}, \underbrace{u_1, u_2, \cdots, u_N}_{\boldsymbol{u_k}}) \tag{4.52}$$

$$:= \boldsymbol{0}_N \otimes \boldsymbol{u_k}. \tag{4.53}$$

Proof. Suppose $\boldsymbol{v} = \boldsymbol{v_1} \otimes \boldsymbol{v_2} \in \mathbb{R}^N \otimes \mathbb{R}^N$ is an eigenvector of J with eigenvalue λ. Then we have:

$$\lambda \boldsymbol{v_1} = -A\boldsymbol{v_1} - M\boldsymbol{v_2} \tag{4.54}$$

$$\lambda \boldsymbol{v_2} = \boldsymbol{v_1} \tag{4.55}$$

Substituting (4.55) in (4.54):

$$0 = M\boldsymbol{v_2} + \lambda A \boldsymbol{v_2} + \lambda^2 \boldsymbol{v_2} \tag{4.56}$$

$$0 = \boldsymbol{v_2}^\dagger M \boldsymbol{v_2} + \boldsymbol{v_2}^\dagger A \boldsymbol{v_2} \lambda + \boldsymbol{v_2}^\dagger \boldsymbol{v_2} \lambda^2 \tag{4.57}$$

$$= \kappa_1^2 + \kappa_2^2 \lambda + \kappa_3^2 \lambda^2, \tag{4.58}$$

where

$$\kappa_1^2 = \boldsymbol{v_2}^\dagger M \boldsymbol{v_2} \quad \geq 0, \quad \text{(M is positive semi-definite)} \tag{4.59}$$

$$\kappa_2^2 = v_2{}^\dagger A v_2 \qquad \geq 0, \quad (\alpha_j \geq 0) \tag{4.60}$$
$$\kappa_3^2 = v_2{}^\dagger v_2 \qquad \geq 0, \tag{4.61}$$

such that

$$\lambda = \frac{-\kappa_2^2 \pm \sqrt{\kappa_2^4 - 4\kappa_1^2 \kappa_3^2}}{2\kappa_3^2}. \tag{4.62}$$

This implies $\Re(\lambda) \leq 0$, which proves the first part of the Lemma. Moreover, $\Re(\lambda) = 0 \iff \kappa_1^2 = 0$, which happens only if $M v_2 = 0$. This can be checked by expanding v_2 in the eigenbasis of M. This proves the second part. $\qquad\square$

Using the technical results presented above, we now analyze the stability and bifurcations in more detail. We show that stability is entirely determined by the Hesse matrix M and independent of the damping coefficients α_j. In many cases, M can be interpreted as a Laplacian matrix [52], such that the stability can be analyzed in terms of the topology of the grid.

Before we proceed, we note that by construction the Hesse matrix M has one zero eigenvalue (proof in Corollary 4.A.1) with the eigenvector:

$$u_1 = (1, 1, \cdots, 1) \tag{4.63}$$
$$M u_1 = 0 \tag{4.64}$$

For notational convenience we denote the eigenvalues of M sorted in ascending order of absolute values: $0 = |\mu_1| \leq |\mu_2| \leq |\mu_3| \leq \cdots \leq |\mu_N|$.

Theorem 4.3.1. *Let θ^* be a fixed point of the oscillator model* (4.20). *Then $\theta^* + \Delta(1, 1, \cdots, 1)^T$ is also a fixed point for all $\Delta \in \mathbb{R}$. If $\mu_j > 0$ for all $j \in \{2, 3, \ldots, N\}$, then the fixed point is transversely asymptotically stable.*

Proof. If $\mu_j > 0$ for all $j \in \{2, 3, \ldots, N\}$, Lemma 4.3.2 shows that the Jacobian J will have only one zero eigenvalue. We can see from (4.63) that the eigenvector corresponding to zero eigenvalue is

$$v^* = \mathbf{0}_N \otimes (1, 1, \cdots, 1). \tag{4.65}$$

This eigenvector implies that a perturbation around a fixed point in the direction

$$\Delta \dot{\theta}_j^* = 0, \quad \Delta \theta_j^* = \text{constant} \tag{4.66}$$

is neutrally stable. However, this is simply due to the fact that the equations of motion (4.20) remains unchanged on adding a uniform global shift to the phase angles θ_j.

Since all other eigenvalues of the Jacobian J are less than 0, as guaranteed by Lemma 4.3.2, we see that all small perturbations transverse to the global shift (4.66) decay to zero with time. Transverse asymptotic stability therefore follows from the center manifold theorem (cf. [82]). $\qquad \square$

Lemma 4.3.3. *A stable fixed point of the oscillator model* (4.20) *can be lost only via an inverse saddle-node bifurcation where one of the* μ_j *as defined in* (4.50) *becomes zero.*

Proof. To analyze the nature of bifurcations consider first the hamiltonian limit $\alpha_j = 0$. In a hamiltonian system only two types of bifurcation are possible when a parameter is varied smoothly [81]: a saddle-node bifurcation or a Krein bifurcation. At a Krein bifurcation complex quadruplets of eigenvalues emerge. However, this is impossible for the given dynamical system as eigenvalues of the Jacobian J are always purely real or purely imaginary for $\alpha = 0$, as demonstrated in (4.62). Thus the only possible bifurcation scenario is that of a saddle-node bifurcation. As the position (Theorem 4.3.1) and stability properties (Lemma 4.3.2) of fixed points are both independent of α_j the bifurcation remains the same also for the non-Hamiltonian case $\alpha_j > 0$. $\qquad \square$

We note that in the Hamiltonian limit $\alpha = 0$ stability always means neutral stability. A minimum of the potential function $V(\boldsymbol{\theta})$ is an "elliptic fixed point" or "center" of the dynamical system as all eigenvalues of the Jacobian are purely imaginary. For $\alpha_j > 0$ all eigenvalues of the Jacobian acquire a negative real part, such that the fixed point becomes asymptotically stable.

We note that Theorem 4.3.1 also implies that the fixed points of the oscillator model share identical position and linear stability properties with the famous Kuramoto model [2] because $-M$ happens to be the Jacobian of the Kuramoto system.

4.4   ELEMENTARY EXAMPLE

To illustrate the mathematical results of the previous section, we first consider the simplest non-trivial grid, a two-element system consisting of one generator and one consumer. We assume that the power is balanced, i.e. $-P_1 = P_2$ and damping is uniform, i.e. $\alpha_1 = \alpha_2 = \alpha$. Therefore, $\ddot{\theta}_1 + \ddot{\theta}_2 = -\alpha(\dot{\theta}_1 + \dot{\theta}_2)$ and the mean phase $\theta_1 + \theta_2$ of the grid reaches a constant value exponentially in time. We thus consider only the dynamics of the phase difference $x = \theta_2 - \theta_1$. With $\Delta P = P_2 - P_1$ the equation of motion for this system reads

$$\frac{d^2 x}{dt^2} = \Delta P - \alpha \frac{dx}{dt} - 2K \sin(x). \tag{4.67}$$

As the phase difference is defined modulo 2π, the phase space is cylindrical, $(\dot{x}, x) \in \mathbb{R} \times 2\pi \mathrm{S}^1$ (however, for illustration purposes and
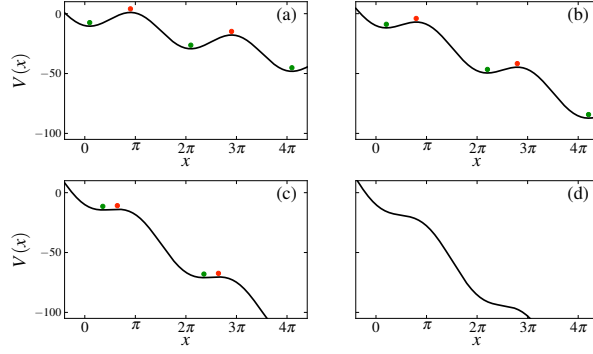
Figure 4.1: The tilted washboard potential (4.73) for $K = 5$ and (a) $\Delta P = 3$, (b) $\Delta P = 6$, (c) $\Delta P = 9$ and (d) $\Delta P = 12$, respectively. The green (red) points illustrate the local minima (maxima) of the potential determining the location of a stable (unstable) fixed point.

for comparing to the Hamiltonian case, it might be helpful to "unravel" the cylinder, i.e. assume that phases can take arbitrary values in $\mathbb{R}$).

Two fixed points exist for $2K > \Delta P$. The physical reason is that a steady operation of the grid is possible only when the transmission capacity of the line is larger than the power that must be transmitted. The location of the two fixed points $F_k = (x^*, \dot{x}^*)$ are specified by the conditions $\dot{x}^* = 0, \ddot{x}^* = 0$. The eigenvalues of the Jacobian at these points are given by

$$F_1 : \ x^* = \arcsin \frac{\Delta P}{2K} \tag{4.68}$$

$$\lambda_\pm^{(1)} = -\frac{\alpha}{2} \pm \sqrt{\left(\frac{\alpha}{2}\right)^2 - 2K \cos\left(\arcsin \frac{\Delta P}{2K}\right)} \tag{4.69}$$

$$F_2 : \ x^* = \pi - \arcsin \frac{\Delta P}{2K} \tag{4.70}$$

$$\lambda_\pm^{(2)} = -\frac{\alpha}{2} \pm \sqrt{\left(\frac{\alpha}{2}\right)^2 + 2K \cos\left(\arcsin \frac{\Delta P}{2K}\right)}. \tag{4.71}$$

The fixed point F_1 is stable: Depending on α, the eigenvalues are either both real and negative or complex with negative real values. The fixed point F_2 is a saddle, as $\lambda_+^{(1)}$ is always real and positive while $\lambda_-^{(1)}$ is always real and negative.

At $2K = \Delta P$ these two fixed points vanish in an inverse saddle-node bifurcation. No steady operation is possible for $2K < \Delta P$ as the load exceeds the capacity of the link. The nature of this bifurcation becomes most obvious when we consider the potential function introduced in the Hamiltonian formulation (4.36). The dynamical system (4.67) can be viewed as the equation of motion of a mechanical particle moving in a tilted washboard potential with friction

$$\frac{d^2 x}{dt^2} = -\alpha \frac{dx}{dt} - \frac{dV(x)}{dx} \tag{4.72}$$
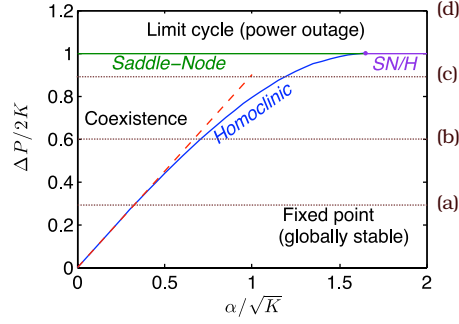
Figure 4.2: Global stability phase diagram in parameter space for an elementary power grid consisting of one generator and one consumer (cf. [84]). The dashed red line shows the approximate phase boundary (4.85) in the case of low friction α. The dotted horizontal lines labelled by letters indicate the parameter values at which the potential V has been drawn in Fig. 4.1.

$$\text{with } V(x) \;=\; -\Delta P x - K\cos(x). \tag{4.73}$$

The tilted washboard potential $V(x)$ and the critical points are illustrated in Fig. 4.1. When the tilting ΔP is increased, maxima and minima approach each other. At $\Delta P = 2K$ the critical points collide and vanish in an inverse saddle-node bifurcation, as previously explained by the form of the eigenvalues (4.68). This mechanical analog has been analyzed in great detail in statistical physics (see [83, 84] and references therein).

4.5   LOCAL VS. GLOBAL STABILITY

How about the *global* stability? Here we focus on the mathematical aspects of global stability and confine ourselves to the elementary example introduced in the previous section. Numerical studies for large complex networks were recently presented in [85, 73].

The global stability properties of the two-element grid are summarized in the parametric portrait in Fig. 4.2, cf. also [83]. For $\Delta P > 2K$, there is no fixed point as discussed above. All trajectories converge to the global attractor – a limit cycle representing a run-away solution. For $\Delta P < 2K$ and strong damping, the stable fixed point F_1 is a global attractor. For weak damping, there exists a stable limit cycle, which coexists with the stable fixed point. The system will converge to either of them, depending on which basin of attraction the initial conditions belong to. This weak damping regime characterizes regular power grid operation such that the coexistence might be typical of real world power grids.

The critical damping $\alpha_c(\Delta P, K)$ is defined by the boundary that separates these two regions in the parametric portrait. At the boundary, the limit cycle emerges from a homoclinic orbit of the saddle fixed point in a homoclinic bifurcation, as illustrated in Fig. 4.3. Along the homoclinic
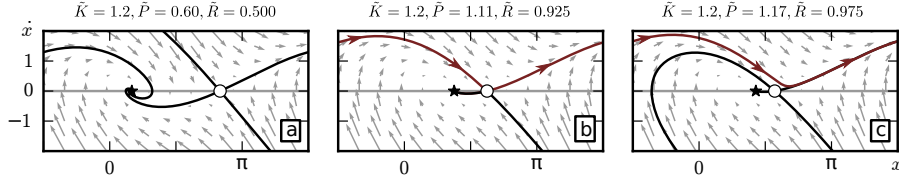
Figure 4.3: Homoclinic bifurcation from globally stable fixed point to coexistence of limit cycle and fixed point in the two-element system. Black lines indicate the stable/unstable manifolds of the fixed points, brown lines indicate the homoclinic orbit. (a) In the globally stable region all trajectories converge to the stable focus ($\star$). (b) At the bifurcation, a homoclinic orbit (brown) is attached to the saddle ($\circ$). (c) The coexistence region. One unstable manifold of the saddle extends to the limit cycle, which has emerged from the homoclinic orbit. Parameters are: $\widetilde{K} = \frac{2K}{\alpha^2}, \widetilde{P} = \frac{\Delta P}{\alpha^2}, \widetilde{R} = \frac{\Delta P}{2K}$.

orbit, the phase x increases 2π. The boundary intersects the saddle-node bifurcation line ($\Delta P = 2K$) at a numerically determined value of $\frac{\alpha}{\sqrt{K}} \approx 1.69$. For $\frac{\alpha}{\sqrt{K}} \gtrsim 1.69$, the saddle-node bifurcation and the homoclinic bifurcation combine to a saddle-node homoclinic bifurcation (cf. [86], Fig. 7.2).

An analytical approximation for the border between the globally stable and the coexistence regime can be obtained in the low-friction limit [84]. In order to determine stability criteria according to Lyapunov's second method [87], we define the energy E of the system as

$$E = \frac{(\dot{x})^2}{2} - 2K\cos(x). \tag{4.74}$$

It is to be noted that this energy E is not identical with the Hamiltonian H since this does not include the tilting introduced by the damping α. The change of energy is thus

$$\frac{dE}{dt} = \ddot{x}\dot{x} + 2K\sin(x)\dot{x}. \tag{4.75}$$

Inserting equation (4.67) into (4.75) yields

$$\frac{dE}{dt} = (\Delta P - 2K\sin(x) - \alpha\dot{x})\,\dot{x} + 2K\sin(x)\dot{x} \tag{4.76}$$

$$= \Delta P\dot{x} - \alpha(\dot{x})^2. \tag{4.77}$$

If the average energy over one full period T decreases for all initial conditions for all time, the system is in the globally stable regime. The condition for the border between the globally stable and the coexistence regime is therefore described by:

$$\overline{\frac{dE}{dt}}^T = 0. \tag{4.78}$$

Hence

$$\Delta P \overline{\dot{x}}^T - \alpha \overline{\dot{x}^2}^T = 0 \tag{4.79}$$

is the condition for the border between the globally stable and the coexistence regime.

We can now calculate

$$\bar{\dot{x}}^T = \frac{1}{T} \int_0^T \dot{x}dt = \frac{1}{T} \int_{-\pi}^{\pi} dx = \frac{2\pi}{T} \tag{4.80}$$

and

$$\overline{\dot{x}^2}^T = \frac{1}{T} \int_0^T \dot{x}^2 dt = \frac{1}{T} \int_{-\pi}^{\pi} \dot{x}dx \tag{4.81}$$

$$= \frac{1}{T} \int_{-\pi}^{\pi} \sqrt{2E(x,\dot{x}) + 4K\cos(x)}dx. \tag{4.82}$$

Inserting equation (4.79), we get

$$\Delta P \frac{2\pi}{T} = \frac{\alpha}{T} \int_{-\pi}^{\pi} \sqrt{2E(x,\dot{x}) + 4K\cos(x)}dx. \tag{4.83}$$

At the parameters where a globally stable fixed point loses global stability, there will exist a trajectory of x which will satisfy $\dot{x} = 0$ at each successive peak of the potential landscape (cf. Fig. 4.1). Therefore we have $E_{\text{peak}} = 2K$. At the low friction approximation, we can neglect energy dissipation and hence assume E to be constant throughout the period. So we substitute $E(x,\dot{x}) = 2K$ in (4.83):

$$\int_{-\pi}^{\pi} \sqrt{4K + 4K\cos(x)}dx = 8\sqrt{2K}. \tag{4.84}$$

We thus find for the low-friction approximation the following border between the globally stable and the coexistence regime (cf. (4.83))

$$\Delta P = \frac{4\sqrt{2}}{\pi} \cdot \alpha\sqrt{K}. \tag{4.85}$$

The excellent agreement of the low-friction approximation (red line) for $\alpha/\sqrt{K} < 0.6$ with the numerically calculated border (blue curve) separating the two regimes is illustrated in Fig. 4.2.

4.6 INSTABILITIES WITH AND WITHOUT OVERLOAD

The regular operation of a power grid is described by a stable fixed point of the oscillator model (4.20). When a parameter, such as the power P_j or the transmission capacity K_{jk}, is varied smoothly, in some cases this fixed point can be lost, which signals an eventual desynchonization of the grid. If the local frequency deviates from the reference Ω by more than a fixed security margin (typically 200 mHz, cf. [88]), an emergency shutdown is carried out which can lead to a large-scale power outage (see, e.g., [89, 56, 57]). In this section we discuss the physical aspects of this instability.

We first note that a stable fixed point can be lost only via a saddle-node bifurcation as described by Lemma 4.3.3. The fixed point is stable iff the real part of all eigenvalues of the Jacobian is smaller than or equal to zero. The bifurcation thus occurs when

$$\Re(\lambda_{\ell\pm}) \to 0 \qquad \Leftrightarrow \qquad \mu_\ell \to 0. \tag{4.86}$$

for any $\ell \in \{2,\dots,N\}$. We recall that $\mu_1 = 0$, which corresponds to a global shift of the phases θ_j, has no physical significance.

Interestingly, the loss of a stable fixed point is generally *not* equivalent to an overload of one or more transmission lines. In particular, we can distinguish two different scenarios.

4.6.1 *In normal operation, instability implies overload*

When a power grid is only weakly loaded, the phase differences along each edge remain small. The power flow over the transmission line (j,k) increases monotonically with the phase difference as long as $|\theta_j - \theta_k| \leq \pi/2$ (cf. equation (4.15)). If this condition holds for all edges in the network, the grid is dynamically stable, as proved in Corollary 4.6.1 below, and we can find a direct graph theoretic interpretation of any bifurcation. We call this *normal operation*.

Corollary 4.6.1. *A fixed point is stable if $|\theta_i^* - \theta_j^*| \leq \pi/2$ holds for all edges (i,j) of the network.*

Proof. We define the *residual capacity* of each transmission line as

$$K_{ij}^{\mathrm{red}} \;=\; K_{ij}\cos(\theta_j - \theta_i). \tag{4.87}$$

If $|\theta_i^* - \theta_j^*| \leq \pi/2$ holds for all edges, then $\forall i,j \in Z_N$

$$
\begin{aligned}
0 &\geq K_{ij}\cos(\theta_i^* - \theta_j^*) & \tag{4.88}\\
&= K_{ij}\sqrt{1 - \sin^2(\theta_j - \theta_i)} \\
&= \sqrt{K_{ij}^2 - F_{ij}^2} & \tag{4.89}
\end{aligned}
$$

where $F_{ij} = K_{ij}\sin(\theta_j - \theta_i)$ is the power flow from node j to node i. Let us define a meta-graph $\widetilde{G}$ with the same set of vertices and edges as the original power grid, but with edge weights $w_{ij} = K_{ij}^{\mathrm{red}}$. The Hesse matrix M as defined in (4.48) then becomes the Laplacian matrix of the meta-graph (details in Appendix 4.A). It is a well known result [52] that the eigenvalues of the Laplacian of a graph with *non-negative* edge weights satisfy:

$$0 = \mu_1 \leq \mu_2 \leq \cdots \leq \mu_N. \tag{4.90}$$

Stability of the fixed point directly follows from theorem 4.3.1. $\square$
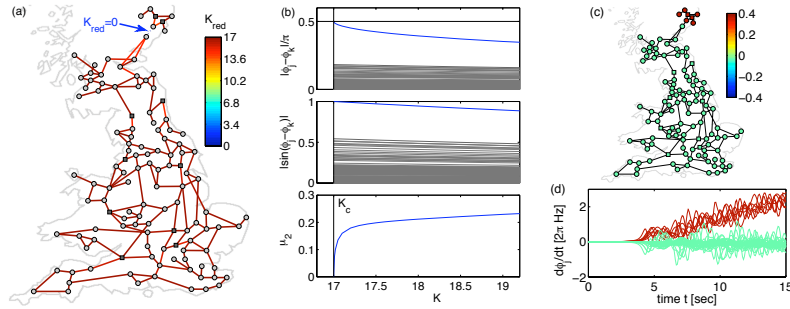
Figure 4.4: Bifurcation due to an isolated overload. At the bifurcation the marked edge becomes overloaded and the meta-graph $\widetilde{G}$ decomposes into two fragments. (a) Model network based on the topology of the British high-voltage transmission grid [90, 26]. Ten out of 120 nodes are randomly chosen to be generators with $P_j = +11\mathrm{s}^{-1}$ ($\square$), all others have $P_j = -1\mathrm{s}^{-1}$ ($\circ$). All edges have the same transmission capacity K. The color code shows K^{red} defined in (4.87) at the bifurcation $K = K_c$. (b) The second eigenvalue μ_2 of the matrix M, the phase difference $\theta_j - \theta_k$ and the load $\sin(\theta_j - \theta_k)$ for all edges as a function of the transmission capacity K. At the bifurcation exactly one edge (marked in panel (a)) is fully loaded, $\theta_j - \theta_k = \pi/2$. (c) The Fiedler vector v_2 at the bifurcation. (d) Dynamical instability after reducing the transmission capacity to $K = 0.98 \times K_c$. The color coding of the nodes is the same as in panel (c).

Corollary 4.6.2. *If $|\theta_i^* - \theta_j^*| \leq \pi/2$ holds for all edges (i, j), then whenever a fixed point undergoes a bifurcation, all connections between two components of the grid will become fully loaded.*

Proof. As shown in Corollary 4.6.1, if $|\theta_i^* - \theta_j^*| \leq \pi/2$ holds for all edges (i, j), then M is the Laplacian of the meta graph $\widetilde{G}$. It is shown in Corollary 4.A.1 that the multiplicity of the eigenvalue 0 in a graph's Laplacian equals the number of connected components of the graph [91, 92].

Theorem 4.3.1 tells us that any bifurcation of a fixed point will be accompanied by one more eigenvalue of the Hesse matrix M becoming 0, which implies $\widetilde{G}$ splitting into one more component. This is equivalent to all edges between the components becoming fully loaded:

$$|F_{ij}| = K_{ij} \quad \Longleftrightarrow \quad K_{ij}^{\mathrm{red}} = 0. \tag{4.91}$$

$\square$

An example for such a bifurcation is shown in Fig. 4.4 for a model grid based on the topology of the British high-voltage transmission grid [26]. The second eigenvalue μ_2 indicating dynamical stability is decreasing with decreasing transmission capacity K and vanishes at the bifurcation point $K = K_c$. At the bifurcation a single edge connecting the north of Scotland to the rest of the grid is fully loaded, $\theta_j - \theta_k = \pi/2$, such

that the meta-graph $\widetilde{G}$ gets disconnected. Physically speaking, the fixed point is lost because of transmission line overload.

When the fixed point is lost for $K < K_c$, the disconnected components lose synchrony with each other. The components may remain synchronous internally, as depicted in Fig. 4.4 (c), where the two components, colored green and red, diverge from each other with time, but the frequencies within each component remain close.

The two components are readily identified by the eigenvector $\boldsymbol{v_2}$ associated with μ_2, the so-called Fiedler vector [93, 52, 94]:

$$M\boldsymbol{v_2} = \mu_2 \boldsymbol{v_2}. \tag{4.92}$$

When $\widetilde{G}$ becomes disconnected at the bifurcation, the Fiedler vector is given by

$$\boldsymbol{v_2} = \frac{1}{\sqrt{N_1 + N_2}} \big(\underbrace{\sqrt{N_2/N_1}, \ldots}_{N_1 \text{ times}}, \underbrace{-\sqrt{N_1/N_2}, \ldots}_{N_2 \text{ times}} \big)^T, \tag{4.93}$$

assuming that the nodes are labeled such that the first component is given by $1, \ldots, N_1$ and the second by $N_1 + 1, \ldots, N_1 + N_2$. The Fiedler vector thus predicts the dynamics when stability is lost as shown in Fig. 4.4 (d).
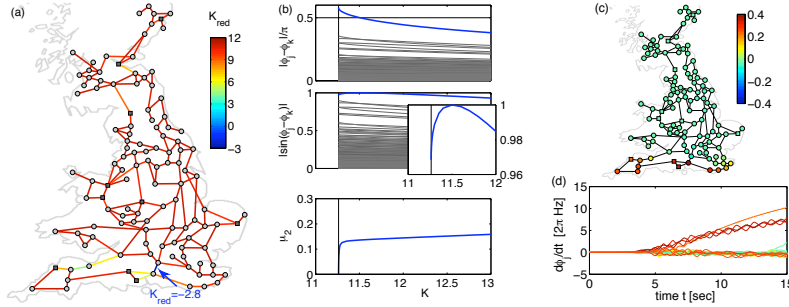
Figure 4.5: Bifurcation without overload. At the bifurcation the marked edge is operating "beyond" an overload. (a) Model network based on the topology of the British high-voltage transmission grid [90, 26]. Ten out of 120 nodes are randomly chosen to be generators with $P_j = +11\mathrm{s}^{-1}$ ($\square$), all others have $P_j = -1\mathrm{s}^{-1}$ ($\circ$). All edges have the same transmission capacity K. The color code shows K^{red} defined in (4.87) at the bifurcation $K = K_c$. (b) The second eigenvalue μ_2 of the matrix M, the phase difference $\phi_j - \phi_k$ and the load $\sin(\phi_j - \phi_k)$ for all edges as a function of the transmission capacity K. At the bifurcation one edge (marked by an arrow in panel (a)) is operating beyond overload $|\phi_j - \phi_k| > \pi/2$. (c) The Fiedler vector $\boldsymbol{v_2}$ at the bifurcation. (d) Dynamical instability after reducing the transmission capacity to $K = 0.98 \times K_c$. The color coding of the nodes is the same as in panel (c).

4.6.2   *Instability* without *overload*

A different scenario can occur when the condition $|\theta_i^* - \theta_j^*| \leq \pi/2$ is not satisfied for one or more edges. This is possible for a stable fixed point in complex networks at the edge of the stable parameter region. Then we can have $K_{jk}^{\text{red}} < 0$ such that the meta-graph is no longer a *non-negative* graph and the results discussed in the previous section do not apply.

In this case the bifurcation of a fixed point is generally *not* associated with any overload. In particular, the grid is already operating 'beyond' an overload at the bifurcation point. An example of such a bifurcation is shown in Fig. 4.5. The marked edge has a phase difference of $|\theta_j^* - \theta_k^*| > \pi/2$ such that $K_{jk}^{\text{red}} < 0$. The loss of stability is a collective effect of the entire grid and in particular there is no simple graph theoretical interpretation of the bifurcation. Consequently, the Fiedler vector defined in (4.92) only gives a limited insight into the desynchronization dynamics when the fixed point is lost.

4.6.3   *Relevance of bifurcation scenarios*

The two bifurcation scenarios regularly occur in networks with complex topologies. We have analyzed the bifurcation for 200 realizations of the model network based on the topology of the British power grid with random generator positions (see Fig. 4.6). We find that the loss of the steady state is caused by an isolated overload in approximately 40% of the sample networks while the grid is operating beyond overload in the remaining 60% of all cases.

We note that the loss of a steady state and the following desynchronization generally leads to a large-scale power outage (cf. [89, 56, 57]). In current power grids this can happen only in periods of extreme loads while the phase difference is generally much smaller than $\pi/2$ in periods of average load. However, extreme loads are expected to become much more likely in the future if the power grid is not sufficiently adapted to the energy transition to renewable sources [64].

The two examples shown in Fig. 4.4 and Fig. 4.5 capture the essential mathematical aspects of this bifurcation for two model networks. Hence they are of interest both for fundamental research and as a guideline for the the analysis of real-world power grids though being simplified. In the figures we have illustrated the system stability for two model networks as a function of the parameter K in the very tradition of the physics literature on oscillator models (cf. [1, 4, 2] and references therein). In real world grids, the connectivity K_{ij} is generally fixed while generation and load can change strongly. As an essential parameter affecting stability is the transported power P *relative to* the connectivity K_{ij}, we vary K_{ij} to study qualitative changes in the collective dynamics of the network.
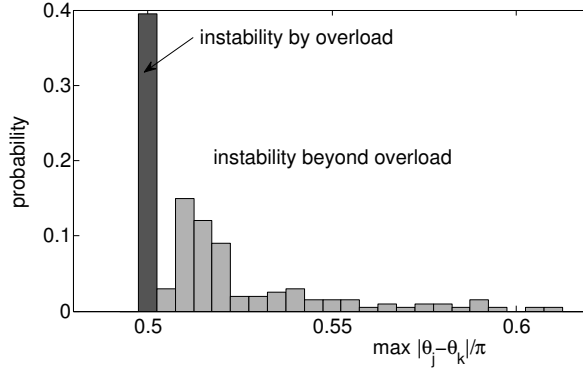
Figure 4.6: Statistical analysis of the different bifurcation scenarios based on an ensemble of 200 different model networks. Shown is a histogram of the maximum phase difference $\max_{\text{edges}(j,k)} |\theta_j - \theta_k|$ at the bifurcation point. In approximately 40% of all realizations the steady state is lost because of an isolated overload as shown in Fig. 4.4. In approximately 60% of all realizations the grid is operating beyond an overload at the bifurcation point, i.e. $|\theta_j - \theta_k| > \pi/2$ for at least one edge, as shown in Fig. 4.5. Results have been obtained for 200 realizations of the model network based on the topology of the British power grid with random generator positions.

4.6.4   *Braess' paradox*

We finally note that a variety of parameter changes can induce a bifurcation. Stability can be lost due to an increase of the power load or the damage of a transmission line, but surprisingly also by *increasing* the transmission capacity or even by putting a new line into operation. Fig. 4.7 shows an example of this effect called Braess' paradox [32]. A detailed discussion of Braess' paradox in supply networks is presented in [36, 37].

In this example (Fig. 4.7) the stable fixed point ceases to exist after a saddle node bifurcation when the capacity of the upper transmission line is increased to a critical value $\kappa > \kappa_c = 17.15$. Again, we find that the grid is no longer in normal operation in the vicinity of the bifurcation as the phase difference $\theta_5^* - \theta_4^*$ exceeds $\pi/2$ already for $\kappa > 15.2$. This constitutes a clear example that adding lines or improving line capacities may also induce instabilities without overloads via Braess' paradox [36, 37].

4.7   CONCLUSIONS AND DISCUSSION

How can supply networks become unstable? In simple systems where the loads are the only relevant variables, the answer is simple: instabilities emerge if and only if one or more elements overload, cf. also [95].

As we intended, we have demonstrated in this article how instability can also emerge in the absence of any overloads. We have explicated stability conditions for fixed points (steady operation) of oscillatory power grid models [19, 26, 71], where in addition to the pure flows, phase variables play a crucial role. We linked a Hamiltonian description to existence and bifurcation types of fixed points. In particular, we demonstrated that instabilities may emerge with and without transmission line overloads and that – through Braess' paradox [36, 37] – adding new lines may also create collective instabilities without line overloads.
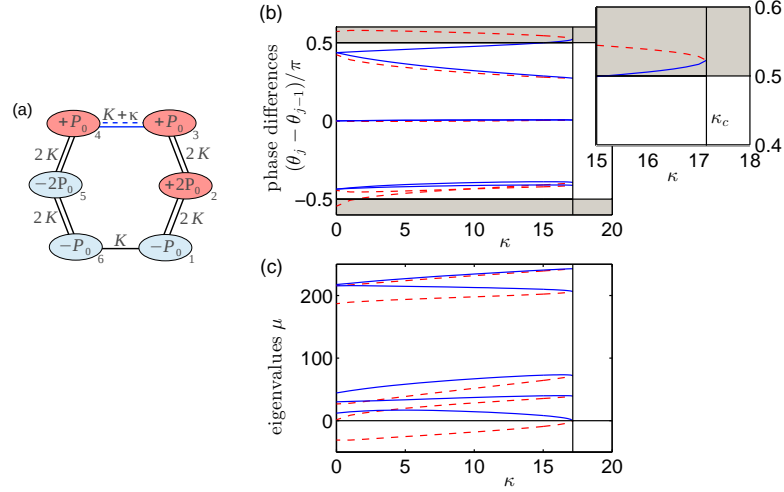
Figure 4.7: Loss of stability due to the *increase* of local transmission capacity in a circular network. A stable (—) and an unstable (− − −) fixed point vanish in a saddle-node bifurcation at the critical point $\kappa_c = 17.15$. The stable fixed point (blue) is lost. (a) Topology of the network. The capacity of the upper edge $(3,4)$ is increased by an amount κ. (b) Phase differences along the edges of the cycle. Close to the bifurcation, the phase difference $|\theta_5 - \theta_4|$ exceeds $\pi/2$ for the stable fixed point (see inset). (c) Eigenvalues of the Hesse matrix M, which yield the eigenvalues of the Jacobian via (4.62). Parameters are $K = 50$ and $P_0 = 49$.

Like the coupled phase oscillator model described here in the context of power grids, the function of many physical and biological supply networks depends on and involves quantities other than the network load. A notable example from biology is leaf vasculature and stomatal patchiness. Stomatal patchiness is the oscillatory dynamics of the opening and closing of patches of leaf stomata, which is believed to be the result of hydraulic and elastic coupling between neighbouring stomata. This dynamics can arise in a self organised manner in situations where a uniform stomatal aperture should be expected. Although recent progress has been made, stomatal patchiness is still not completely understood [96], especially in the context of the underlying hydraulic coupling of the stomata to the vascular system.

Similarly, the plant phloem is a dynamical transport system involving a number of interdependent quantities. The phloem vascular elements transfer sap (a sugar rich water solution) from and between the photosynthesising tissues to the rest of the plant. Sugars are being loaded in the phloem actively or passively at the sites of photosynthesis and the rate of sugar production and loading (determining the vascular network operation) can vary from site to site. The sugar concentration is a field of independent variables coupled to the network load (phloem fluid flow), and depending on the loading regime, the system has a potential of a rich dynamical behaviour [97, 98]. The plant phloem might thus constitute a biological candidate system where instabilities of normal supply function may emerge without overloads.

ACKNOWLEDGEMENT

APPENDIX

Definition 4.A.1. *Let G be a weighted graph with n nodes with all the edge weights $w_{ij} \geq 0$. The Laplacian M is an $N \times N$ matrix given by:*

$$M_{ij} = -w_{ij} + \delta_{ij} \sum_{k=1}^{N} w_{ik} \tag{4.94}$$

Theorem 4.A.1. *In a fully connected graph G, the Laplacian L has exactly one zero eigenvalue.*

Proof. The Laplacian M obviously has one zero eigenvalue: the corresponding eigenvector being $\boldsymbol{v_0} = (1, 1, \cdots, 1)$:

$$
\begin{aligned}
(M\boldsymbol{v_0})_i &= \sum_j M_{ij} v_{0j} \\
&= \sum_j M_{ij} \\
&= \sum_j \left[\sum_k \delta_{ij} w_{ik} - w_{ij} \right] \\
&= 0
\end{aligned}
\tag{4.95}
$$

Suppose there is another eigenvector $\boldsymbol{v}'$ with eigenvalue 0. Then:

$$
\begin{aligned}
0 &= \boldsymbol{v'}^T M \boldsymbol{v'} \\
&= \sum_{ij} v_i' M_{ij} v_j' \\
&= \sum_{ij} v_i' \left(\sum_k \delta_{ij} w_{ik} - w_{ij} \right) v_j' \\
&= \sum_j \left(\sum_k w_{jk} \right) v_j'^2 - \sum_{ij} w_{ij} v_i' v_j' \\
&= \sum_{i<j} \left[\sqrt{w_{ij}} \left(v_i' - v_j' \right) \right]^2
\end{aligned}
\tag{4.96}
$$

Therefore it follows that $\sqrt{w_{ij}}(v_i' - v_j') = 0$ for all $i, j \in Z_N$. This implies whenever two nodes are connected by an edge ($w_{ij} \neq 0$), $v_i = v_j$. Now, by virtue of G being connected, $v_i' = v_j'$ must hold for all (i, j). But that implies $\boldsymbol{v}' = \boldsymbol{v_0}$, up to a multiplicative constant. $\square$

Corollary 4.A.1. *The multiplicity of 0 eigenvalue in the Laplacian of a graph equals its number of connected components.*

Proof. For a graph with c connected components, if the node indices are chosen properly, the Laplacian L will be in a block diagonal form with c blocks. Then following the same reasoning as in Theorem 4.A.1, the result follows. □

REFERENCES

[1] Y. Kuramoto. "Self-entrainment of a population of coupled non-linear oscillators." In: *International Symposium on on Mathematical Problems in Theoretical Physics.* Ed. by H. Araki. Lecture Notes in Physics Vol. 39. New York: Springer, 1975, p. 420.

[2] Juan A Acebrón et al. "The Kuramoto model: A simple paradigm for synchronization phenomena." In: *Reviews of modern physics* 77.1 (2005), p. 137.

[4] Steven H. Strogatz. "From Kuramoto to Crawford: Exploring the onset of synchronization in populations of coupled oscillators." In: *Physica D: Nonlinear Phenomena* 143 (2000), p. 1.

[19] Giovanni Filatrella, Arne Hejde Nielsen, and Niels Falsig Pedersen. "Analysis of a power grid using a Kuramoto-like model." In: *The European Physical Journal B - Condensed Matter and Complex Systems* 61.4 (2008), pp. 485–491.

[26] Martin Rohden et al. "Self-organized synchronization in decentralized power grids." In: *Physical review letters* 109.6 (2012), p. 064101.

[32] Dietrich Braess. "Über ein Paradoxon aus der Verkehrsplanung." In: *Unternehmensforschung* 12.1 (1968), pp. 258–268.

[36] Dirk Witthaut and Marc Timme. "Braess's paradox in oscillator networks, desynchronization and power outage." In: *New journal of physics* 14.8 (2012), p. 083036.

[37] Dirk Witthaut and Marc Timme. "Nonlocal failures in complex supply networks by single link additions." In: *The European Physical Journal B* 86.9 (2013), p. 377.

[49] Florian Dörfler, Michael Chertkov, and Francesco Bullo. "Synchronization in complex oscillator networks and smart grids." In: *Proceedings of the National Academy of Sciences* 110.6 (2013), pp. 2005–2010.

[52] M. E. J. Newman. *Networks – An introduction.* Oxford: Oxford University Press, 2010. ISBN: 978-0-19-920665-0.

[56] U.S.-Canada Power System Outage Task Force. https://reports.energy.gov/BlackoutFinal-Web.pdf. 2004.

[57] Union for the Coordination of Transmission of Electricity. *Final report on the system disturbance on 4 November 2006*. `http://www.entsoe.eu/~library/publications/ce/otherreports/Final-Report-20070130.pdf`. 2007.

[62] Emma Marris. "Energy: Upgrading the grid." In: *Nature News* 454.7204 (2008), pp. 570–573.

[63] John A Turner. "A realizable renewable energy future." In: *Science* 285.5428 (1999), pp. 687–689.

[64] Thiemo Pesch, H-J Allelein, and J-F Hake. "Impacts of the transformation of the German energy system on the transmission grid." In: *The European Physical Journal Special Topics* 223.12 (2014), pp. 2561–2575.

[65] Dominik Heide et al. "Seasonal optimal mix of wind and solar power in a future, highly renewable Europe." In: *Renewable Energy* 35.11 (2010), pp. 2483–2489.

[66] Frank Böttcher, Joachim Peinke, et al. "Small and large scale fluctuations in atmospheric wind speeds." In: *Stochastic environmental research and risk assessment* 21.3 (2007), pp. 299–308.

[67] Patrick Milan, Matthias Wächter, and Joachim Peinke. "Turbulent character of wind energy." In: *Physical review letters* 110.13 (2013), p. 138701.

[68] Arthur R Bergen and David J Hill. "A structure preserving model for power system stability analysis." In: *IEEE Transactions on Power Apparatus and Systems* 1 (1981), pp. 25–35.

[69] David J Hill and Guanrong Chen. "Power systems as dynamic networks." In: *Circuits and Systems, 2006. ISCAS 2006. Proceedings. 2006 IEEE International Symposium on*. IEEE. 2006, 4–pp.

[70] Jan Machowski, Janusz W Bialek, and James Richard Bumby. *Power system dynamics, stability and control*. New York: John Wiley & Sons, 2008.

[71] Martin Rohden et al. "Impact of network topology on synchrony of oscillatory power grids." In: *Chaos: An Interdisciplinary Journal of Nonlinear Science* 24.1 (2014), p. 013123.

[72] Adilson E Motter et al. "Spontaneous synchrony in power-grid networks." In: *Nature Physics* 9.3 (2013), pp. 191–197.

[73] Peter J Menck et al. "How dead ends undermine power grid stability." In: *Nature communications* 5 (2014).

[74] Prabha Kundur, Neal J Balu, and Mark G Lauby. *Power system stability and control*. Vol. 7. McGraw-hill New York, 1994.

[75] Yoshihiko Susuki, Igor Mezic, and Takashi Hikihara. "Global swing instability of multimachine power systems." In: *Decision and Control, 2008. CDC 2008. 47th IEEE Conference on*. IEEE. 2008, pp. 2487–2492.

[76] Yoshihiko Susuki, Igor Mezić, and Takashi Hikihara. "Coherent swing instability of power grids." In: *Journal of nonlinear science* 21.3 (2011), pp. 403–439.

[77] Florian Dorfler and Francesco Bullo. "Kron reduction of graphs with applications to electrical networks." In: *IEEE Transactions on Circuits and Systems I: Regular Papers* 60.1 (2013), pp. 150–163.

[78] Katrin Schmietendorf et al. "Self-organized synchronization and voltage stability in networks of synchronous machines." In: *The European Physical Journal Special Topics* 223.12 (2014), pp. 2577–2592.

[79] Hsiao-Dong Chiang, Felix Wu, and P Varaiya. "Foundations of direct methods for power system transient stability analysis." In: *IEEE Transactions on Circuits and systems* 34.2 (1987), pp. 160–173.

[80] CJ Perez and F Ritort. "A moment-based approach to the dynamical solution of the Kuramoto model." In: *Journal of Physics A: Mathematical and General* 30.23 (1997), p. 8095.

[81] James Howard. "Stability of Hamiltonian equilibria." In: *Scholarpedia* 8 (2013), p. 3627. DOI: 10.4249/scholarpedia.3627.

[82] Hassan K Khalil and JW Grizzle. *Nonlinear systems*. Vol. 3. Prentice hall Upper Saddle River, 2002.

[83] M Levi, Frank C Hoppensteadt, and WL Miranker. "Dynamics of the Josephson junction." In: *Quarterly of Applied Mathematics* 36.2 (1978), pp. 167–198.

[84] Hannes Risken. *Fokker-planck equation*. Springer, 1996, pp. 63–95.

[85] Peter J Menck et al. "How basin stability complements the linear-stability paradigm." In: *Nature Physics* 9.2 (2013), pp. 89–92.

[86] Yuri A Kuznetsov. *Elements of applied bifurcation theory*. Vol. 112. Springer Science & Business Media, 2013.

[87] Patrick C Parks. "AM Lyapunov's stability theory - 100 years on." In: *IMA journal of Mathematical Control and Information* 9.4 (1992), pp. 275–303.

[88] Union for the Coordination of Transmission of Electricity. *Continental Europe Operation Handbook*. https://www.entsoe.eu/publications/system-operations-reports/operation-handbook/Pages/default.aspx. 2014.

[89]   Peter Fairley. "The unruly power grid." In: *IEEE Spectrum* 41.8 (2004), pp. 22–27.

[90]   Ingve Simonsen et al. "Transient dynamics increasing network vulnerability to cascading failures." In: *Physical review letters* 100.21 (2008), p. 218701.

[91]   William N Anderson Jr and Thomas D Morley. "Eigenvalues of the Laplacian of a graph." In: *Linear and multilinear algebra* 18.2 (1985), pp. 141–145.

[92]   Bojan Mohar et al. "The Laplacian spectrum of graphs." In: *Graph theory, combinatorics, and applications* 2.871-898 (1991), p. 12.

[93]   Miroslav Fiedler. "Algebraic connectivity of graphs." In: *Czechoslovak mathematical journal* 23.2 (1973), pp. 298–305.

[94]   Santo Fortunato. "Community detection in graphs." In: *Physics reports* 486.3 (2010), pp. 75–174.

[95]   Surya D Pathak et al. "Complexity and adaptivity in supply networks: Building supply network theory using a complex adaptive systems perspective." In: *Decision sciences* 38.4 (2007), pp. 547–580.

[96]   Antônio MT Ramos and Carmen PC Prado. "Role of hysteresis in stomatal aperture dynamics." In: *Physical Review E* 87.1 (2013), p. 012719.

[97]   Kåre Hartvig Jensen et al. "Optimality of the Münch mechanism for translocation of sugars in plants." In: *Journal of the Royal Society Interface* 8.61 (2011), pp. 1155–1165.

[98]   JW Patrick. "Phloem unloading: sieve element unloading and post-sieve element transport." In: *Annual review of plant biology* 48.1 (1997), pp. 191–222.

Debsankha Manik[1], Marc Timme[1,2,3], Dirk Witthaut[4,5]

[1] Network Dynamics, Max Planck Institute for Dynamics and Self-Organization (MPI DS), D-37077 Göttingen, Germany

[2] Chair for Network Dynamics, Institute for Theoretical Physics and Center for Advancing Electronics Dresden (cfaed), Technical University of Dresden, 01069 Dresden, Germany

[3] Department of Physics, Technical University Darmstadt, 64289 Darmstadt, Germany

[4] Forschungszentrum Jülich, Institute for Energy and Climate Research – Systems Analysis and Technology Evaluation (IEK-STE), 52425 Jülich, Germany

[5] Institute for Theoretical Physics, University of Cologne, 50937 Köln, Germany

Original contribution:
I carried out most of the analytical calculations behind the results. I performed the numerical computations for Sec V, and contributed all results for Sec II, III, V.C–V.F. I wrote most of the text sections, including Discussion and Conclusion. I revised manuscript during revision process, updating texts and figures as per referee reports.

Cycle flows and multistability in oscillatory networks

Debsankha Manik,[1] Marc Timme,[1,2,3] and Dirk Witthaut[4,5]

[1]*Network Dynamics, Max Planck Institute for Dynamics and Self-Organization (MPIDS), 37077 Göttingen, Germany*
[2]*Chair for Network Dynamics, Institute for Theoretical Physics and Center for Advancing Electronics Dresden (cfaed), Technical University of Dresden, 01069 Dresden, Germany*
[3]*Department of Physics, Technical University Darmstadt, 64289 Darmstadt, Germany*
[4]*Forschungszentrum Jülich, Institute for Energy and Climate Research - Systems Analysis and Technology Evaluation (IEK-STE), 52425 Jülich, Germany*
[5]*Institute for Theoretical Physics, University of Cologne, 50937 Köln, Germany*

We study multistability in phase locked states in networks of phase oscillators under both Kuramoto dynamics and swing equation dynamics—a popular model for studying coarse-scale dynamics of an electrical AC power grid. We first establish the existence of geometrically frustrated states in such systems—where although a steady state flow pattern exists, no fixed point exists in the dynamical variables of phases due to geometrical constraints. We then describe the stable fixed points of the system with phase differences along each edge not exceeding $\pi/2$ in terms of cycle flows—constant flows along each simple cycle—as opposed to phase angles or flows. The cycle flow formalism allows us to compute tight upper and lower bounds to the number of fixed points in ring networks. We show that long elementary cycles, strong edge weights, and spatially homogeneous distribution of natural frequencies (for the Kuramoto model) or power injections (for the oscillator model for power grids) cause such networks to have more fixed points. We generalize some of these bounds to arbitrary planar topologies and derive scaling relations in the limit of large capacity and large cycle lengths, which we show to be quite accurate by numerical computation. Finally, we present an algorithm to compute all phase locked states—both stable and unstable—for planar networks. © 2017 Author(s). All article content, except where otherwise noted, is licensed under a Creative Commons Attribution (CC BY) license (http://creativecommons.org/licenses/by/4.0/). [http://dx.doi.org/10.1063/1.4994177]

The functions of many networked systems in physics, biology, or engineering rely on a coordinated or synchronized dynamics of their constituents. In power grids for example, all generators must run at the *same frequency* and their phases need to lock to guarantee a steady power flow. Here, we analyze the existence and multitude of states exhibiting this phase locking behaviour. Focusing on edge and cycle flows instead of the nodal phases, we derive rigorous results on the existence and number of such states. Generally, multiple phase-locked states coexist in networks with edges capable of carrying high flows, long elementary cycles, and a homogeneous spatial distribution of natural frequencies or power injections. Utilizing concepts from the graph theory, we derive scaling relations for the number of such states in plane embedded networks. We also offer an algorithm to systematically compute all phase-locked states, both stable and unstable.

I. FROM KURAMOTO OSCILLATORS TO POWER GRIDS

Coupled oscillator models are ubiquitous in science and technology, describing the collective dynamics of various systems on micro- to macro-scale. Research on coupled oscillators dates back to Christian Huygens, who noticed that two clocks synchronize when they are coupled.[1] One of the most important mathematical models was introduced by Kuramoto[2,3] and successfully applied to describe the collective dynamics of coupled Josephson junctions,[4] neuronal networks,[5] chemical oscillators,[6] and a variety of other synchronization phenomena.[7–10]

That model[3] describes the dynamics of N coupled limit cycle oscillators. The equations of motions for the phases θ_j, $j \in \{1, \ldots, N\}$ are given by

$$\frac{d}{dt}\theta_j = \omega_j + \sum_{\ell=1}^{N} K_{j,\ell} \sin\left(\theta_\ell - \theta_j\right). \tag{1}$$

The coupling matrix is assumed to be symmetric, $K_{j,\ell} = K_{\ell,j}$, and ω_j are the natural frequencies of the oscillators. Throughout this article, we consider systems where all $K_{j,\ell} \geq 0$, i.e., the units attract each other and do not repel.

A similar model of second-order oscillators describes the collective phenomena of animal flocks[11,12] or human crowds[13] as well as the coarse-scale dynamics of power grids.[14–20]

For power grids, for instance, the units j describe synchronous machines, generators, or motors, whose state is completely described by their phase θ_j and the phase velocity $\dot{\theta}_j$ relative to the reference frequency of the grid, typically rotating at 50 Hz or 60 Hz. The acceleration (deceleration) of the machines is proportional to the sum of the mechanical power P_j generated (consumed) by the machine including

damping and electric power exchanged with the grid. The detailed equations of motion are given by

$$M_j \frac{d^2}{dt^2}\theta_j + D_j \frac{d}{dt}\theta_j = P_j + \sum_\ell K_{j,\ell}\sin\left(\theta_\ell - \theta_j\right), \quad (2)$$

where M_j is an inertia term and D_j a damping constant. The coupling constants $K_{j,\ell} = U^2 B_{j,\ell}$ are determined by the voltage U of the grid, which is assumed to be constant, and the admittance $B_{j,\ell}$ of the electrical transmission line joining node j and node ℓ. The flow of electric real power from node ℓ to node j is

$$F_{j,\ell} = K_{j,\ell}\sin(\theta_\ell - \theta_j) = K_{j,\ell}S_{j,\ell}. \quad (3)$$

It is useful to describe the interaction topology of the system as a weighted graph $G(V, E)$, whose vertex set V is identical to the set of oscillators and edge set E is given by the set of all inter-oscillator coupling pairs, i.e., all pairs with $K_{\ell,j} > 0$. We use the term network[21] (rather than the term graph) for the entire system with given natural frequencies ω_j or the powers P_j.

Here, we distinguish two types of synchronization in oscillator networks. Traditionally, the emergence of partial synchrony has received the most interest of the physics community.[2,3,7,8] In his seminal work, Kuramoto investigated a set of oscillators with global coupling, $K_{j,\ell} = K/N$, and natural frequencies drawn at random from a unimodal symmetric distribution $g(\omega)$. If the coupling constant K exceeds a critical value K_c, a fraction of the oscillators start to synchronize in the sense that they rotate at the same angular velocity although their natural frequencies differ. In this state of *partial frequency locking*, commonly referred to in the Kuramoto oscillator literature as "partial synchrony,"[8] the phases of parts of the oscillators are ordered, but they are not strictly phase-locked, such that the phase difference of two synchronized oscillators $(\theta_j - \theta_\ell)$ is generally small but not constant.

In this article, we analyze the properties of *globally phase-locked states*, where all oscillators synchronize and the phase differences $(\theta_j - \theta_\ell)$ are constant for all pairs (j, ℓ). These states are especially important for power grids, as they describe the regular synchronous operation of the grid.[14–18] If this state is lost due to local outages or accidents, the grid will fragment into asynchronous islands which can no longer exchange electric energy.[22] For instance, the European power grid fragmented into three asynchronous areas on November 4th 2006 after the shutdown of one transmission line in Northern Germany. As a result, southwestern Europe suffered an under-supply on the order of 10 GW and approximately 10 million households were disconnected.[23]

Without loss of generality, we take $\sum_j \omega_j = 0$ or $\sum_j P_j = 0$, respectively, by invoking a transformation to a co-rotating frame of reference. The globally phase-locked states are then the *fixed points* of the system. For both the Kuramoto model and the power grid model, these states are given by the solutions of the transcendental equations

$$P_j + \sum_{\ell=1}^{N} K_{j,\ell}\sin\left(\theta_\ell - \theta_j\right) = 0 \quad \text{for all } j \in \{1, ..., N\}, \quad (4)$$

replacing P_j by ω_j for the Kuramoto model. In the following, we analyze the influence of the network topology given by the coupling matrix $K_{j,\ell}$ on the existence of a fixed point. All results below hold for both models; nevertheless, our intuition heavily relies on the interpretation of $F_{j,\ell} = K_{j,\ell}\sin\left(\theta_\ell - \theta_j\right)$ as a flow which is inspired from the power grid model. The results can be generalized to arbitrary coupling functions f instead of the sine (see, e.g., Refs. 24 and 25). In the following, we mostly restrict ourselves to the common sine coupling for the sake of clarity.

We note that the second order power grid model (2) evidently describes a different system from the first order Kuramoto model (1). Nevertheless, there are deep underlying connections between these two. In the context of power grids, in the overdamped limit, one recovers the first order Kuramoto model. The relation of first and second order models in the context of coupled Josephson Junctions was discussed in detail in Refs. 26 and 27. Partial synchronization in first and second order models was reviewed in Ref. 28.

II. THE NATURE AND BIFURCATIONS OF FIXED POINTS

Both the Kuramoto system and the oscillator model of power grids share the same set of fixed points (4). It has been shown that the similarity between these two systems runs deeper, namely, the linear stability properties of those fixed points are identical.[29,30] In this section, we briefly review some basic results on the stability of the fixed points.

We analyze the dynamical stability of a certain fixed point $\boldsymbol{\theta}^* = (\theta_1^*, ..., \theta_N^*)$ by defining the potential function

$$V(\theta_1, \theta_2, ..., \theta_N) = -\sum_j P_j \theta_j - \frac{1}{2}\sum_{i,j} K_{ij}\cos\left(\theta_i - \theta_j\right). \quad (5)$$

The fixed points correspond to the local extrema of this potential, where $\frac{\partial V}{\partial \theta_j} = 0$ for all j. A fixed point $\boldsymbol{\theta}^*$ is asymptotically stable if the Hesse matrix H of the potential function

$$H(\boldsymbol{\theta}^*) = \begin{pmatrix} \sum_\ell K_{1,\ell}^{\text{red}} & -K_{1,2}^{\text{red}} & \cdots \\ -K_{2,1}^{\text{red}} & \sum_l K_{2,\ell}^{\text{red}} & \cdots \\ \vdots & \vdots & \ddots \end{pmatrix} \quad (6)$$

with the residual capacity

$$K_{j,\ell}^{\text{red}} = K_{j,\ell}\cos(\theta_j^* - \theta_\ell^*) \quad (7)$$

has positive eigenvalues only. It is worth noting that H has one eigenvector $\boldsymbol{v}_1 = (1, 1, ..., 1)$ with eigenvalue $\mu_1 = 0$ because any fixed point $\boldsymbol{\theta}^*$ is arbitrary up to an additive constant c. As such a global phase shift does not affect the locking of the phases, we can discard it in the following and concentrate on the stability transversely to the solution space $\{\boldsymbol{\theta}^* + c(1, 1, ..., 1)|c \in \mathbb{R}\}$.

Lemma 1. Let the eigenvalues of H be ordered such that $\mu_1 = 0$ and $\mu_2 \leq \cdots \leq \mu_N$. If for a given network topology and a given fixed point,

$$\mu_k > 0, \quad \text{for all } k \in \{2, 3, ..., N\}, \qquad (8)$$

then this fixed point is transversally asymptotically stable for both the Kuramoto system and the power grid model system. If one of the $\mu_k < 0$, then the dynamical system is linearly unstable (this lemma and its proof have been presented in Ref. 29).

Using some results from the bifurcation theory, it has been shown in Ref. 29 that a stable fixed point can only be lost by an inverse saddle-node bifurcation when one of the eigenvalues becomes zero, $\mu_2 = 0$. At this point, linear stability analysis is not sufficient to predict the stability of the fixed point, but it is expected that the fixed point is unstable.[31]

More insights into the loss of a fixed point when the phase differences across all edges in the network are sufficiently small can be gained:

Corollary 1. Consider a connected network. It is sufficient (but not necessary) for a fixed point $\boldsymbol{\theta}^*$ to be transversally asymptotically stable; if the condition

$$\cos(\theta_i^* - \theta_j^*) > 0 \qquad (9)$$

holds for all edges (i, j) in the network, then the network is said to be in "normal operation."

Proof. To this end, we first define a metagraph as follows.

Definition 1 (Metagraph). *Given a graph $G(V, E)$ and a set of flows F_{uv} across each edge $e(u, v)$, its metagraph $\tilde{G}$ is an undirected graph with vertex set V and edge set E' defined as follows. For all edges $e(u, v) \in E$, with weight K_{uv}, $\exists$, an edge $e(u, v) \in E'$ with weight $K_{uv}^{\text{red}} = \sqrt{K_{uv}^2 - F_{uv}^2}$, as per (7).*

Then, the matrix H as defined in (6) is seen to be the Laplacian matrix of the metagraph $\tilde{G}$. The eigenvalues of a Laplacian of a connected undirected graph with positive edge weights are always non-negative[21] such that we obtain the result. $\square$

We note that this sufficient condition for stability has been shown in Ref. 32 using the Gershgorin circle theorem.

During normal operation, an eigenvalue of the Hesse matrix H, as defined in (6), can become 0 only when $\tilde{G}$ disconnects into two (or more) components. Such a split-up occurs only when $K_{j,\ell}^{\text{red}} = 0$ for all the transmission lines connecting two certain parts (denoted by G_1 and G_2) of the network, meaning that these lines are completely saturated

$$\sin(\theta_j^* - \theta_\ell^*) = \pm 1 \quad \Rightarrow \quad |F_{j,\ell}| = K_{j,\ell}$$
$$\text{for all } (j, \ell) \in E, j \in G_1, \ell \in G_2. \qquad (10)$$

Another scenario for the loss of stability is that one or more transmission lines leave normal operation. Then, the edge weights become effectively negative, such that a simple graph-theoretic interpretation of the bifurcation is no longer possible.[29,58]

III. CYCLE FLOWS AND GEOMETRIC FRUSTRATION

A. Flow conservation and the dynamics condition

It is instructive to divide the defining equation (4) of a fixed point into two parts. First, every fixed point has to satisfy a dynamic condition which is nothing but the conservation of the flow at every node of the network

$$P_j + \sum_{\ell=1}^N K_{j,\ell} S_{j,\ell} = 0 \quad \text{for all } j \in \{1, ..., N\}, \qquad (11a)$$

$$|S_{j,\ell}| \leq 1 \quad \text{for all edges } (j, \ell). \qquad (11b)$$

Here, $\sum_\ell K_{j,\ell} S_{j,\ell}$ is the sum of all flows from the neighboring nodes to the node j, while P_j is a source or sink term. The second part of this condition reflects the fact that the transmission capacity of each link is bound, such that the magnitude of the flow $|F_{j,\ell}|$ cannot exceed the capacity $K_{j,\ell}$. The dynamic condition (11) holds for all flow networks also including DC networks (i.e., Kirchhoff's rules) and biological network models.[33,34]

To obtain a better understanding of the possible solutions, we slightly rephrase the dynamic condition (11). In particular, we label all the L edges in the network with $e \in \{1, ..., L\}$. As the flows are directed, we have to keep track of the ordering of the vertices connected by the edge e. That is, each e corresponds to a directed link (j, ℓ) in the following. The ordering is arbitrary but must be kept fixed. Then, we write $S_e = S_{j,\ell}$ and $F_e = F_{j,\ell}$ for the flow over a link $e \hat{=} (j, \ell)$. Furthermore, we define the unweighted edge incidence matrix $I \in \mathbb{R}^{N \times L}$ (Ref. 21) via

$$I_{j,e} = \begin{cases} +1 & \text{if node } j \text{ is the head of edge } e \hat{=} (j, \ell), \\ -1 & \text{if node } j \text{ is the tail of edge } e \hat{=} (j, \ell), \\ 0 & \text{otherwise}, \end{cases} \qquad (12)$$

and the weighted edge incidence matrix $\tilde{K} \in \mathbb{R}^{N \times L}$ with the components $\tilde{K}_{je} = K_e I_{je}$.

The dynamic condition (11) then reads

$$P_j + \sum_{e=1}^L I_{j,e} F_e = 0 \quad \text{for all } j = 1, ..., N, \qquad (13a)$$

$$|F_e| \leq K_e \quad \text{for all } e = 1, ..., L \qquad (13b)$$

in terms of the flows or

$$P_j + \sum_{e=1}^L \tilde{K}_{j,e} S_e = 0 \quad \text{for all } j = 1, ..., N, \qquad (14a)$$

$$|S_e| \leq 1 \quad \text{for all } e = 1, ..., L \qquad (14b)$$

in terms of the sine factors. Here, $\boldsymbol{F} = (F_1, ..., F_L)^T$ and $\boldsymbol{S} = (S_1, ..., S_L)^T$ are vectors in $\mathbb{R}^L$. The matrix $\tilde{K}$ has N rows, but its rank is only $(N - 1)$. This is due to the fact that the sum of all rows is zero as $\sum_j \tilde{K}_{j,e} = 0$ since each edge has exactly one head and one tail. Hence, the solutions of the linear set of Eq. (14a) span an affine subspace of $\mathbb{R}^L$ whose dimension is $(L - N + 1)$. This statement will later be

rigorously proved in Lemma 2. In many important applications, L is much larger than the number of nodes N, such that we have a high dimensional submanifold $\mathbb{B}$ of $\mathbb{R}^L$ with every $S \in \mathbb{B}$ being a solution of (14) and hence a candidate for a fixed point of (1) and (2). However, the set of solutions of the dynamical equations can also be empty if the capacities $K_{j,\ell}$ are too small. In fact, the condition (14b) defines a bound convex polytope in $\mathbb{R}^L$. The solution of the full dynamical conditions (14) is given by the intersection of this polytope and the $(L - N + 1)$ dimensional affine subspace.

We can further characterize the solution of the dynamic conditions by establishing that the homogeneous solutions of the system (14a) are just the *cycle flows* which do not affect flow conservation. As the number of fundamental cycles in a network is $(L - N + 1)$, the dimension of the solution space is also given by $(L - N + 1)$. The derivation of these results is as follows.

Definition 2 (*Simple cycle*). *Given an undirected graph $G(V, E)$, a closed path $c = (v_1, v_2, ..., v_l, v_1)$ where no vertex apart from v_1 occurs twice is called a simple cycle (Ref. 36, p. 21).*

Definition 3 (*Cycle basis*). *Given a connected graph $G(V, E)$ with L edges and N vertices, the set of all simple cycles $\mathfrak{C}$ forms a vector space over the two element field $GF(2) = \{0, 1\}$, with the set symmetric difference being the addition operator. This vector space has dimension $L - N + 1$. A basis B_C of this vector space is called a **cycle basis** of the graph G.*

Definition 4 (*Signed characteristic vector of a cycle*). *An arbitrary assignment of a direction to each edge of an undirected graph G, which results in a directed graph, is called an orientation G^σ.[36] Given a graph G with L edges and N vertices and one such orientation, there exists an injective mapping from the set $\mathfrak{C}$ of all simple cycles of G to $\mathbb{R}^L$ as follows:*

$$\mathfrak{C} \to \mathbb{R}^L,$$
$$c \mapsto z^c,$$
$$z_e^c = \begin{cases} 0, & \text{if } e \text{ is not in } c, \\ 1, & \text{if } e = (v_i, v_{i+1}) \text{ and } v_{i+1} \text{ is the head of } e, \\ -1, & \text{if } e = (v_i, v_{i+1}) \text{ and } v_{i+1} \text{ is the tail of } e. \end{cases}$$

z^c *is called the signed characteristic vector of each cycle.*

Now, we show that any fixed point of the system can be uniquely specified by a *cycle flow* along each cycle belonging to a cycle basis of the underlying graph, along with an arbitrary solution of (13).

Definition 5 (*Cycle flow*). *Given a simple cycle $c = (v_1, v_2, ..., v_l, v_1)$ belonging to an undirected graph $G(V, E)$, a flow F is called a cycle flow if*

$$F_{j,k} = \begin{cases} f_c & \text{if } (j,k) \in \{(v_1, v_2), (v_2, v_3), ..., (v_{l-1}, v_l), (v_l, v_1)\}, \\ 0 & \text{otherwise,} \end{cases}$$
$$(15)$$

i.e., it is a constant nonzero flow along the cycle.

Lemma 2. *Let $\mathbb{S}_G$ be the set of all fixed points of a network G satisfying the normal operation criteria (9). Then,*

there exists a one-to-one function $f_c : \mathbb{S}_G \mapsto \mathbb{R}^{L-N+1}$ that maps each fixed point to a cycle flow vector.

Proof. Let $\boldsymbol{\theta}^{(0)}$ be one (arbitrarily chosen) fixed point. Let $\boldsymbol{\theta}$ be another. Then, we construct the mapping f_c by proving that the flows for these two fixed point differ only by *cycle flows* along each cycle.

Let $\boldsymbol{F}^{(0)} = (F_{e_1}^{(0)}, F_{e_2}^{(0)}, ..., F_{e_L}^{(0)})$ and $\boldsymbol{F} = (Fe_1, Fe_2, ..., Fe_L)$ be the flows for the fixed points $\boldsymbol{\theta}^{(0)}$ and $\boldsymbol{\theta}$, respectively. Then,

$$\boldsymbol{F} - \boldsymbol{F}^{(0)} = \sum_{c \in B_C} f_c z^c, \qquad (16)$$

due to the result from the graph theory that the flow space of an oriented graph G^σ is spanned by the signed characteristic vectors (Definition 4) of its cycles (Ref. 37, p. 311). Since by definition the cycles in B_C form a basis of the cycle space, the coefficients f_c are guaranteed to be unique. This concludes the proof. $\square$

We note that this mapping between fixed points and cycle flows has previously been presented in slightly different ways in Refs. 18 (supplementary material) and 38.

B. The winding number and the geometric condition

In addition to the dynamic condition, there is a geometric condition for the existence of a fixed point: a fixed point exists if the flows $F_{j,\ell} = K_{j,\ell}S_{j,\ell}$ satisfy the dynamic condition (14) *and if*

$$\text{for all edges } (\ell, j): \ \exists (\theta_1, ..., \theta_N) \ \text{ such that } S_{j,\ell} = \sin(\theta_\ell - \theta_j).$$
$$(17)$$

We now rephrase this condition in a more instructive way. To this end, we assume that we have already obtained a solution of the dynamic condition (14). Then, we can try to successively assign a phase θ_j to every node j in the network. Starting at a node j_0 with an arbitrary phase θ_{j_0}, we assign the phases of all neighboring nodes j_1 such that $\sin(\theta_{j_1} - \theta_{j_0}) = S_{j_0,j_1}$. We then proceed in this way through the complete network to assign the phase of an arbitrary node j_n,

$$\theta_{j_n} = \theta_{j_0} + \sum_{s=0}^{n-1} \Delta_{j_s, j_{s+1}}, \qquad (18)$$

where $(j_0, j_1, ..., j_n)$ is an arbitrary *path* from j_0 to j_n and we have used a solution of the equation

$$S_{j,\ell} = \sin(\Delta_{j,\ell}) \qquad (19)$$

for every edge (j, ℓ).

In general, a given node j_n can be reached from j_0 via a multitude of different paths. To define a unique set of phases that satisfy the geometric condition (17), we must ensure that Eq. (18) yields a unique phase regardless of which path is taken from j_0 to j_n. This is equivalent to the condition that the phase differences over every *simple cycle* (as defined in Definition 2) in the network must add up to an integer multiple of 2π.

$$\sum_{(j,\ell)\in \text{cycle } c} \Delta_{j,\ell} = 2m\pi, \quad \text{for some } m \in \mathbb{Z}, \qquad (20)$$

where $\Delta_{j,\ell}$ is a solution of Eq. (19). Furthermore, it is sufficient if (20) is satisfied by the cycles in the cycle basis of the network defined in Definition 3: it will then automatically be satisfied for all simple cycles of the network since the simple cycles form a vector space.

However, there are two distinct solutions

$$\Delta_{j,\ell}^+ = \arcsin(S_{j,\ell}), \qquad (21a)$$

$$\Delta_{j,\ell}^- = \pi - \arcsin(S_{j,\ell}) \qquad (21b)$$

of Eq. (19) which satisfy $\Delta_{j,l}^{\pm} \in [-\pi, \pi)$. To consider both, we define a partition of the edge set

$$E = E_+ \cup E_-, \qquad (22)$$

$$E_+ = \{(j,\ell) \in E | \Delta_{j,\ell} = \Delta_{j,\ell}^+\}, \qquad (23)$$

$$E_- = \{(j,\ell) \in E | \Delta_{j,\ell} = \Delta_{j,\ell}^-\}. \qquad (24)$$

Alternatively, we can define the two sets in terms of the nodal phases as

$$E_+ = \{(i,j) \in E | \cos(\theta_i - \theta_j) > 0\}, \qquad (25)$$

$$E_- = \{(i,j) \in E | \cos(\theta_i - \theta_j) \le 0\}. \qquad (26)$$

We note that a fixed point where the plus sign is realized for all edges ($E_- = \{\}$) is guaranteed to be linearly stable according to corollary 1. We refer to it as *normal operation*.

To operationalize the geometric condition, we now define the winding number (27) following the terminology used by Ochab and Gora[38] and Wiley *et al.*[39]

Definition 6 *(Winding vector). Consider a connected network with flows $\boldsymbol{F}$. For every fundamental cycle c, the winding number with respect to a partition $E = E_+ + E_-$ is defined as*

$$\varpi_c = \frac{1}{2\pi}\sum_{e \in E} z_e^c \Delta_e(F_e) \qquad (27)$$

with

$$\Delta_e(F_e) = \begin{cases} \arcsin(F_e/K_e) & \text{for} \quad e \in E_+ \\ \pi - \arcsin(F_e/K_e) & e \in E_-. \end{cases} \qquad (28)$$

The winding vector is defined as

$$\boldsymbol{\varpi} = (\varpi_1, \ldots, \varpi_{L-N+1})^T. \qquad (29)$$

Using the winding number, we can reformulate the conditions for the existence of a fixed point and establish a correspondence between the description of fixed points in terms of nodal phases of edge flows.

Theorem 7. *Consider a connected network with power injections $\boldsymbol{P} \in \mathbb{R}^N$ and coupling matrix $K \in \mathbb{R}^{N\times N}$. Then, the following two statements are equivalent:*

1. $\boldsymbol{\theta}^*$ *is a fixed point, i.e., a real solution of* Eq. (4).

2. $\boldsymbol{F} \in \mathbb{R}^L$ *satisfies the dynamic condition (13) and $\boldsymbol{\varpi} \in \mathbb{Z}^{L-N+1}$ for some partition $E = E_+ + E_-$.*

Proof. We prove the theorem in two parts.

(1) $\Rightarrow$ (2): If $\boldsymbol{\theta}^*$ is a fixed point, then the flows $\boldsymbol{F}$ satisfying the dynamical condition (13) as given by (3) are

$$F_{j,k} = K_{j,k}\sin(\theta_k - \theta_j). \qquad (30)$$

Let us partition the edge set into E^+ and E^- by

$$e = (j,k) \in \begin{cases} E^+ & \text{if } \cos(\theta_k - \theta_j) > 0 \\ E^- & \text{if } \cos(\theta_k - \theta_j) \le 0. \end{cases} \qquad (31)$$

We note the identity that

$$\arcsin(\sin(x))$$
$$= \begin{cases} -x + (2m_x + 1)\pi & \text{if } \cos(x) \le 0 \\ x + 2m_x\pi & \text{if } \cos(x) > 0, \text{ for some } m_x \in \mathbb{Z}. \end{cases} \qquad (32)$$

Combining this identity with the definition of Δ_e in (28) and our chosen set partition (31) results in

$$\begin{aligned} \text{for all } (j,k) \in E^+, \quad \Delta_{j,k} &= \arcsin(F_{jk}/K_{jk}), \\ &= \arcsin(\sin(\theta_k - \theta_j)), \\ &= 2m_{jk}\pi + (\theta_k - \theta_j), \qquad (33) \end{aligned}$$

$$\begin{aligned} \text{for all } (j,k) \in E^-, \quad \Delta_{j,k} &= \pi - \arcsin(F_{jk}/K_{jk}), \\ &= \pi - \arcsin(\sin(\theta_k - \theta_j)), \\ &= -2m_{jk}\pi + (\theta_k - \theta_j). \qquad (34) \end{aligned}$$

Combining (33) and (34), we obtain $\Delta_{jk} = 2m_{jk}\pi + (\theta_k - \theta_j)$, $m_{jk} \in \mathbb{Z}$ (choosing the $+$ sign for $2m_{jk}\pi$ without loss of generality).

Then, for any simple cycle $c = (v_1, v_2, \ldots, v_l, v_1)$ in the cycle basis B_C, the winding number is

$$\varpi_c = \frac{1}{2\pi}\sum_{e \in E} z_e^c \Delta_e(F_e), \qquad (35)$$

$$= (m_{12} + m_{23}, \ldots, m_{l1}) \in \mathbb{Z}, \qquad (36)$$

thus completing the first part of the proof.

(2) $\Rightarrow$ (1): Given a set of flows satisfying the dynamic condition (13) and having integral winding numbers, the fixed point $\boldsymbol{\theta}^*$ can be constructed following Eqs. (17) and (18).

This concludes the proof. $\qquad\square$

C. Geometric frustration

The previous reasoning shows that we can face the following situation: given an oscillator network characterized by the frequencies P_j and the capacity matrix $K_{j,\ell}$, we can find a solution of the dynamical conditions, such that the flow is conserved at all nodes of the network. Nevertheless, no fixed point exists as these solutions are incompatible with the geometric conditions. In this case, we say that phase locking is inhibited due to *geometric frustration*. We

summarize this in a formal definition before giving some examples for the importance of this phenomenon.

Definition 8. *An oscillator network is said to be geometrically frustrated if a solution of the dynamic conditions (11) exists, but all solutions are incompatible with the geometric conditions (20) such that no fixed point exists.*

This definition builds on a generalized notion of geometric frustration introduced in mathematical physics.[40] In that context, a system with multiple state variables $(x_1, x_2, ..., x_n)$ is called geometrically frustrated if for certain pair-wise correlations between those variables, no steady state exist satisfying all these correlations simultaneously.

IV. EXAMPLES AND APPLICATIONS

In this section, we discuss the importance of geometric aspects for the fixed points of an oscillator network with different topologies. In particular, we analyze the number of fixed points and show that geometric frustration can inhibit phase locking, which may lead to counter-intuitive phenomena.

A. Trees do not suffer from frustration

By definition, a tree does not contain any cycle such that the geometric condition (20) does not apply. Therefore, the calculation of a fixed point of the power grid oscillator model and the Kuramoto model as defined by Eq. (4) on a tree reduces to the solution of the dynamic condition (11), which is a linear set of equations. Moreover, we can find a strong result on the number of stable and unstable fixed points—see Corollary 2.

B. Multiple solutions in the cycle

We now consider the simplest nontrivial topology of a cyclic network with only three nodes and three links with equal strength K. The dynamical condition for the existence of a fixed point then reads

$$K \begin{pmatrix} 0 & 1 & -1 \\ -1 & 0 & 1 \\ 1 & -1 & 0 \end{pmatrix} \begin{pmatrix} S_{1,2} \\ S_{2,3} \\ S_{3,1} \end{pmatrix} = \begin{pmatrix} P_3 \\ P_1 \\ P_2 \end{pmatrix} \qquad (37)$$

and $|S_{j,\ell}| \leq 1$. In particular, for $P_j = 0$, any solution is a cycle flow $(S_{1,2}, S_{2,3}, S_{3,1}) = S \times (1, 1, 1)$.

Taking into account that there are two possible solutions for the phase difference along each edge as per (21) and since in order to satisfy the geometric condition (20), the sum of phase differences along the cycle must equal $2m\pi$ for some integer $m \in \mathbb{Z}$, we see that all fixed points must satisfy

$$\Delta_{12}^{\pm} + \Delta_{23}^{\pm} + \Delta_{31}^{\pm} = 2m\pi. \qquad (38)$$

Taking all combinations of either Δ^+ or Δ^- and corresponding possible values of m, we see that there are three intersections corresponding to three fixed points. These fixed points are illustrated in Fig. 1. This shows that stationary states are generally not unique, not even for the simplest cycle network. In the present case, only one of the solutions is dynamically stable, but this is generally not true in larger cycles as we will show in the following.

C. Frustration induces discreteness

We now extend the above example to a single cycle with an arbitrary number of nodes with the same power $P_j \equiv 0$. All links have an equal strength K as above. For the sake of notational convenience, we label the nodes as $1, 2, ..., N$ along the cycle and identify node 1 with $N+1$ and 0 with N. In order to have a non-trivial closed cycle, we need $N \geq 3$. The dynamic conditions for fixed points are then given by

$$F_{j+1,j} = F_{j,j-1} \equiv F \qquad \text{for all } j = 1, ..., N, \qquad (39)$$

$$|F| \leq K. \qquad (40)$$

We stress that the dynamic conditions have a continuum of solutions, i.e., all F values in the interval $[-K, K]$ are allowed.

The phase difference along the edges $(j+1, j)$ is given by Eq. (21), leaving two possible solutions $\Delta_{j,\ell}^+$ and $\Delta_{j,\ell}^-$. Choosing the minus sign for at least one edge $(\ell+1, \ell)$ yields $\tilde{K}_{\ell+1,\ell}^{\text{red}} = -\sqrt{K^2 - F^2} < 0$. In this case, one can show that the Hesse matrix H is not positive semi-definite such that the fixed point must be unstable. Restricting ourselves to the dynamically stable states, we find that the phase differences are all equal and given by

$$\theta_{j+1} - \theta_j = \arcsin(F/K). \qquad (41)$$
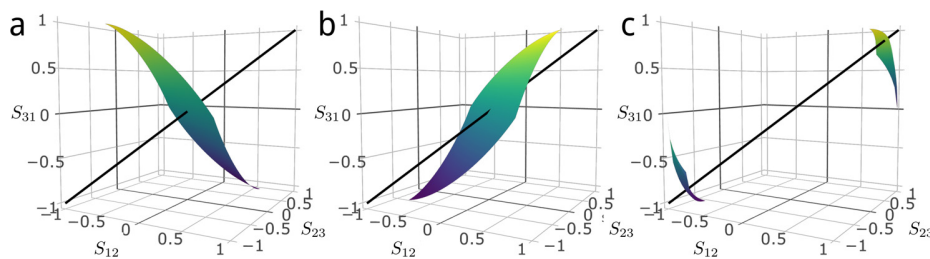
FIG. 1. Illustration of geometric frustration and multistability in the simplest cyclic network with 3 nodes with $P_j = 0$ and three links with equal strength K. Subplots show different branches of (38) obtained by choosing $+$ or $-$ sign for Δ_{12}, Δ_{23}, and Δ_{31}. The black lines denote the solution space of the dynamical condition (37), $S_{1,2} = S_{2,3} = S_{3,1} = S$. (a) Branch $(+++)$ with $m = 0$. (b) Branch $(--+)$ with $m = 1$. The branches $(+--)$ and $(-+-)$ yield solutions at $S = (0, 0, 0)$ in an analogous way. (c) Branch $(---)$ with $m = 1$ (upper part) and $m = 2$ (lower part). The branches $(++-)$, $(+-+)$, and $(-++)$ do not yield a solution.

The geometric condition now yields

$$N \arcsin(F/K) = 0 \quad (\mathrm{mod}\, 2\pi), \qquad (42)$$

which can be satisfied only for certain *discrete* values of F. The geometric condition thus induces a "quantization" of the phase differences as previously reported in Refs. 37 and 39

$$\theta_{j+1} - \theta_j = \frac{n}{N} 2\pi,$$

$$\text{with } n \in \left\{ -\left\lfloor \frac{N-1}{4} \right\rfloor, -\left\lfloor \frac{N-1}{4} \right\rfloor + 1, \ldots, +\left\lfloor \frac{N-1}{4} \right\rfloor \right\}, \qquad (43)$$

where $\lfloor \cdot \rfloor$ denotes the floor function. We note that solutions with $(\theta_{j+1} - \theta_j) = \pm\pi/2$ have Jacobian eigenvalues $\mu_k = 0$ for all $k \in \{1, \ldots, N\}$. In this case, linear stability analysis fails to determine dynamical stability properties (see the study by Khazin und Shnol[31] for details). For two coupled oscillators, it is rather easy to see that the fixed point is nonlinearly unstable. In total, we thus find $2 \times \lfloor (N-1)/4 \rfloor + 1$ different stable stationary states.

This example is very simple but illustrates three important general results. First, there can be *multiple* stable fixed points in cyclic networks as previously noticed in Refs. 38 and 41–43. This fact has been discussed in power engineering in Ref. 44, but rigorous results on conditions on the existence of multistability and the number of fixed points are rare probably because most authors in this community concentrate on fully connected networks which arise after a Kron reduction.[17,41] Second, the oscillator model (2) allows for stable fixed points with a persistent current around a cycle. Interestingly, these states are phase locked but *not phase ordered* in the sense that the phase order parameter[7]

$$re^{i\psi} := \frac{1}{N} \sum_j e^{i\theta_j} \qquad (44)$$

vanishes exactly for $K > 0$. Third, the geometric condition induces the *discreteness* of the phase differences although the dynamic condition allows for continuous values of cycle flows.

D. Braess' paradox

Here, we introduce a special example which illustrates the paradoxical effects of geometric frustration most clearly. We consider the oscillator network depicted in Fig. 2(a) consisting of $N = 4$ nodes placed on a cyclic network, where nodes 1 and 3 have power injection $-P$ and nodes 2 and 4 have power injections P. In particular, we analyze what happens if the capacity of the upper edge $(1, 2)$ is increased from K to $K' = K + \kappa$.

The dynamic condition for this network reads

$$0 = P_j + (K_{j+1,j} S_{j+1,j} - K_{j,j-1} S_{j,j-1}), \qquad (45)$$

and $|S_{j+1,j}| \leq 1$, identifying node $j = 5$ with $j = 1$. For notational convenience, we define the vector
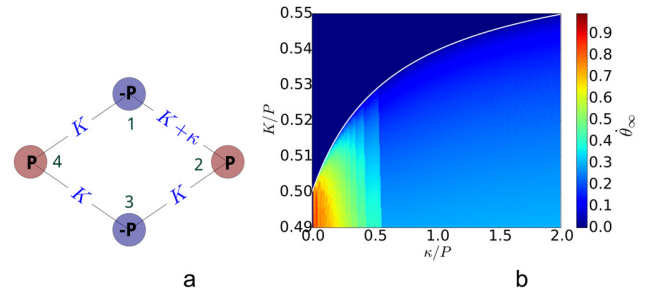

FIG. 2. Geometric frustration induces Braess' paradox. (a) Topology of the network under consideration. (b) Average phase velocities $\dot{\theta}_\infty$ defined in (49) for different values of K and κ. For fixed points, $\dot{\theta}_\infty = 0$. The white line shows the critical coupling K_c. The fixed point can be lost when the local transmission capacity κ *increases*.

$$\boldsymbol{S} = (S_{4,1}, S_{1,2}, S_{2,3}, S_{3,4}). \qquad (46)$$

The solutions of the linear system of Eq. (45) span a one-dimensional affine space parametrized by a real number ϵ,

$$\boldsymbol{S} = \frac{P}{K}(\boldsymbol{S}_a - \epsilon \boldsymbol{S}_b). \qquad (47)$$

The vector $\boldsymbol{S}_a = (-1, 0, -K/K', 0)$ is an inhomogeneous solution of the linear system (45), and the vector $\boldsymbol{S}_b = (1, 1, K/K', 1)$ is a homogeneous solution corresponding to a cycle flow. Evaluating the condition $|S_{j+1,j}| \leq 1$ yields a necessary condition for the existence of a fixed point

$$2K \geq P. \qquad (48)$$

For $\kappa = 0$, this condition is also sufficient for the existence of a stable fixed point. If the capacity of the upper link increases, $\kappa > 0$, geometric frustration inhibits phase locking. A solution of the dynamical conditions always exists for $2K \geq P$, but this can become incompatible with the geometric condition. We illustrate this in the stability diagram in Fig. 2(b). A stable fixed point exists only in the parameter region above the white line. As we see in Fig. 2(b), the minimum K required to maintain steady operation, the *critical coupling K_c*, increases when κ is increased.

To further characterize the long-time behavior of the oscillator network, we define $\dot{\theta}_\infty$ as the average phase velocities of all the nodes in the limit of large time

$$\dot{\theta}_\infty = \lim_{T \to \infty} \frac{1}{\tau} \int_T^{T+\tau} \frac{1}{N} \sum_{j=1}^{N} |\dot{\theta}_j(t)| dt. \qquad (49)$$

Therefore, $\dot{\theta}_\infty$ must be zero for steady operation to take place. As expected, we find $\dot{\theta}_\infty = 0$ in the stable parameter region above the white line $K > K_c$ and $\dot{\theta}_\infty > 0$ in the unstable parameter region below the white line $K < K_c$. Remarkably, $\dot{\theta}_\infty$ is the largest for small values of κ and, of course, $K < K_c(\kappa)$.

This leads to the paradoxical effect that an increase in local transmission capacity reduces the ability of the network to support a phase locked fixed point. This behavior can also be seen as an example of Braess' paradox[45,46] which has been first predicted for traffic networks.[47]

It is noted that the existence of cycles is a necessary condition for this paradoxical behavior in oscillator networks. A fundamental example of Braess' paradox was investigated in Ref. 30, starting from a chain network which has no cycles and thus shows no frustration and Braess behavior. Then, a single line is added creating a single cycle and necessary conditions being established under which conditions the closing of the cycles induced Braess' paradox.

V. MULTISTABILITY AND THE NUMBER OF FIXED POINTS

The previous examples show that there can be a large number of stable fixed points in a cyclic network. In the following, we derive conditions for the existence and bounds for the number of stable fixed points depending on the network structure. We start with a deeper analysis of the dynamic condition for arbitrary networks, which is a necessary prerequisite for the existence of a stable fixed point. Then, we turn to the geometric condition and derive bounds for the number of fixed points. The arguments depend heavily on the network structure such that we will start with trees and simple cycles before we turn to more complex topologies.

A. The dynamic condition

We first analyze whether the dynamic condition (13) admits a solution. The problem reduces to the Multi-source multi-sink maximum flow problem, which can be solved by a variety of different algorithms.[48,49]

So, let $G = (V, E)$ be a connected graph with N nodes and L edges. Each edge is assigned a capacity given by $K_1, \ldots, K_L$, and each node has an in- or outflux given by $P_1, \ldots, P_N$. We define an extended graph $G' = (V', E')$, illustrated in Fig. 3, by adding two vertices s and t to the vertex set,

$$V' = V \cup \{s, t\}, \tag{50}$$

and adding directed links connecting $s(t)$ to all nodes with positive (negative) power injection

$$E = E \cup \{(s \to j)|j \in V, P_j \geq 0\} \cup \{(j \to t)|j \in V, P_j < 0\}. \tag{51}$$

The capacity of the newly added links is infinite. Then, one finds the theorem:
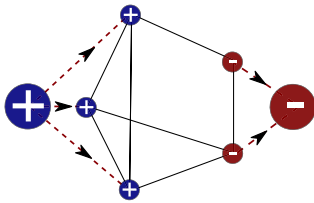

FIG. 3. Illustration of Theorem 9. The original network G (smaller nodes and solid edges) admits solution to the dynamic condition if and only if the extended graph G' with a super source s (big blue node) and a super sink t (big red node) admits an s-t flow larger than the sum of all positive input powers in G.

Theorem 9. *A solution of the dynamic condition (13) exists if and only if the value of the maximum s-t-flow $\mathcal{F}_{st}$ in the network G' is larger than or equal to the cumulated input power*

$$\mathcal{F}_{st} \geq \sum_{j \in V, P_j \geq 0} P_j. \tag{52}$$

Alternatively, a sufficient condition for the existence of a solution can be found by dividing the graph into parts: let (V_1, V_2) be an arbitrary partition of V and $E(V_1, V_2)$ the cut-set induced by this partition (see Fig. 4). Then, we define

$$\bar{P}_1 = \sum_{v_j \in V_1} P_{v_j}, \quad \bar{P}_2 = \sum_{v_j \in V_2} P_{v_j}, \quad \bar{K}_{12} = \sum_{e \in E(V_1, V_2)} K_e. \tag{53}$$

We note that have assumed that $\sum_j P_j = 0$, without loss of generality, such that we always have $\bar{P}_1 + \bar{P}_2 = 0$.

Theorem 10. *If for all partitions (V_1, V_2) we have*

$$|\bar{P}_1| = |\bar{P}_2| \leq \bar{K}_{12}, \tag{54}$$

then there exists a solution of the dynamic condition (13).

Proof. The idea is to prove the following:
($\not\exists$ a solution of the dynamic condition (13a) and (13b).
$\iff$ All solutions of (13a) violate (13b)).
$\Rightarrow \exists$ a partition (V_1, V_2) with $|\bar{P}_1| \geq \bar{K}_{12}$.

Reversing arguments then yields the theorem. It remains to show that the statement "$\Rightarrow$" is true.

Let $\boldsymbol{F}$ be a solution of (13a). According to our assumption, the set of overloaded edges

$$E_{\text{ov}} = \{e \in E||F_e| > K_e\} \tag{55}$$

is not empty. Now, consider one overloaded edge $e_0 = (u, v) \in E_{\text{ov}}$. We assume without loss of generality that the flow is from u to v, i.e., $F_{v,u} > K_{v,u} > 0$. We define the weighted directed network $\tilde{G}(V, \tilde{E})$ with $\tilde{E} = E \backslash e_0$ and coupling constants

$$W_{j,i} = \max\{0, K_{j,i} - F_{j,i}\}. \tag{56}$$

We determine the maximum flow pattern $\Delta F_e, e \in \tilde{E}$ with the value $\Delta F_{\max}$ from u to v in the network $\tilde{G}$. According to the max-flow min-cut theorem, there is a partition (V_1, V_2) with $u \in V_1$ and $v \in V_2$ and the associated cutset $\tilde{E}(V_1, V_2)$ such that

$$\Delta F_e = W_e \quad \text{for all } e \in \tilde{E}(V_1, V_2). \tag{57}$$

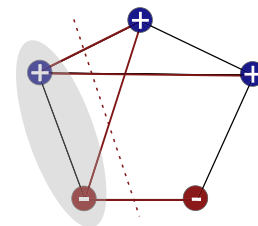Now, consider the flow pattern $\boldsymbol{F}'$ defined by

FIG. 4. Illustration of Theorem 10. For each partition of the node set of a graph into V_1 (shaded grey) and V_2, the induced cutset (edges coloured red) must have capacity not less than the absolute value of input power in V_1 or V_2.

$$F'_e = F_e + \Delta F_e \qquad e \in \tilde{E}, \tag{58}$$

$$F'_{e_0} = F_{e_0} - \Delta F_{\max}. \tag{59}$$

This is a new solution of the condition (13a). Basically, we have rerouted the maximum possible flow from the edge $e_0 = (u, v)$ to alternative paths from u to v. Furthermore, we define the edge set $E(V_1, V_2) = e_0 \cup \tilde{E}(V_1, V_2)$, which is a cut of the original graph G.

We now have to distinguish two cases:

Case 1: The maximum flow value $\Delta F_{\max} < F_{e_0} - K_{e_0}$. Then, the edge e_0 is still overloaded, i.e., we have $F'_{e_0} > K_{e_0}$. Summing up Eq. (13a) over the nodes in V_1 and V_2 yields

$$\bar{P}_1 = -\bar{P}_2 = \sum_{e \in E(V_1, V_2)} F'_e. \tag{60}$$

However, we know that $F'_{e_0} > K_{e_0}$ and $F'_e = K_e$ for all other $e \in E(V_1, V_2)$ such that

$$\sum_{e \in E(V_1, V_2)} F'_e > \bar{K}_{12} \tag{61}$$

and the statement "⇒" follows.

Case 2: The maximum flow value $\Delta F_{\max} \geq F_{e_0} - K_{e_0}$. e_0 is no longer overloaded with respect to the flow pattern $\boldsymbol{F}'$. The set of edges which is still overloaded

$$E'_{\text{ov}} = \{e \in E \,||F'_e| > K_e\} \tag{62}$$

does no longer contain e_0, i.e., $E'_{\text{ov}} \in E_{\text{ov}} \backslash e_0$. However, this set cannot be empty as we have assumed that there is no solution of (13a) satisfying (13b). Then, we can just restart the procedure, by selecting an edge $e_1 \in E'_{\text{ov}}$ and finding a max. flow between its adjacent vectors. Finally, we must arrive at case 1 for which the statement "⇒" follows.   □

These two theorems have a straightforward energetic interpretation. In Theorem 10, we assume that the grid is decomposed into two parts and calculate the cumulated power in the two parts V_1 and V_2. A steady state can only exist if it is possible to transmit the cumulated power from one part to the other one. This condition must hold for all partitionings of the networks. Theorem 9 is basically a reformulation of this task in the sense of the max-flow min-cut theorem from the graph theory. We accumulate all sources in a super-source and all sinks in a super-sink. A steady state can only exist if there is a valid flow from the super-source to the super-sink.

B. Tree network

In Sec. IV we have argued that multistability arises due to the possibility of cycle flows. In a tree, there are no cycles and thus no multistability, and we obtain the following result.

Corollary 2 *In a tree network, either there is no fixed point or there are 2^{N-1} fixed points of which one is stable and $2^{N-1} - 1$ are unstable.*

Whether the fixed points exist or not can then be decided solely on the basis of the dynamical condition (11), respectively, using Theorem 9.

Proof. By definition, a tree has $L = N - 1$ edges such that the space of solutions of the linear system (14a) has dimension $L - N + 1 = 0$. That is, there is either zero or exactly one unique solution for the flows $F_{j,\ell}$. In the first case, no fixed point exists. In the latter case, there are 2 possible values for the phase difference for each of the edges given by Eq. (21). Hence, there are $2^L = 2^{N-1}$ fixed points. Choosing the +-sign in Eq. (21) yields one stable fixed point as shown in corollary 1.

It remains to show that all other fixed points are unstable. So, consider a fixed point with one edge where the cosine of the phase difference is smaller than zero. The network is a tree such that it is decomposed into two parts which are only connected by this edge. We label the nodes by $1, \ldots, \ell$ in one part and by $\ell + 1, \ldots, N$ in the other part. Then, the Hesse matrix H (see Sec. II) has the form

$$H = \begin{pmatrix} H_1 & 0 \\ 0 & H_2 \end{pmatrix} + \begin{pmatrix} \ddots & & & & & \\ & 0 & 0 & 0 & 0 & \\ & 0 & K^{\text{red}}_{\ell,\ell+1} & -K^{\text{red}}_{\ell,\ell+1} & 0 & \\ & 0 & -K^{\text{red}}_{\ell,\ell+1} & K^{\text{red}}_{\ell,\ell+1} & 0 & \\ & 0 & 0 & 0 & 0 & \\ & & & & & \ddots \end{pmatrix}, \tag{63}$$

where $K^{\text{red}}_{\ell,\ell+1} < 0$ and H_1 and H_2 are defined as in Eq. (6) for the two parts of the network. Now define the vector

$$\boldsymbol{v} = (\underbrace{1, \ldots, 1}_{\ell \text{ times}}, \underbrace{0, \ldots, 0}_{(N-\ell) \text{ times}})^T. \tag{64}$$

Due to the structure of the matrix H_1, we have $H_1(1, \ldots, 1)^T = 0$ such that

$$\boldsymbol{v}^T H \boldsymbol{v} = K^{\text{red}}_{\ell,\ell+1} < 0. \tag{65}$$

Thus, the Hesse matrix H is not positive semi-definite, i.e., it has at least one negative eigenvalue and the fixed point is unstable (cf. Lemma 1).   □

We note that this can also be seen as a consequence of Taylor's lemma in Ref. 41, showing that for stable fixed points, there cannot be a partition of a graph so that the sum of cosines of the phase differences across all edges in the induced cutset is less than zero.

C. Cycle flows and winding vector

In the following, we want to operationalize theorem (7), which characterizes fixed points in terms of the flows and winding numbers, to derive strict bounds for the number of fixed points in a network. Restricting ourselves to normal operation ($E_- = \{\}$) and using the decomposition (16), the definition of the winding numbers (27) reads

$$\varpi_c = \frac{1}{2\pi} \sum_{e=1}^{L} z_e^c \arcsin\left(\frac{F_e}{K_e}\right)$$

$$= \frac{1}{2\pi} \sum_{e=1}^{L} z_e^c \arcsin\left(\frac{F_e^{(0)} + \sum_{c' \in B_C} f_{c'} z_e^{c'}}{K_e}\right), \quad (66)$$

using Eq. (16). The concept of winding numbers is particularly useful when they are unique. If we can find upper and lower bounds for ϖ_c, then we can simply count the number of solutions $\boldsymbol{\varpi} \in \mathbb{Z}^{L-N+1}$ to obtain the number of fixed points. Uniqueness is rigorously shown for planar graphs in the following lemma.

A graph is called planar if it can be drawn in the plane without any edge crossings. Such a drawing is called a plane graph or a planar embedding of the graph, and any cycle that surrounds a region without any edges is called a face of the graph.[35] For the sake of simplicity, we adopt the convention that for plane graphs, the cycle basis B_C is built up from the faces in the following. Notably, many power grids and other supply networks are actually planar. Crossing of power lines is not forbidden *a priori* but is rare.

Lemma 3. *For a planar network, let $\boldsymbol{\theta}$ and $\boldsymbol{\theta}'$ be two fixed points satisfying the "normal operation" criterion (9). If $\boldsymbol{\varpi}(\boldsymbol{\theta}) = \boldsymbol{\varpi}(\boldsymbol{\theta}')$, then both fixed points are the same, i.e., the phases differ only by an additive constant*

$$\boldsymbol{\theta} = \boldsymbol{\theta}' + c(1, 1, ..., 1)^T. \quad (67)$$

In other words, no two different fixed points in planar networks can have an identical winding vector.

Proof. Choose as the cycle basis B_C the faces of the plane embedding. The two fixed points can differ only via cycle flows such that the flows can be written as

$$\text{fixed point } \boldsymbol{\theta}: \quad F_e = F_e^{(0)} + \sum_{c \in B_C} f_c z_e^c, \quad (68)$$

$$\text{fixed point } \boldsymbol{\theta}': \quad F_e' = F_e^{(0)} + \sum_{c \in B_C} f_c' z_e^c, \quad (69)$$

defining two cycle flow vectors $\boldsymbol{f}$ and $\boldsymbol{f}'$. We write $\boldsymbol{\varpi}(\boldsymbol{f}')$ and $\boldsymbol{\varpi}(\boldsymbol{f})$ in short-hand notation for the corresponding winding vectors. We show that $\boldsymbol{\varpi}(\boldsymbol{f}') = \boldsymbol{\varpi}(\boldsymbol{f})$ implies $\boldsymbol{f}' = \boldsymbol{f}$ and thus $\boldsymbol{F}' = \boldsymbol{F}$. As we are assuming normal operation, we can reconstruct the phases via (18) and thus find $\boldsymbol{\theta} = \boldsymbol{\theta}' + c(1, 1, ..., 1)^T$ as we need to show.

So, assume that $\boldsymbol{\varpi}(\boldsymbol{f}') = \boldsymbol{\varpi}(\boldsymbol{f})$ and $f_c' \neq f_c$ for at least one cycle c. We show that this leads to a contradiction such that the lemma follows. First, consider the case that $f_c' - f_c$ is the same for all cycles: $f_c' - f_c = \Delta f \neq 0$ for all $c \in B_C$. Then, choose a cycle k at the boundary. If $\Delta f > 0$, we find $\varpi_k(\boldsymbol{f}') > \varpi_k(\boldsymbol{f})$, and if $\Delta f < 0$, we find $\varpi_k(\boldsymbol{f}') < \varpi_k(\boldsymbol{f})$. This contradicts the assumption and the lemma follows.

Otherwise, choose a cycle for which the quantity $f_c' - f_c$ is the largest. We can find a cycle k such that

$$f_k' - f_k \geq f_\ell' - f_\ell \quad \text{for all } \ell \neq k, \quad (70)$$

$$f_k' - f_k > f_n' - f_n \quad \text{for at least one cycle } n \text{ adjacent to } k. \quad (71)$$

or, equivalently,

$$f_k' - f_\ell' \geq f_k - f_\ell \quad \text{for all } \ell \neq k, \quad (72)$$

$$f_k' - f_n' > f_k - f_n \quad \text{for at least one cycle } n \text{ adjacent to } k. \quad (73)$$

We now exploit that any edge belongs to at most two cycles, according to Mac Lane's planarity criterion.[50] Choosing an edge e which is part of both the cycles k and n, we have $z_e^k z_e^k = 1$ and $z_e^k z_e^n = -1$. For all other cycles $\ell \neq k, n$, we have $z_e^\ell = 0$. Thus, we find [using (73)]

$$z_e^k F_e^{(0)} + \underbrace{z_e^k z_e^k}_{=+1} f_k' + \underbrace{z_e^k z_e^n}_{=-1} f_n' + \sum_{\ell \neq k,n} \underbrace{z_e^k z_e^\ell}_{=0} f_\ell' > z_e^k F_e^{(0)}$$
$$+ \underbrace{z_e^k z_e^k}_{=+1} f_k + \underbrace{z_e^k z_e^n}_{=-1} f_n + \sum_{\ell \neq k,n} \underbrace{z_e^k z_e^\ell}_{=0} f_\ell, \quad (74)$$

$$\rightarrow \quad z_e^k F_e^{(0)} + \sum_c z_e^k z_e^c f_c' > z_e^k F_e^{(0)} + \sum_c z_e^k z_e^c f_c. \quad (75)$$

For every other edge e' in cycle k, we find by the same procedure [using (72)] that

$$z_{e'}^k F_{e'}^{(0)} + \sum_c z_{e'}^k z_{e'}^c f_c' \geq z_{e'}^k F_{e'}^{(0)} + \sum_c z_{e'}^k z_{e'}^c f_c. \quad (76)$$

Substituting these two inequalities in the definition (66) and using that arcsin is monotonically increasing and point-symmetric about the origin such that $\arcsin(z_e^k x) = z_e^k \arcsin(x)$, we find

$$\varpi_k(\boldsymbol{f}') > \varpi_k(\boldsymbol{f}). \quad (77)$$

This contradicts our contrary assumption, which concludes the proof.   □

We note that Delabays *et al.* have proved this lemma using completely different techniques in Ref. 51.

D. Simple cycles

For networks containing a single cycle (a ring network), tight upper and lower bounds can be obtained for the number of fixed points satisfying $\cos(\theta_i^* - \theta_j^*) > 0$ for all edges (i, j). These states correspond to the normal operation of a power grid and are guaranteed to be stable by corollary 1. Other stable steady states can exist in particular at the border of the stable parameter region.[29] We label the nodes as $1, 2, ..., N$ along the cycle, fixing the direction of counting in the counter-clockwise direction and identify node 1 with $N + 1$ and 0 with N. Likewise, we fix the orientation of the edges $e \in \{1, ..., L\}$ such that $F_e > 0$ describes a counter-clockwise flow and $F_e < 0$ a clockwise flow.

We will first calculate the exact number of fixed points counting the number of different allowed winding numbers. However, this result depends on one particular solution of the dynamic conditions (11), thereby limiting its applicability. We therefore also derive lower and upper bounds for the number of fixed points in terms of a few simple characteristics of the grid, in particular, the maximum partial net power. These bounds do not depend on any particular solution of the dynamical condition.

Remark 11. *For any ring network $\mathcal{R}_N$ with N nodes, the cycle flow vector defined in (2) and the winding vector defined in (29) naturally reduce into single numbers. We refer to them as cycle flow f_c and winding number ϖ_c, following Ref. 39. These two quantities will be crucial in establishing the results in the rest of this section.*

Theorem 12. *For a ring network $\mathcal{R}_N$, the number of normal operation fixed points (denoted by $\mathcal{N}$) is given by*

$$\mathcal{N} = \left\lceil \frac{1}{2\pi} \sum_j \arcsin\left(\frac{F_{j+1,j}^{(0)} + f_c^{\max}}{K_{j+1,j}}\right) \right\rceil$$
$$- \left\lfloor \frac{1}{2\pi} \sum_j \arcsin\left(\frac{F_{j+1,j}^{(0)} + f_c^{\min}}{K_{j+1,j}}\right) \right\rfloor - 1, \quad (78)$$

where $\lfloor \cdot \rfloor$ denotes the floor function and $\lceil \cdot \rceil$ denotes the ceiling function. $F_{ij}^{(0)}$ is one particular solution to the dynamic condition (11) and

$$f_c^{\max} = \min_j(K_{j+1,j} - F_{j+1,j}^{(0)}),$$
$$f_c^{\min} = \max_j(-K_{j+1,j} - F_{j+1,j}^{(0)}). \quad (79)$$

Proof. Suppose that we have one fixed point θ_0 with the flows $F_{ij}^{(0)}$ and analyze (as per Theorem 3) which cycle flow values f_c lead to different valid fixed points. First, the cycle flow bounds both above and below since the flow $F_{j,j+1}$ along each edge cannot exceed in absolute value the capacity $K_{j,j+1}$

$$f_c^{\min} < f_c < f_c^{\max}, \quad (80)$$

$$f_c^{\max} = \min_j(K_{j,j+1} - F_{j,j+1}^{(0)}), \quad (81)$$

$$f_c^{\min} = \max_j(-K_{j,j+1} - F_{j,j+1}^{(0)}). \quad (82)$$

We emphasize that f_c cannot be equal to $f_c^{\max}$ or $f_c^{\min}$ because otherwise one edge would be fully loaded with $\cos(\theta_i - \theta_j) = 0$, contradicting our assumption.

Second, all fixed points have to satisfy the geometric condition (cf. Theorem 7)

$$\varpi(f_c) \in \mathbb{Z}. \quad (83)$$

Since we restrict ourselves to normal operation, the winding number for a single cycle reads

$$\varpi(f_c) = \frac{1}{2\pi} \sum_j \arcsin\left(\frac{F_{j+1,j}^{(0)} + f_c}{K_{j+1,j}}\right). \quad (84)$$

Using the bound for the cycle flow strength (80) and the fact that arcsin is a monotonically increasing function, we find that the winding number is also bound by

$$\varpi(f_c^{\min}) \leq \varpi \leq \varpi(f_c^{\max}). \quad (85)$$

As the winding numbers are unique (see Lemma 3), the distinct fixed points correspond to the following values of the winding number:

$$\varpi_{\text{fixedpoint}} = \lfloor \varpi(f_c^{\min}) \rfloor + 1, \lfloor \varpi(f_c^{\min}) \rfloor + 2, ..., \lceil \varpi(f_c^{\max}) \rceil - 1. \quad (86)$$

Counting these values and inserting the values of $f_c^{\min}$ and $f_c^{\max}$ then yield the number of fixed points $\mathcal{N}$. $\qquad \square$

For practical applications, it is desirable to determine the number of fixed points from the properties of the network alone, without referring to a particular solution $F^{(0)}$. To obtain suitable bounds for the number of fixed points $\mathcal{N}$, we first define some properties which characterize the network.

Definition 13. *For a ring network $\mathcal{R}_N$ with $N \in \mathbb{N}$ nodes indexed by $1, 2, ..., N$ along the cycle, a **fragment** $\mathcal{F}_{i,j}$ is defined as the path starting at node i and ending at node j. For any fragment $\mathcal{F}_{i,j}$, the **partial net power** $\bar{P}_{ij}$ is defined as*

$$\bar{P}_{ij} = \sum_{k=i}^{j} P_k. \quad (87)$$

*and the **maximal partial net power** is defined as*

$$\bar{P}_{\max} = \max_{i,j} \bar{P}_{i,j}. \quad (88)$$

This concept is illustrated in Fig. 5. *Furthermore, we define the maximum and minimum transmission capacities*

$$K_{\max} = \max_j K_{j+1,j} \quad \text{and} \quad K_{\min} = \min_j K_{j+1,j}. \quad (89)$$

Lemma 4. *For any ring fragment $\mathcal{F}_{i,j}$, the partial net power is equal to the net outward flow*

$$\bar{P}_{ij} = F_{j+1,j} - F_{i-1,i} \quad (90)$$

and

$$\bar{P}_{\max} = \max_j F_{j+1,j} - \min_i F_{i-1,i}. \quad (91)$$

Lemma 4 is a formalization of energy conservation. The net outward flow from a segment must equal the cumulated power injections in the fragment. We then seek the fragment maximizing the total flow exchanged with the rest of the ring. We note that the definitions of $\bar{P}_{ij}$ and $\bar{P}_{\max}$ appeared previously in Ref. 51.

Corollary 3. *For a ring network $\mathcal{R}_N$, the number of normal operation fixed points (denoted by $\mathcal{N}$) is bound from above and below by*

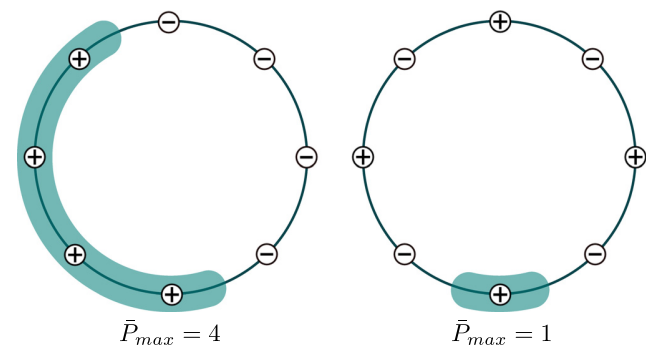$$0 \leq \mathcal{N} \leq 2\left\lfloor \frac{N}{4} \right\rfloor + 1 \quad (92)$$

$$\bar{P}_{max} = 4 \qquad \bar{P}_{max} = 1$$

FIG. 5. The maximum partial net power $\bar{P}_{\max}$ in different ring networks.

and by

$$\left\lceil \frac{N}{4} \frac{2K_{\max} - \bar{P}_{\max}}{K_{\min}} \right\rceil \geq \mathcal{N} \geq \left\lceil \frac{N}{2\pi} \frac{2K_{\min} - \bar{P}_{\max}}{K_{\max}} \right\rceil - 1. \quad (93)$$

Proof. According to Lemma 12, the number of fixed points $\mathcal{N}$ is given by

$$\mathcal{N} = \lceil \varpi(f_c^{\max}) \rceil - \lfloor \varpi(f_c^{\min}) \rfloor - 1. \quad (94)$$

We make use of the fact that the arcsin function is bound, $\arcsin(x) \in [-\pi/2, +\pi/2]$, such that

$$\varpi(f_c^{\max}) = \frac{1}{2\pi} \sum_{j=1}^{N} \arcsin\left(\frac{F_{j+1,j}^{(0)} + f_c^{\max}}{K_{j+1,j}}\right) < \frac{N}{4},$$

$$\varpi(f_c^{\min}) = \frac{1}{2\pi} \sum_{j=1}^{N} \arcsin\left(\frac{F_{j+1,j}^{(0)} + f_c^{\min}}{K_{j+1,j}}\right) > -\frac{N}{4}. \quad (95)$$

This proves the first part (92) of the corollary. To prove the second part, we start from

$$\lceil \varpi(f_c^{\max}) - \varpi(f_c^{\min}) \rceil - 1 \leq \mathcal{N} \leq \lceil \varpi(f_c^{\max}) - \varpi(f_c^{\min}) \rceil. \quad (96)$$

Now, one can obtain upper and lower bounds for all terms in the sum using the trigonometric relation

$$x - y \leq \arcsin(x) - \arcsin(y) \leq \frac{\pi}{2}(x - y), \quad (97)$$

which holds for all $-1 \leq y \leq x \leq 1$. This yields

$$\frac{1}{2\pi} \sum_j \frac{\Delta f_c}{K_{j+1,j}} \leq \varpi(f_c^{\max}) - \varpi(f_c^{\min}) \leq \frac{1}{4} \sum_j \frac{\Delta f_c}{K_{j+1,j}}, \quad (98)$$

where we define $\Delta f_c = f_c^{\max} - f_c^{\min}$. Furthermore, this quantity can be bound as

$$\begin{aligned}
\Delta f_c &= \min_j (K_{j+1,j} - F_{j+1,j}^{(0)}) - \max_j (-K_{j+1,j} - F_{j+1,j}^{(0)}) \\
&\geq 2K_{\min} + \min_j (-F_{j+1,j}^{(0)}) - \max_j (-F_{j+1,j}^{(0)}), \\
&= 2K_{\min} + \max_j (F_{j,j+1}^{(0)}) - \max_j (-F_{j+1,j}^{(0)}), \\
&= 2K_{\min} - \bar{P}_{\max} \quad \text{(using (92))}, \quad (99)
\end{aligned}$$

such that the fraction in Eq. (98) becomes

$$\frac{\Delta f_c}{K_{j+1,j}} \geq \frac{2K_{\min} - \bar{P}_{\max}}{K_{\max}}. \quad (100)$$

In a similar way, we find

$$\Delta f_c \leq 2K_{\max} - \bar{P}_{\max}. \quad (101)$$

Substituting these bounds into Eq. (98) yields

$$\begin{aligned}
\varpi(f_c^{\max}) - \varpi(f_c^{\min}) &\geq \frac{N}{2\pi} \frac{2K_{\min} - \bar{P}_{\max}}{K_{\max}}, \\
\varpi(f_c^{\max}) - \varpi(f_c^{\min}) &\leq \frac{N}{4} \frac{2K_{\max} - \bar{P}_{\max}}{K_{\min}},
\end{aligned} \quad (102)$$

which combined with (96) completes the proof. $\square$

We note that the first part of this bound (92) had previously been shown by Ochab and Gora[38] as well as by Delabays *et al.*[37]

Corollary 4. *For homogeneous rings* $\mathcal{R}_N$*, i.e.,* $K_{i,i+1} = K$*, Eq.* (93) *simplifies to*

$$\left\lceil \frac{N}{\pi} - \frac{N\bar{P}_{\max}}{2K\pi} \right\rceil - 1 \leq \mathcal{N} \leq \left\lceil \frac{N}{2} - \frac{N\bar{P}_{\max}}{4K} \right\rceil. \quad (103)$$

In particular, ring networks $\mathcal{R}_N$ *with* $N \leq 4$ *do not have multiple stable fixed points. Ring network* $\mathcal{R}_N$ *with* $N \geq 7$ *nodes will have multiple stable fixed points* $(\mathcal{N} \geq 2)$ *if*

$$\bar{P}_{\max} < 2K_{\min} - \frac{4\pi}{N} K_{\max}. \quad (104)$$

These relations can be proven by simply evaluating the bounds in Corollary 3.

Corollary 5. *As K is decreased in a homogeneous ring network, the fixed points with the largest infinity norm of the flows*

$$||\boldsymbol{F}||_\infty := \max_j |F_{j,j+1}|$$

will be the first ones to vanish.

Proof. We can see from (95) that both $\varpi(f_c^{\max})$ and $\varpi(f_c^{\min})$ are monotonically increasing functions of $f_c^{\max}$ and $f_c^{\min}$, respectively. According to (80), when K is decreased, $f_c^{\max}$ decreases and $f_c^{\min}$ increases. The corollary follows. $\square$

We illustrate how the bounds scale with the connectivity K and $\bar{P}_{\max}$ for a sample ring of size $N = 16$ in Fig. 6. We see in Fig. 6(a) that increasing K results in more stable fixed points. Whereas Fig. 6(b) demonstrates that if the power generators ($P_j \geq 0$) are clustered together, then the system has less fixed points, as opposed to the case where they are more distributed.
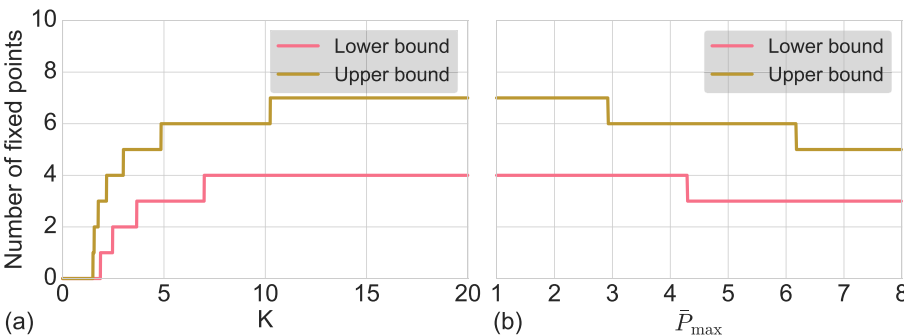

FIG. 6. Upper and lower bounds for the number of fixed points $\mathcal{N}$ for a sample 16 element ring as a function of (a) $K = K_{j,j+1}$ for all $1 \leq j \leq 16$ at $\bar{P}_{\max} = 3$ and (b) $\bar{P}_{\max}$ at $K = 10$.
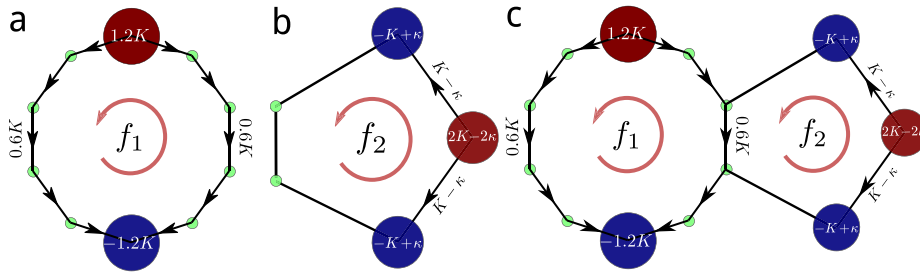
FIG. 7. Difficulties in finding bound for the number of stable fixed points in the complex network. The network motifs shown in (a) and (b) have 3 and 1 stable fixed points, respectively, whereas the fused network shown in (c) has no stable fixed point at all. The power injections P_j are given in the nodes. All edges have transmission capacity K.

E. Complex networks

Obtaining bounds for the number of fixed points is hard in general, as we cannot simply decompose a network into single cycles, unless no two cycles of a network share an edge. The difficulty arises because cycle flows in two faces sharing one or more edges can cancel or enhance each other. This is why one cannot simply multiply the bounds for a number of fixed points for each cycle to obtain a bound for the total number of fixed points for a network. We demonstrate this using two examples.

1. Two cycle flows destroying each other

First, we show that even if all single cycles support (multiple) fixed points in case they are isolated, the full network may not have a single fixed point at all. This is illustrated in Fig. 7 for a network consisting of just two cycles. The network motifs shown in panels (a) and (b) have 3 and 1 stable fixed points, respectively, whereas the full network shown in panel (c) does not have a stable fixed point. Isolated cycle 2, i.e., the network shown in Fig. 7(b), has a stable fixed point, but two edges are heavily loaded such that there is nearly no security margin and no available capacity for cycle flows. Fusing the two cycles as in Fig. 7(c) disturbs the geometric condition for both cycles. To restore the geometric condition $\boldsymbol{\varpi} \in \mathbb{Z}^2$, we would have to add some cycle flows. But this is impossible in cycle 2 such that there is no stable fixed point in the full network.

2. Two cycle flows getting created

So, we have seen that getting a *lower bound* for a number of fixed points of a general network is hard, as multiplying lower bounds for each cycle in a cycle basis does not yield a valid lower bound. Next, we will show why obtaining a good *upper bound* is also hard.

Consider any of the two identical single loop networks in Fig. 8. It consists of one generator and one consumer, generating and consuming $2.1K$ power, respectively. Each edge has capacity K. None of the two single loop networks have any fixed point: simply because the network does not have enough capacity to transport the $2.1K$ amount of power from the
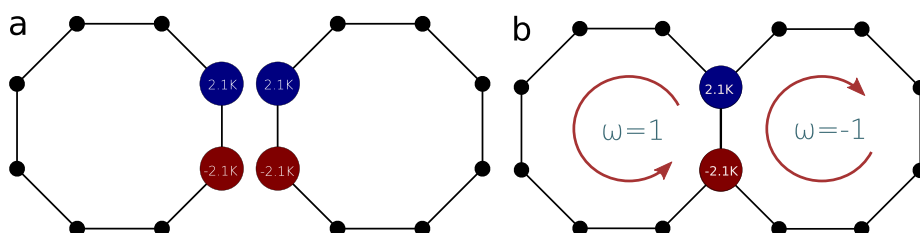
generator to the consumer. However, when those two are fused together, two cycle flows emerge and a stable fixed point with winding vector $\boldsymbol{\omega} = (1, -1)$ comes into existence. This should not come as a surprise: fusing two cycles in this case ended up with an alternate pathway for the powerflow being created.

F. Planar networks

Although obtaining estimates for a number of fixed points for general topologies is quite difficult, we now show that for planar topologies, it is possible to obtain some analytical insights.

1. Upper bound

Theorem 14. *Consider a finite planar network. Choose the faces of the graph as the cycle basis B_C. Then, the number of normal operation fixed points, i.e., fixed points satisfying* $\cos(\theta_i^* - \theta_j^*) > 0$ *for all edges (i, j), is bound from above by*

$$\mathcal{N} < \prod_{c=1}^{L-N+1} 2 \left\lfloor \frac{N_c}{4} \right\rfloor + 1, \qquad (105)$$

where N_c is the number of nodes in cycle c.

Proof. In a planar network, no two different fixed points can have the same winding vector $\boldsymbol{\varpi}$ (see Lemma 3) such that we can just count the different allowed winding vectors. For each fundamental cycle $c \in B_C$, we have

$$-\lfloor N_c/4 \rfloor < \varpi_c = \frac{1}{2\pi} \sum_{e \in \text{cycle } c} \Delta_e < +\lfloor N_c/4 \rfloor \qquad (106)$$

because $-\pi/2 < \Delta_e < +\pi/2$ in normal operation. Counting the number of different possible values of the winding numbers $\varpi_1, \ldots, \varpi_{L-N+1}$ respecting these upper and lower bounds yields the result. □

Delabays *et al.* have presented[37] this bound in the case of uniform power injections P_j at all nodes. They have also determined topological conditions that are sufficient to ensure that *all* fixed points are under normal operation, thus making the upper bound in (105) valid for all fixed points in a certain class of networks.

FIG. 8. Two ring networks, each with no fixed point, when merged by an edge, gain a fixed point.
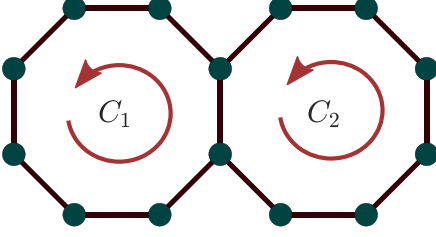
FIG. 9. A 2-cycle network. We use the convention that cycles are counter-clockwise. Therefore, we assign positive magnitudes to counter-clockwise cycle flows and negative magnitudes to clockwise cycle flows.

Intriguingly, this upper bound has been demonstrated to be *invalid*[51] outside normal operation.

2. Asymptotic behaviour

We have shown in Subsection V E that it is not straightforward to obtain bounds for the number of fixed points $\mathcal{N}$ in complex networks, unlike simple cycles. However, in the limit of $N \gg 1, K \gg 1$, we can nevertheless derive the scaling behaviour for $\mathcal{N}$.

3. Two-cycle network

For simplicity, we first consider a network with homogeneous transmission capacities consisting of two cycles C_1 and C_2, as illustrated in Fig. 9. Suppose that there are n_1 edges belonging only to cycle 1, n_2 edges belonging only to cycle 2

and n_{12} edges belonging to both. Let one fixed point be θ^* with flows in each cycle and the intersection be bound by

$$F_1^{\min} \leq F_e \leq F_1^{\max}, \quad \text{for all} \quad e \in C_1 - C_2 \quad (107)$$

$$F_2^{\min} \leq F_e \leq F_2^{\max}, \quad \text{for all} \quad e \in C_2 - C_1 \quad (108)$$

$$F_{12}^{\min} \leq F_e \leq F_{12}^{\max}, \quad \text{for all} \quad e \in C_2 - C_1. \quad (109)$$

Then, the possible cycle flows in each cycle are bound inside a convex polygon $\mathcal{D}$ described by

$$-K - F_1^{\min} \leq f_1 \leq K - F_1^{\max}, \quad (110)$$

$$-K - F_2^{\min} \leq f_2 \leq K - F_2^{\max}, \quad (111)$$

$$-K - F_{12}^{\min} \leq f_1 - f_2 \leq K - F_{12}^{\max}. \quad (112)$$

Then, for $K \gg 1, n_1 \gg 1, n_2 \gg 1$, the number of fixed points converges to the area of the image set of $\mathcal{D}$ under the mapping ϖ.

$$\mathcal{N} \approx \int_{\varpi(\mathcal{D})} d\varpi_1 d\varpi_2, \quad (113)$$

$$= \int_{\mathcal{D}} df_1 df_2 \det J(\varpi), \quad (114)$$

where the Jacobian $J(\varpi)$ for the change in the variable can be computed from the expression for ϖ in (66), which yields

$$
\det J(\varpi) = \frac{1}{4K^2\pi^2}
$$
$$
\times \det \begin{pmatrix} \sum\limits_{e \in C_1} \dfrac{1}{\sqrt{1 - \left(\dfrac{F_e + f_1}{K}\right)^2}} + \sum\limits_{e \in C_1 \cap C_2} \dfrac{1}{\sqrt{1 - \left(\dfrac{F_e + f_1 - f_2}{K}\right)^2}} & -\sum\limits_{e \in C_1 \cap C_2} \dfrac{1}{\sqrt{1 - \left(\dfrac{F_e + f_1 - f_2}{K}\right)^2}} \\[2em] -\sum\limits_{e \in C_1 \cap C_2} \dfrac{1}{\sqrt{1 - \left(\dfrac{F_e + f_1 - f_2}{K}\right)^2}} & \sum\limits_{e \in C_2} \dfrac{1}{\sqrt{1 - \left(\dfrac{F_e + f_2}{K}\right)^2}} + \sum\limits_{e \in C_1 \cap C_2} \dfrac{1}{\sqrt{1 - \left(\dfrac{F_e + f_1 - f_2}{K}\right)^2}} \end{pmatrix}.
$$
$$(115)$$

Taking the limits

$$\lim_{K \to \infty} \frac{F_e + f_1}{K} = \frac{f_1}{K},$$
$$\lim_{K \to \infty} \frac{F_e + f_2}{K} = \frac{f_2}{K}, \quad (116)$$

leads to

$$
\mathcal{N} \approx \frac{1}{4K^2\pi^2} \int_{\tilde{\mathcal{D}}} df_1 df_2 \det \begin{pmatrix} \dfrac{n_1}{\sqrt{1 - \left(\dfrac{f_1}{K}\right)^2}} + \dfrac{n_{12}}{\sqrt{1 - \left(\dfrac{f_1 - f_2}{K}\right)^2}} & -\dfrac{n_{12}}{\sqrt{1 - \left(\dfrac{f_1 - f_2}{K}\right)^2}} \\[2em] -\dfrac{n_{12}}{\sqrt{1 - \left(\dfrac{f_1 - f_2}{K}\right)^2}} & \dfrac{n_2}{\sqrt{1 - \left(\dfrac{f_2}{K}\right)^2}} + \dfrac{n_{12}}{\sqrt{1 - \left(\dfrac{f_1 - f_2}{K}\right)^2}} \end{pmatrix}.
$$

$$\tilde{\mathcal{D}} := \{(f_1, f_2) : (f_1, f_2) \in \mathbb{R}^2, |f_1| \leq K, |f_2| \leq K, |f_1 - f_2| \leq K\}. \quad (117)$$

Redefining $f_1 \to f_1/K, f_2 \to f_2/K$, we obtain

$$\mathcal{N} \approx \frac{1}{4\pi^2} \int_{\tilde{\mathcal{D}}} df_1 df_2 \det \begin{pmatrix} \dfrac{n_1}{\sqrt{1-f_1^2}} + \dfrac{n_{12}}{\sqrt{1-(f_1-f_2)^2}} & -\dfrac{n_{12}}{\sqrt{1-(f_1-f_2)^2}} \\ -\dfrac{n_{12}}{\sqrt{1-(f_1-f_2)^2}} & \dfrac{n_2}{\sqrt{1-f_2^2}} + \dfrac{n_{12}}{\sqrt{1-(f_1-f_2)^2}} \end{pmatrix}, \tag{118}$$

$$= \frac{1}{4\pi^2} \left(n_1 n_2 \int_{\tilde{\mathcal{D}}} \frac{1}{\sqrt{1-f_1^2}} \frac{1}{\sqrt{1-f_2^2}} df_1 df_2 + n_1 n_{12} \int_{\tilde{\mathcal{D}}} \frac{1}{\sqrt{1-f_1^2}} \frac{1}{\sqrt{1-(f_1-f_2)^2}} df_1 df_2 \right.$$

$$\left. + n_2 n_{12} \int_{\tilde{\mathcal{D}}} \frac{1}{\sqrt{1-f_2^2}} \frac{1}{\sqrt{1-(f_1-f_2)^2}} df_1 df_2 \right), \tag{119}$$

$$= \frac{1}{4\pi^2} \left(n_1 n_2 \int_{\tilde{\mathcal{D}}} \frac{1}{\sqrt{1-f_1^2}} \frac{1}{\sqrt{1-f_2^2}} df_1 df_2 + (n_1 + n_2) n_{12} \int_{\tilde{\mathcal{D}}} \frac{1}{\sqrt{1-f_1^2}} \frac{1}{\sqrt{1-(f_1-f_2)^2}} df_1 df_2 \right). \tag{120}$$

In the last line, we use the symmetry in f_1 and f_2, both in the integrand and the domain of integration. We can simplify even further, by using the following change in variables in the second integral:

$$(f_1, f_2) \mapsto (f_2 - f_1, f_2).$$

We note that the domain remains the same after this change in the variable and the determinant of the Jacobian $\det(J) = -1$. This allows the simplification

$$\mathcal{N} \approx (n_1 n_2 + (n_1 + n_2) n_{12}) \underbrace{\frac{1}{4\pi^2} \int_{\tilde{\mathcal{D}}} \frac{1}{\sqrt{1-f_1^2}} \frac{1}{\sqrt{1-f_2^2}} df_1 df_2}_{\gamma},$$

with

$$\gamma = \frac{1}{4\pi^2} \left\{ \int_{-1}^{0} \frac{df_1}{\sqrt{1-f_1^2}} \int_{-1}^{f_1+1} \frac{df_2}{\sqrt{1-f_2^2}} + \int_{0}^{1} \frac{df_1}{\sqrt{1-f_1^2}} \int_{f_1-1}^{1} \frac{df_2}{\sqrt{1-f_2^2}} \right\},$$

$$= \frac{1}{4\pi^2} \left\{ \int_{-1}^{0} \frac{\arcsin(f_1+1) + \dfrac{\pi}{2}}{\sqrt{1-f_1^2}} df_1 + \int_{0}^{1} \frac{\dfrac{\pi}{2} - \arcsin(f_1-1)}{\sqrt{1-f_1^2}} df_1 \right\},$$

$$= \frac{1}{4\pi^2} \left\{ \frac{\pi^2}{4} + \int_{-1}^{0} \frac{\arcsin(f_1+1)}{\sqrt{1-f_1^2}} df_1 + \frac{\pi^2}{4} + \int_{0}^{1} \frac{\arcsin(f_1-1)}{\sqrt{1-f_1^2}} df_1 \right\},$$

$$= \frac{1}{8} + \frac{1}{2\pi^2} \int_{-1}^{0} \frac{\arcsin(f_1+1)}{\sqrt{1-f_1^2}} df_1,$$

$$\approx 0.1576,$$

to finally yield this scaling result

$$\lim_{n_1, n_2 \to \infty} \mathcal{N} = \gamma (n_1 n_2 + (n_1 + n_2) n_{12}), \tag{121}$$

$$\gamma \approx 0.1576.$$

To evaluate the accuracy of (121), we apply it to two special cases. First, we consider networks with $n = n_1 = n_2$, $n_{12} = 1$, i.e., two identical cycles sharing only one single edge. In this case, (121) becomes

$$\mathcal{N}(n, n, 1) \approx (n^2 + 2n)\gamma. \tag{122}$$

Second, we consider networks with $n = n_1 = n_2$, $n_{12} = n$, i.e., two identical cycles sharing half of their edges. In this case, (121) becomes

$$\mathcal{N}(n, n, n) \approx 3\gamma n^2. \tag{123}$$

We see in Fig. 10 that in both these cases, the scaling relations are quite accurate even for not very large network sizes, such as $n = 50$.

4. General planar graphs

The scaling results for two-cycle networks can be extended to general planar graphs; to this end, we define a few quantities.

Definition 15 (*Loopy dual graph*). *Given a planar graph $G(V, E)$ and an embedding, we choose a cycle basis B_C consisting of the faces of the embedding. The loopy dual graph $G^{\text{dual}}(G)$ is an undirected multigraph whose vertex set is equal to B_C. Its edge set E' is as follows. For each edge*
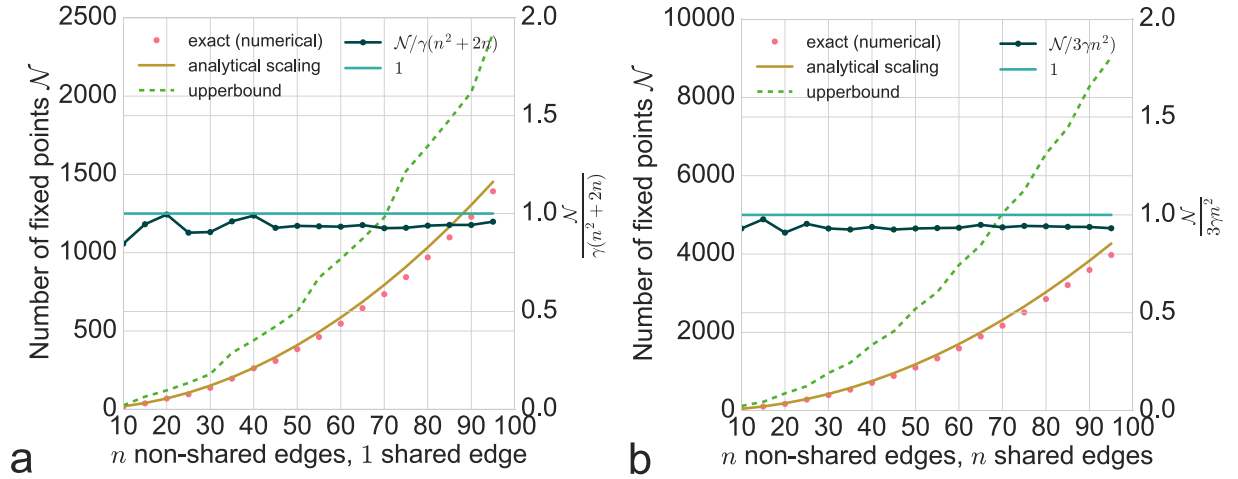
FIG. 10. (a) Scaling of the number of fixed points for two-cycle networks at zero power injection and infinite edge capacity limit. (a) Each cycle has $n+1$ edges, and they share one edge between them. (Left y-axis) The dots show the exact number of fixed points computed numerically. The solid line shows the predicted number as per scaling relation (121). The dashed line shows the upper bound (105). (Right y-axis) The dotted line shows the number of fixed points divided by $n^2 + 2n$ converging to a constant value, that is close to the analytically predicted value $\gamma = 0.1576$, as per equation (121). (b) The same as (a), but for networks where each cycle has $2n$ edges, they share n edges between them.

$e \in E$, if it is shared between two cycles c_1 and c_2, then an edge between c and c' is added to E'. If e is at the boundary and belongs to only one cycle c, then a self-loop is added at node c. We illustrate this definition in Fig. 11.

Now, consider a planar graph and an arbitrarily chosen fixed point with flows F_e. Let us denote by $\tilde{L}^{\text{loopy}}$ the loopy Laplacian of its metagraph, as defined in Definition 1.

Then, Eq. (117) generalizes to

$$\mathcal{N} \approx \frac{1}{(2K\pi)^{L-N+1}} \int_{\tilde{\mathcal{D}}} df_1 df_2 \cdots df_{L-N+1} \det \tilde{L}^{\text{loopy}}, \quad (124)$$

$$\tilde{\mathcal{D}} := \{(f_1, f_2, \ldots f_{L-N+1}) : |f_i| \leq K, |f_i - f_j| \leq K$$
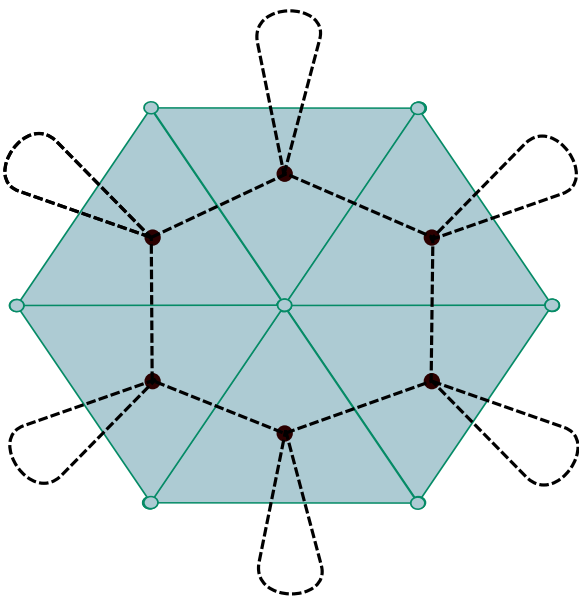$$\text{if cycles } i, j \text{ share an edge}\}.$$

FIG. 11. A planar graph (solid edges, unfilled circular nodes) and its loopy dual (dashed edges, filled circular nodes) corresponding to this specific embedding.

VI. UNSTABLE FIXED POINTS

In principle, we can generalize the cycle flow approach to find fixed points which do not satisfy the normal operation condition, too. These fixed points are typically linearly unstable (cf. the discussion in Ref. 30) However, most of the results on the number of fixed points cannot be generalized to this case. As an instructive example, consider again a homogeneous ring as in Sec. IV C. We label the nodes as $1, 2, \ldots, N$ along the cycle and assume that N is an integer multiple of 4. All nodes have a vanishing power injection $P_j \equiv 0$, and all links have an equal strength K as before. Then, it is easy to see that

$$\theta^* = (0, \delta, \pi, \pi + \delta, 2\pi, 2\pi + \delta, 3\pi, \ldots)^T \quad (125)$$

is a fixed point of the dynamics for each value of $\delta \in [0, \pi)$. This class of fixed points represents a pure cycle flow

$$F_{j,j+1} = K \sin(\theta_{j+1} - \theta_j) = K \sin(\delta) \quad (126)$$

for all edges $(j, j+1)$. The winding number is $\varpi = N/4$ independent of the value of δ and the edges belong alternately to E_+ and E_-

$$E_+ = \{(1,2); (3,4); (5,6); \ldots\},$$
$$E_- = \{(2,3); (4,5); (6,7); \ldots\}. \quad (127)$$

This simple example shows that two main assumptions made for the normal operation fixed points (where $E_- = \{\}$) do not longer hold: first, the set of fixed points is no longer discrete. Instead, we find a continuum of solutions parametrized by the real number δ. Second, different fixed points yield the same winding number. Thus, we cannot obtain the number of fixed points by counting winding numbers in general.

VII. CALCULATING ALL FIXED POINTS

The cycle flow approach yields a convenient method to calculate multiple fixed points for oscillator networks.

Generally, it is hard to make sure that a numerical algorithm yields all solutions for a nonlinear algebraic equation. However, we have shown that the winding numbers are unique at least for normal operation fixed points in planar networks. Thus, we can scan the allowed values of the winding numbers and try to find a corresponding solution. This can be done by starting from an arbitrary solution of the dynamical condition and adding cycle flows until we obtain the desired winding numbers.

In particular, we can calculate all fixed points in normal operation for a planar network using the following algorithm:

1. Find a solution $F^{(0)}$ of the dynamic condition.
2. Fix a plane embedding and a cycle basis.
3. Vary the number z_c in the interval $[-\frac{N_c}{4}, \frac{N_c}{4}]$, for all cycles $c = 1, \ldots, L - N + 1$.
4. Try to solve the set of equations

$$\varpi_c(f) = z_c \qquad \text{for all } c = 1, \ldots, L - N + 1, \qquad (128)$$

where the winding numbers are given by Eq. (27). Dropping the assumption of a normal operation, we lose the guarantee of uniqueness as discussed in Sec. VI. Nevertheless, the method can be readily adapted to find *most*

of the unstable fixed points, at least if the number $|E_-|$ is small. This can be very useful, as a systematic calculation of such fixed points is generally not straightforward. The results can be applied, among other things, to assess the global stability of a stable fixed point by analyzing the stability boundary[52,53] or the stability in the presence of stochastic fluctuations.[54] In particular, we must add another step to the algorithm to loop over all possible sets E_-:

3a.   Vary $k = 0, \ldots, L$. Then, sample all k-tuples from the edge set E to define the set E_-.
3b.   Vary the number z_c in the interval $[-\frac{N_c}{4}, \frac{N_c}{4}]$, for all cycles $c = 1, \ldots, L - N + 1$.

The output of this algorithm is shown in Fig. 12 for a small test network and $|E_-| \leq 2$. For this small network, we have only $L - N + 1 = 3$ fundamental cycles of which one is decoupled. Hence, we can graphically check that we have obtained *all* fixed points.
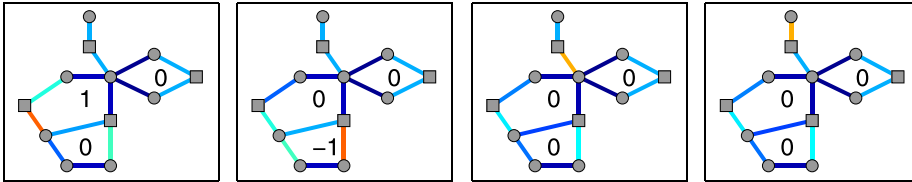
VIII. DISCUSSION

Oscillator networks are ubiquitous in nature and technology. A lot of research in statistical physics starting from

Fixed points with $|E_-| = 0$ (normal operation):
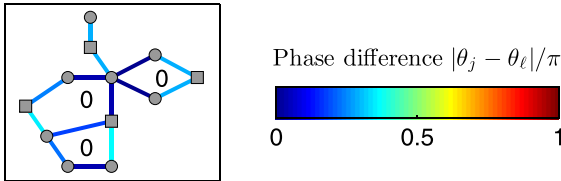
Fixed points with $|E_-| = 1$:

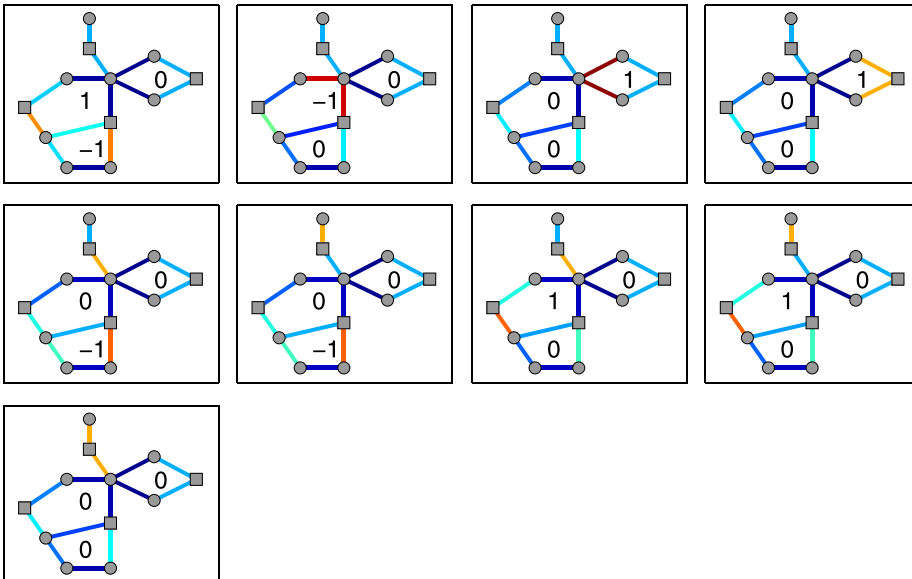Fixed points with $|E_-| = 2$:

FIG. 12. All fixed points with $|E_-| \leq 2$ in a network with three cycles calculated using the algorithm described in the main text. The winding number of each cycle is displayed. Squares represent the generators with $P = +2P_0$ and circles the consumers with $P = -P_0$. All links have a coupling strength of $K = 24/19 \times P_0$.

Kuramoto's seminal work[2] has been devoted to the onset of partial synchronization in large networks. However, in some applications, global synchronization is required. In particular, in electrical power grids, all generators have to run with exactly the same frequency and have to be strictly phase-locked to enable stable power flows to the customers. A desynchronization generally has catastrophic consequences. An example is provided by the European power blackout in November 2006. Following a shutdown of one transmission line and unsuccessful attempts to restore stable operation, the European grid fragmented in three mutually asynchronous clusters.[23] In the end, more than 10 million customers were cut from the power supply.

In this article, we have analyzed the existence of stable fixed points in finite oscillator networks. The main methodological advancement is to split the calculation into two parts: first, we calculate the flows which satisfy the continuity equation at all nodes. Then, we single out the specific solution which leads to consistent phases of the oscillators. We thus move the focus of the calculation from the nodes (phases) to the edges (flows) and cycles. An immediate consequence is that several fixed points can co-exist, which differ by cycle flows. Thus, oscillator networks are in general multistable.

For networks containing a single cycle, we have obtained upper and lower bounds for the number of fixed points in terms of three structural quantities: the maximal partial net power $\bar{P}_{\max}$, which measures the homogeneity of the power injections or natural frequencies and the maximum and minimum edge strength along the cycle. We find that generally the number of stable fixed points is particularly large if (a) the cycle is long, (b) the edge strength is large, and (c) the power sources are distributed homogeneously. However, the example discussed in Sec. IV D shows that extreme care has to be taken for special network topologies. Increasing the strength of the wrong edge can also decrease the number of fixed points. Finding bounds for the number of stable fixed points in general network topologies is much more involved. The results have been obtained for planar networks, but the bounds are much weaker as for networks with single cycles. Interestingly, both tree networks and fully connected networks have at most one stable fixed point. However, networks with intermediate sparsity, which is most realistic for electrical power grids, may exhibit multistability.

Several aspects of multistability have been previously discussed in the literature. Multistability in isolated rings was discussed in Ref. 38. The limits (92) were derived, and the basins of attraction of the different fixed points were studied numerically. The case of a densely connected graph was analyzed by Taylor in Ref. 41. He was able to show that there is at most one stable fixed point if the node degree is at least $0.9395 \times (N - 1)$. Mehta *et al.* investigate multistability in complex networks numerically using a similar approach to the present paper.[43] They argue that the number of fixed points scales with the number of cycles as each cycle can accommodate cycle flows. While this is valid for many graphs, there are counterexamples (Fig. 7). Delabays *et al.*[37] have recently reported their treatment of multistability using

cycle flows. They have extended the upper bounds for fixed points in single rings in Ref. 38 to also include those stable fixed points with phase differences along edges $>\pi/2$. They have also derived upper bounds[51] for a number of fixed points for planar graphs in the case of uniform power injections at all nodes. Xi *et al.*[55] have numerically shown that the spatial heterogeneity of power injections P_j reduces the number of fixed points, which fits with our analytical result in Corollary 3. Intriguingly, they have also found that in heterogeneous ring topologies, the nonlinear stability of fixed points decreases with the ring size N.

In this work, we have obtained a *lower bound* for the number of fixed points and thereby provided a *sufficient condition* for the existence of multistability. Furthermore, we have shown that the length of the cycles N_c and the homogeneity $\bar{P}_{\max}$ are equally important for multistability and thereby arrived at tighter bounds for the number of fixed points than Ochab and Gora[38] and Delabays *et al.*[37] Moreover, we have derived scaling laws at the limit of infinite transmission strengths that are much tighter than the upper bound results previously reported. We have shown the derived scaling behaviour to match numerically computed exact results for moderately sized networks.

Interestingly, our results show that a previous highly recognized result presented by Jadbabaie *et al.* in Ref. 57 is incorrect. The authors claim that for any network of Kuramoto oscillators with different natural frequencies, there exists a K_u such that for $K > K_u$ there is only one stable fixed point. This claim is disproven by the examples presented in Sec. IV C as well as by the rigorous results on the existence of multiple fixed points in Corollary 3. The error in the proof of Ref. 57 is rather technical. The authors define a function $\boldsymbol{L}$ such that the defining equation of a fixed point (4) can be rewritten in the form

$$\boldsymbol{\theta}^* = \boldsymbol{L}(\boldsymbol{\theta}^*). \tag{129}$$

Jadbabaie *et al.* then claim that $\boldsymbol{L}$ is a contraction on the subset of $\boldsymbol{\theta}$ such that $|\theta_i - \theta_j| < \pi/2$ for all edges (i, j), which we called normal operation. Banach's contraction theorem then yields that the algebraic equation (129) has a unique fixed point. The problem is that the range of $\boldsymbol{L}(\theta)$ is generally *not* a subset of subspace of normal operation, even if the domain is. After applying $\boldsymbol{L}$, some phase differences can get out of the interval $[-\pi/2, \pi/2]$. Thus, Banach's contraction theorem cannot be applied, which spoils the proof.

IX. CONCLUSION

In summary, taking cycle flows as a basis of flow patterns, we analyzed the existence and stability of phase locked states in networks of Kuramoto oscillators and second order phase oscillators modeling the phase dynamics of electric power grids. We demonstrated that such systems exhibit multistability. Intriguingly, multistability prevails even under conditions where unique stable operating points were believed to exist in both a power engineering textbook and a major complex network reference on Kuramoto oscillators.[56,57] For classes of network topologies, we have established necessary and sufficient conditions for multistability

and derived lower and upper bounds for the number of fixed points. We explained why generalizing those bounds for arbitrary topologies is hard. Nevertheless, we have derived asymptotic scaling laws at a large loop limit that has been found to match closely numerically obtained exact results.

ACKNOWLEDGMENTS

[1]C. Huygens, *Oeuvres Complétes de Christiaan Huygens* (Martinus Nijhoff, The Hague, The Netherlands, 1893).

[2]Y. Kuramoto, in *International Symposium on Mathematical Problems in Theoretical Physics*, Lecture Notes in Physics Vol. 39, edited by H. Araki (Springer, New York, 1975), p. 420.

[3]Y. Kuramoto, *Chemical Oscillations, Waves, and Turbulence* (Springer, Berlin, 1984).

[4]K. Wiesenfeld, P. Colet, and S. H. Strogatz, Phys. Rev. Lett. **76**, 404 (1996).

[5]F. Varela, J.-P. Lachaux, E. Rodriguez, and J. Martinerie, Nat. Rev. Neurosci. **2**, 229 (2001).

[6]I. Z. Kiss, Y. Zhai, and J. L. Hudson, Science **296**, 1676 (2002).

[7]S. H. Strogatz, Phys. D: Nonlinear Phenom. **143**, 1 (2000).

[8]J. A. Acebrón, L. L. Bonilla, C. J. Pérez Vicente, F. Ritort, and R. Spigler, Rev. Mod. Phys. **77**, 137 (2005).

[9]A. Arenas, A. Díaz-Guilera, J. Kurths, Y. Moreno, and C. Zhou, Phys. Rep. **469**, 93 (2008).

[10]D. Witthaut and M. Timme, Phys. Rev. E **90**, 032917 (2014).

[11]B. Ermentrout, J. Math. Biol. **29**, 571 (1991).

[12]S.-Y. Ha, E. Jeong, and M.-J. Kang, Nonlinearity **23**, 3139 (2010).

[13]S. H. Strogatz, D. M. Abrams, A. McRobie, B. Eckhardt, and E. Ott, Nature **438**, 43 (2005).

[14]A. R. Bergen and D. J. Hill, IEEE Trans. Power Appar. Syst. **PAS-100**, 25 (1981).

[15]G. Filatrella, A. H. Nielsen, and N. F. Pedersen, Eur. Phys. J. B **61**, 485 (2008).

[16]M. Rohden, A. Sorge, M. Timme, and D. Witthaut, Phys. Rev. Lett. **109**, 064101 (2012).

[17]A. E. Motter, S. A. Myers, M. Anghel, and T. Nishikawa, Nat. Phys. **9**, 191 (2013).

[18]F. Dörfler, M. Chertkov, and F. Bullo, Proc. Natl. Acad. Sci. **110**, 2005 (2013).

[19]M. Rohden, A. Sorge, D. Witthaut, and M. Timme, Chaos **24**, 013123 (2014).

[20]B. Schäfer, M. Matthiae, M. Timme, and D. Witthaut, New J. Phys. **17**, 015002 (2015).

[21]M. E. J. Newman, *Networks—An Introduction* (Oxford University Press, Oxford, 2010).

[22]D. Witthaut, M. Rohden, X. Zhang, S. Hallerberg, and M. Timme, Phys. Rev. Lett. **116**, 138701 (2016).

[23]Union for the Coordination of Transmission of Electricity, https://www.entsoe.eu/fileadmin/user_upload/_library/publications/ce/otherreports/Final-Report-20070130.pdf for Final report on the system disturbance; accessed 4 November 2006 (2007).

[24]S. Watanabe and S. H. Strogatz, Phys. Rev. Lett. **70**, 2391 (1993).

[25]C. Bick, M. Timme, D. Paulikat, D. Rathlev, and P. Ashwin, Phys. Rev. Lett. **107**, 244101 (2011).

[26]G. Filatrella, N. F. Pedersen, and K. Wiesenfeld, Phys. Rev. E **61**, 2513 (2000).

[27]G. Filatrella, N. F. Pedersen, and K. Wiesenfeld, Phys. Rev. E **75**, 017201 (2007).

[28]S. Gupta, A. Campa, and S. Ruffo, J. Stat. Mech.: Theory Exp. **2014**, R08001.

[29]D. Manik, D. Witthaut, B. Schäfer, M. Matthiae, A. Sorge, M. Rohden, E. Katifori, and M. Timme, Eur. Phys. J. Spec. Top. **223**, 2527 (2014).

[30]T. Coletta and P. Jacquod, Phys. Rev. E **93**, 032222 (2016).

[31]L. G. Khazin and E. Schnol, *Stability of Critical Equilibrium States* (Manchester University Press, 1991).

[32]C. J. Tavora and O. J. Smith, IEEE Trans. Power Appar. Syst. **PAS-91**, 1138–1144 (1972).

[33]E. Katifori, G. J. Szöllősi, and M. O. Magnasco, Phys. Rev. Lett. **104**, 048704 (2010).

[34]H. Ronellenfitsch, M. Timme, and D. Witthaut, IEEE Trans. Power Syst. **32**, 1007 (2016).

[35]R. Diestel, *Graph Theory* (Springer, New York, 2010).

[36]C. Godsil and G. F. Royle, *Algebraic Graph Theory* (Springer Science & Business Media, 2013), Vol. 207.

[37]R. Delabays, T. Coletta, and P. Jacquod, J. Math. Phys. **57**, 032701 (2016).

[38]J. Ochab and P. Gora, Acta Phys. Pol. Ser. B, Proc. Suppl. **3**, 453 (2010).

[39]D. A. Wiley, S. H. Strogatz, and M. Girvan, Chaos: Interdiscip. J. Nonlinear Sci. **16**, 015103 (2006).

[40]M. Wolf, F. Verstraete, and J. Cirac, Int. J. Quantum Inf. **1**, 465 (2003).

[41]R. Taylor, J. Phys. A: Math. Theor. **45**, 055102 (2012).

[42]F. Ionita, D. Labavic, M. A. Zaks, and H. Meyer-Ortmanns, Eur. Phys. J. B **86**, 511 (2013).

[43]D. Mehta, N. Daleo, F. Dörfler, and J. D. Hauenstein, Chaos **25**, 053103 (2015).

[44]A. Korsak, IEEE Trans. Power App. Syst. **PAS-91**, 1093 (1972).

[45]D. Witthaut and M. Timme, New J. Phys. **14**, 083036 (2012).

[46]D. Witthaut and M. Timme, Eur. Phys. J. B **86**, 377 (2013).

[47]D. Braess, Unternehmensforschung **12**, 258 (1968).

[48]Y. Nussbaum, preprint arXiv:1012.4767 (2010).

[49]L. R. Ford, Jr. and D. R. Fulkerson, *Flows in Networks* (Princeton University Press, 2015).

[50]S. Mac Lane, Fundam. Math. **28**, 22 (1937).

[51]R. Delabays, T. Coletta, and P. Jacquod, J. Math. Phys. **58**, 032703 (2017).

[52]P. J. Menck, J. Heitzig, N. Marwan, and J. Kurths, Nat. Phys. **9**, 89 (2013).

[53]H.-D. Chiang, F. Wu, and P. Varaiya, IEEE Trans. Circuits Syst. **34**, 160 (1987).

[54]B. Schäfer, M. Matthiae, X. Zhang, M. Rohden, M. Timme, and D. Witthaut, Phys. Rev. E **95**, 060203 (2017).

[55]K. Xi, J. L. Dubbeldam, and H. X. Lin, Chaos: Interdiscip. J. Nonlinear Sci. **27**, 013109 (2017).

[56]A. Jadbabaie, N. Motee, and M. Barahona, in *Proceedings of the 2004 American Control Conference* (IEEE, 2004), Vol. **5**, pp. 4296–4301.

[57]J. Machowski, J. Bialek, and J. Bumby, *Power System Dynamics, Stability and Control* (John Wiley & Sons, New York, 2008).

[58]W. Chen, D. Wang, J. Liu, T. Basar, K. H. Johansson, and L. Qiu, IFAC-PapersOnLine **49**(22), 97–102 (2016).

6

MANUSCRIPT – BRAESS' PARADOX IN CONTINUOUS FLOW NETWORKS: A NETWORK DYNAMICS PERSPECTIVE

Debsankha Manik[1], Marc Timme[1,2,3], Dirk Witthaut[4,5]

[1] Network Dynamics, Max Planck Institute for Dynamics and Self-Organization (MPI DS), D-37077 Göttingen, Germany

[2] Chair for Network Dynamics, Institute for Theoretical Physics and Center for Advancing Electronics Dresden (cfaed), Technical University of Dresden, 01069 Dresden, Germany

[3] Department of Physics, Technical University Darmstadt, 64289 Darmstadt, Germany

[4] Forschungszentrum Jülich, Institute for Energy and Climate Research – Systems Analysis and Technology Evaluation (IEK-STE), 52425 Jülich, Germany

[5] Institute for Theoretical Physics, University of Cologne, 50937 Köln, Germany

Original contribution:
I conceptualized the article and wrote the first draft of the manuscript. I performed all the analytical calculations behind the results and all numerical computations.

Abstract. Flow networks perform critical functions in various natural and man made systems, e.g. the venation networks in plant leaves and the electrical power transmission grid. Such networks often undergoes *topological changes*, both planned and unplanned: e.g. shutdowns of power lines due to a storm or scheduled maintenance; or leaf veins getting eaten through by bugs. It is therefore very important to understand how such topological changes influence the flows in the network. In the context of traffic networks, it was discovered by traffic engineer D. Braess in 1968 that opening a new street in a street network may *increase* travel time for *everyone*, if each car selfishly chooses the fastest route for oneself. This phenomenon, subsequently named "Braess' paradox" (BP), has been later reported in various other flow networks, including phase oscillator networks, linear flow networks and discrete message passing networks. When a flow network needs to carry more flow, it is a common strategy to strengthen an edge or add new one. If BP is possible in a flow network, such an attempt at improving the network may actually overload or destabilize it. Although the prevalence of this phenomenon is well known, establishing criteria for an edge in a given network to exhibit Braess' paradox is still an unsolved problem. In this article, we consider BP in a class of flow networks that includes Kuramoto networks (that can be used to model the AC power transmission grid) as well as linear flow networks (that can be used to model the fluid flow in leaf veins). Using the notion of network susceptibilities, we take a *differential view* to Braess' paradox, defining BP as an increase in the *maximum load* on infinitesimal increase of the strength of an edge. We reduce the problem of determining Braessian edges in a flow network to a simpler one of determining the flows in the same network topology with a single-source single-sink input. This results in a computational speedup by a factor proportional to the number of edges in the network. More importantly, this approach enables us to obtain a *topological understanding* of which edges are more likely to be Braessian. We use this insight to establish topological classifiers for Braessian edges. Finally, we demonstrate that Braessian edges have a *beneficial effect*: they can be *intentionally damaged* to mitigate overload due to damage at another edge.

6.1 introduction

Braess [32] demonstrated an intriguing phenomena in traffic networks, where opening a new street in a traffic network leads to an *increase* of the travel time for *everyone*. This happened because using the new street was faster for each car compared to all other routes available to it, leading to all cars to use this new street, which had the *collective effect* of increasing travel time for *every car*. In other words, Braess' paradox (BP) was a combined consequence of the network topology (which

allowed high utilization of the newly opened edge to bottleneck the network) and the dynamics (each cars tried to maximize their individual benefits in the *selfish routing strategy*).

Braess' paradox in traffic networks

Subsequently, the topic of BP in selfish routing networks has been extensively explored. Frank [60] presented necessary and sufficient conditions for BP in a 4-node single-source-single-link system, Steinberg and Zangwill [33] as well as Dafermos and Nagurney [34] extended it to general networks. Pas and Principio [35] showed that under non-selfish routing strategies, BP does not occur, however adding a link may lead to no better (nor worse) average performance. Valiant and Roughgarden [61] showed that in large random graphs, BP is not a rare event and it occurs with high probability.

The topic of *preventing* Braess' paradox has been studied in computer networking literature [99, 100] and traffic engineering literature [101]. However, given a flow network, determining which edges would cause BP remains largely unsolved, apart from proofs [99, 100] that certain extremely restricted class of line additions do *not* cause BP, e.g. strengthening (i.e. increasing the edge capacity) the line directly joining the source and sink in a single source/sink network and upgrading all links in a network simultaneously.

Braess' paradox in continuous flow networks

In a *continuous* flow network, e.g. a resistor network conducting electric current or venation networks in plant leaves transporting sap; the dynamics is quite different from routing of discrete entities in street or computer networks. Nevertheless, it has been reported that BP is prevalent in such networks, for example, in electrical circuits with resistors and diodes [102, 103], oscillator networks and models of DC and AC power grid [37, 36] as well as two-dimensional electron systems [104].

Scope and structure of this article

In this context, we ask this question: given a certain continuous flow network, can we predict which edges will exhibit BP without explicitly computing the flows after each edge perturbation? We emphasize that we define Braess' paradox as the *maximum flow* increasing on adding or strengthening an edge, not the *average flow* or *every flow* increasing, in contrast to traffic literature. We do so because increase of maximum flow in a network is known to sometimes cause system wide failures [105], when the initial overload starts a cascade. Coletta and Jacquod [38] showed recently that it is possible to predict whether loads will increase in an oscillator network with one-dimensional chain topology

if a pair of nodes previously unconnected is connected by an edge, from previous steady state phases alone. In the present article, we attack this question in arbitrary topologies and in a wider class of network dynamics that includes both linear flow networks (describing flow of sap in plant leaves and DC flow in a resistor network [14]) and Kuramoto oscillator networks (used to model AC power transmission grid [19]).

In section 6.2, we provide a mathematical definition of BP in a class of flow networks we call "conservative flow networks" and derive an exact mapping between the problem of detecting Braessian edges in a network and the problem of finding steady flows in a linear flow network due to single dipole source (continuous version of which is familiar from electrostatics). In section 6.3, we define an intuitive topological notion of *flow alignment* and demonstrate that edges with flows aligned to the maximally loaded edge are more likely to exhibit BP. In section 6.4, we demonstrate that Braess' paradox has a useful side effect: they can be *intentionally damaged* to reverse an overload caused by damage at another edge.

6.2   NETWORK SUSCEPTIBILITY AND BRAESS' PARADOX

This study on Braess' paradox will be limited to *conservative flow networks* as per definition 2.2.4. Such systems include *linear systems* such as electrical DC flow across a resistor network, flow of water in hydraulic tubes, as well as flow of fluid in venation network in plant leaves [14, 18], as well as *nonlinear systems* such as networks of Kuramoto oscillators [1] as well as the *swing equation model* [19] of electrical AC transmission grid.

We will now define Braess' paradox on such systems, and derive an exact mapping from the problem of finding Braessian edges to the problem of finding steady flows in a linear flow network with a single dipole source.

6.2.1   *Mathematical background*

We introduced the concept on network susceptibilities in [106] to quantify the effect on steady state flows in a flow network (defined in section 2.2) on infinitesimally increasing the weight of an edge. We will now define Braess' paradox in terms of network susceptibilities.

Definition 6.2.1 (Edge-to-edge susceptibility). *Consider a flow network* $(G(\mathbb{V}, \mathbb{E}), I, \mathcal{F})$ *with steady state flows* F_{ij} *for all* $\{i, j\} \in \mathbb{E}$. *Suppose on increasing the weight of a single edge* $\mu := \{s, t\}$ *from* K_{st} *to* $K_{st} + \kappa$, *the steady state flows of another edge* $\nu := \{i, j\}$ *becomes* F'_{ij}. *Then the edge-to-edge susceptibility is defined as*

$$\eta_{\mu \to \nu} := \lim_{\kappa \to 0} \frac{F'_\nu - F_\nu}{\kappa} = \frac{dF_\nu}{dK_\mu} = \frac{dF_{ij}}{dK_{st}}. \tag{6.1}$$

Definition 6.2.2 (Braessian edge). *Consider a flow network $(G, \boldsymbol{I}, \mathcal{F})$. Suppose the maximum absolute flow is across the edge α*

$$\max_{e \in \mathbb{E}} |F_e| = |F_\alpha|.$$

*Then an edge μ is called a **Braessian edge** (BE) if and only if an infinitesimal increase in the weight of edge μ increases the absolute value of the maximal flow F_α*

$$F_\alpha \eta_{\mu \to \alpha} > 0. \tag{6.2}$$

Determining all BE's in a network by Eq. (6.2) requires computing the flow derivatives in Eq. (6.1) $|\mathbb{E}|$ times. We will now establish an equivalent dual problem (that can be solved much faster) exploiting a symmetry property of edge-to-edge susceptibilities for conservative flow networks.

6.2.2 *Edge-to-edge susceptibility in a conservative flow network*

Consider a conservative flow network $(G, \boldsymbol{I}, \mathcal{F})$. Due to the flow conservation property Eq. (2.15), and the flow equation Eq. (2.10), the flows at the edges must satisfy

$$\forall 1 \le j \le |\mathbb{V}|, \quad 0 = I_j + \sum_i K_{ij} f(\varphi_i - \varphi_j). \tag{6.3}$$

Suppose on increasing the weight of a single edge $\mu = \{s, t\}$ by κ, the steady state vertex properties φ_j changes to $\varphi_j + \xi_j$. Then the new flows must still satisfy

$$
\begin{aligned}
0 =& I_j + \sum_i \left(K_{ij} + \kappa \delta_{si} \delta_{tj} + \kappa \delta_{sj} \delta_{ti} \right) f(\varphi_i - \varphi_j + \xi_i - \xi_j) \\
=& I_j + \kappa \delta_{tj} f(\varphi_s - \varphi_j) + \kappa \delta_{sj} f(\varphi_t - \varphi_j) + \sum_i \left\{ K_{ij} \left(f(\varphi_i - \varphi_j) \right. \right. \\
& \left. \left. + f'(\varphi_i - \varphi_j)(\xi_i - \xi_j) \right) \right\} + \mathcal{O}\left((\xi_i - \xi_j)^2 \right).
\end{aligned}
\tag{6.4}
$$

Subtracting Eq. (6.3):

$$
\begin{aligned}
0 =& \kappa \delta_{tj} f(\varphi_s - \varphi_j) + \kappa \delta_{sj} f(\varphi_t - \varphi_j) + \sum_i K_{ij} f'(\varphi_i - \varphi_j)(\xi_i - \xi_j) \\
& + \mathcal{O}\left((\xi_i - \xi_j)^2 \right).
\end{aligned}
\tag{6.5}
$$

We will now recast Eq. (6.5) in a form that is both more intuitive and mathematically enlightening.

Definition 6.2.3 (Meta graph). *Given a flow network $(G, \boldsymbol{I}, \mathcal{F})$ with flows F_{ij} for all edges $\{i, j\} \in \mathbb{E}$, a meta graph $\widetilde{G}$ is a graph with edge set $\mathbb{E}$ and vertex set $\mathbb{V}$, with edge weights given by*

$$\widetilde{K_{ij}} = K_{ij} f'(\varphi_i - \varphi_j). \tag{6.6}$$

We note that $\widetilde{K}_{ij} = \widetilde{K}_{ji}$ because f' is an even function due to f being odd. Furthermore, due to f being monotonically increasing function, $\widetilde{K}_{ij} \geq 0$. Therefore $\widetilde{G}$ is a valid weighted undirected graph with non-negative weights.

Let $\widetilde{L}$ be the Laplacian matrix (see definition 2.1.12) of the meta graph $\widetilde{G}$ of the original graph G, and M be incidence matrix (see definition 2.1.11) of G and assume the edge $\{s, t\}$ to be perturbed is the μ'th one in the edge ordering considered while constructing M.

Then Eq. (6.5) can be rewritten as

$$
\begin{aligned}
\widetilde{L}_{ij}\xi_j &= -\kappa \frac{F_{st}}{K_{st}} \left(\delta_{is} - \delta_{it} \right) \\
\widetilde{L}_{ij}\frac{d\varphi_j}{dK_{st}} &= \widetilde{L}_{ij} \lim_{\kappa \to 0} \frac{\xi_j}{\kappa} \\
&= -\frac{F_{st}}{K_{st}} \left(\delta_{is} - \delta_{it} \right).
\end{aligned}
\tag{6.7}
$$

This allows us to reformulate the edge to edge susceptibilities Eq. (6.1) as

$$
\begin{aligned}
\eta_{(s,t)\to(j,l)} &= \frac{dF_{jl}}{dK_{st}} = K_{jl} \left(\frac{d\varphi_l}{dK_{st}} - \frac{d\varphi_j}{dK_{st}} \right), \\
\widetilde{L}_{ij}\frac{d\varphi_j}{dK_{st}} &= -\frac{F_{st}}{K_{st}} \left(\delta_{is} - \delta_{it} \right).
\end{aligned}
\tag{6.8}
$$

We will now demonstrate that the edge-to-edge susceptibilities $\eta_{(s,t)\to(j,l)}$ given by Eq. (6.8) are equal to the flows in a *linear flow network* with a dipole source placed across the same edge $\{s, t\}$.

CONNECTION TO STEADY FLOWS IN LINEAR FLOW NETWORKS WITH DIPOLE SOURCE

Lemma 6.2.1. *Given a conservative flow network $(G, \boldsymbol{I}, \mathcal{F})$ with flows F_μ for all edges $\mu \in \mathbb{E}$, suppose the flows across a particular edge $\alpha := \{a, b\}$ is directed from a to b.*

Consider a linear flow network $\left(\widetilde{G}, \boldsymbol{I}_{a,b}^{dipole}, \mathcal{F}^{linear} \right)$ consisting of the meta graph $\widetilde{G}$ (see definition 6.2.3) with a single dipole input F_{ab}/K_{ab} at node b and $-F_{ab}/K_{ab}$ at node a. Then the flows $\widetilde{F}_\nu$ at this flow network are equal to the edge-to-edge susceptibilities $\eta_{\alpha \to \nu}$ in the original flow network $(G, \boldsymbol{I}, \mathcal{F})$ for all $\nu \neq \alpha$. An illustration is provided in Figure 6.1.

Proof. For the linear flow network $\left(\widetilde{G}, \boldsymbol{I}_{a,b}^{\text{dipole}}, \mathcal{F}^{\text{linear}} \right)$, the flow conservation condition Eq. (6.3) becomes

$$
\begin{aligned}
\forall 1 \leq j \leq |\mathbb{V}|, \quad 0 &= \left(\delta_{jb} - \delta_{ja} \right) \frac{F_{ab}}{K_{ab}} + \sum_i \widetilde{K}_{ij}(\varphi_i - \varphi_j) \\
\Rightarrow \widetilde{L}_{ij}\varphi_j &= -\frac{F_{ab}}{K_{ab}} \left(\delta_{ja} - \delta_{jb} \right) \\
\widetilde{F}_{jl} &= \widetilde{K}_{jl} \left(\varphi_l - \varphi_j \right).
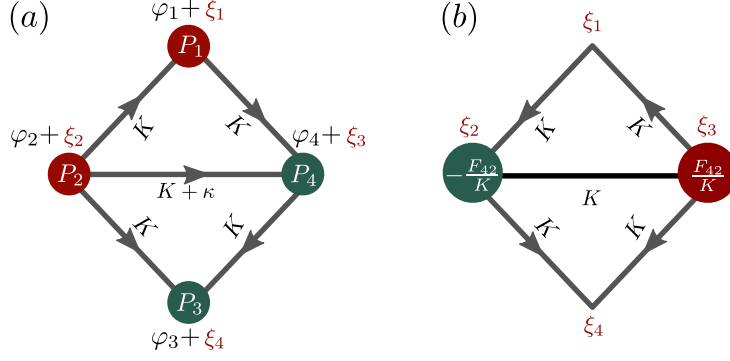\end{aligned}
\tag{6.9}
$$

Figure 6.1: Infinitesimally strengthening an edge in a conservative flow network leads to flow changes at other edges. This incremental change is identical to flows *only due to* a dipole placed across the perturbed edge in a *linear* flow network. Note that the flow change at the *strengthened edge* is an exception.

Comparing Eq. (6.9) with Eq. (6.8), the lemma follows.   □

The consequence of this connection is twofold: firstly, it means understanding the incremental flow change in *any conservative flow network* with *arbitrary inputs* due to infinitesimal strengthening an edge is equivalent to understanding the flow patterns of a *linear* flow network with a single *dipole inputs*: a problem that is well understood in the continuum limit in electrostatics. Secondly, and more relevant to the goal of predicting Braess' paradox, this enables us to exploit a powerful symmetry: flow at an edge $\{i, j\}$ due to dipole current source across edges $\{s, t\}$ is the same as the flow at edge $\{s, t\}$ due to the source across edge $\{i, j\}$. We will now state this symmetry in a precise form and show how this symmetry eases the computational complexity of determining Braessian edges.

Theorem 6.2.1. *Given a flow network* $(G, \mathbf{I}, \mathcal{F})$ *and two specific edges* $\mu := \{s, t\}$ *and* $\nu := \{i, j\}$,

$$F_\nu \frac{dF_\nu}{dK_\mu} = c_{\mu\nu} F_\mu \frac{dF_\mu}{dK_\nu} \tag{6.10}$$
$$c_{\mu\nu} > 0.$$

Proof. Since if $\mu = \nu$, the theorem is vacuously true, we subsequently make the assumption that $\mu \neq \nu$. First we rewrite the edge-to-edge susceptibility from Eq. (6.1) by writing

$$\eta_{\mu \to \nu} = \frac{dF_\nu}{dK_\mu} \tag{6.11}$$

$$= \frac{d}{dK_{st}} K_{ij} f(\varphi_j - \varphi_i) \tag{6.12}$$

$$= K_{ij} f'(\varphi_j - \varphi_i) \left(\frac{d\varphi_j}{dK_{st}} - \frac{d\varphi_i}{dK_{st}} \right) \tag{6.13}$$

$$= \widetilde{K}_\nu \left(\frac{d\varphi_j}{dK_\mu} - \frac{d\varphi_i}{dK_\mu} \right) \tag{6.14}$$

$$= \frac{F_\mu}{K_\mu^2} \widetilde{K}_\nu \left(\widetilde{L}_{ik}^+ M_{k\mu} - \widetilde{L}_{jk}^+ M_{k\mu} \right) \tag{6.15}$$

$$= \frac{F_\mu}{K_\mu^2} \frac{\widetilde{K_\nu}}{K_\nu} M_{l\nu} \widetilde{L}_{lk}^+ M_{k\mu} \quad \text{[using Eq. (6.8), see Appendix 6.A]} \tag{6.16}$$

$$= \frac{F_\mu}{K_\mu^2} \frac{\widetilde{K_\nu}}{K_\nu} \left[M^T \widetilde{L}^+ M \right]_{\nu\mu} \tag{6.17}$$

$$:= \frac{F_\mu}{K_\mu^2} \frac{\widetilde{K_\nu}}{K_\nu} \Xi_{\nu\mu} \tag{6.18}$$

Now we will exploit the fact that Ξ is a symmetric matrix (proof in lemma 6.A.1) to arrive at our result.

From Eq. (6.18), we obtain

$$F_\nu \frac{dF_\nu}{dK_\mu} = F_\nu \frac{F_\mu}{K_\mu^2} \frac{\widetilde{K_\nu}}{K_\nu} \Xi_{\nu\mu} \tag{6.19}$$

$$F_\mu \frac{dF_\mu}{dK_\nu} = F_\mu \frac{F_\nu}{K_\nu^2} \frac{\widetilde{K_\mu}}{K_\mu} \Xi_{\mu\nu} \tag{6.20}$$

$$\Rightarrow F_\nu \frac{dF_\nu}{dK_\mu} = c_{\mu\nu} F_\mu \frac{dF_\mu}{dK_\nu} \tag{6.21}$$

$$c_{\mu\nu} = \frac{K_\nu}{K_\mu} \frac{\widetilde{K_\nu}}{\widetilde{K_\mu}} \tag{6.22}$$

In arriving at Eq. (6.21), we have utilized $\Xi_{\mu\nu} = \Xi_{\nu\mu}$. The monotonicity of f as per Eq. (2.14) guarantees that $c_{\mu\nu} > 0$. The theorem follows. $\square$

Corollary 6.2.1. *Given a flow network $(G, I, \mathcal{F})$, if an infinitesimal increase in weight of edge μ leads to increase in flow in edge ν, then an infinitesimal increase in weight of edge ν would lead to an increase in flow at edge μ.*

Proof. From theorem 6.2.1, we get

$$F_\nu \frac{dF_\nu}{dK_\mu} \gtreqqless 0 \Leftrightarrow F_\mu \frac{dF_\mu}{dK_\nu} \gtreqqless 0. \tag{6.23}$$

The corollary follows. $\square$

Corollary 6.2.2. *Suppose $(G, I, \mathcal{F})$ is a flow network with flows F_μ across each edge $\mu \in \mathbb{E}$. Let the maximum flow be along the edge $\alpha := \{a, b\}$, directed from node a to node b. Denote the set of all Braessian edges in this flow network by $\mathbb{E}_{BE}$. Let $\widetilde{F}_\mu$ for all $\mu \in \mathbb{E}$ be the flows in a linear flow network $\left(\widetilde{G}, I_{a,b}^{dipole}, \mathcal{F}^{linear} \right)$ consisting of the meta graph of G and a single dipole inputs of F_{ab}/K_{ab} at node b and $-F_{ab}/K_{ab}$ at node a. Then $\mu \in \mathbb{E}_{BE}$ if and only if $\widetilde{F}_\mu F_\mu > 0$.*

Proof. Connecting the definition 6.2.2 of Braessian edges, and corollary 6.2.1, we see that μ is Braessian if and only if

$$F_\alpha \frac{dF_\alpha}{dK_\mu} > 0 \Leftrightarrow F_\mu \frac{dF_\mu}{dK_\alpha} > 0. \tag{6.24}$$

Lemma 6.2.1 tells that $\frac{dF_\mu}{dK_\alpha}$ is equal to the flow $\widetilde{F}_\mu$ in the linear flow network $\left(\widetilde{G}, \boldsymbol{I}_{a,b}^{\mathrm{dipole}}, \mathcal{F}^{\mathrm{linear}} \right)$. The Lemma follows. $\qquad\square$

6.2.3 *Efficient algorithm for predicting Braessian edges*

Determining which edges in a flow network is Braessian by brute force requires solving the steady state flows $|\mathbb{E}|$ times: once after increasing one edge weight (alternatively, one can determine them by computing the PTDF matrix [107], which involves computing a Moore-Penrose pseudoinverse). We will now construct an efficient algorithm, based on corollary 6.2.2, to determine *all* BE's in a flow network by solving the steady state flows only *once*, in addition to the original steady flow computations.

Algorithm

DATA: A flow network $(G, \boldsymbol{I}, \mathcal{F})$ with flows F_α for all $\alpha \in \mathbb{E}$.

RESULT: The set of $\mathbb{E}_{\mathrm{BE}}$ of all Braessian edges in the network.

STEP 1: Determine the edge $\nu = \{s, t\}$ with maximum absolute flow

$$|F_\nu| = \max_{\alpha \in \mathbb{E}} |F_\alpha|.$$

STEP 2: Determine the sign of edge susceptibilities $\mathrm{sgn}\left(\frac{dF_{ij}}{dK_{st}} \right)$ using Eq. (6.8)

$$\widetilde{L}_{ij} \frac{d\varphi_j}{dK_{st}} = -\frac{F_{st}}{K_{st}} (\delta_{is} - \delta_{it})$$

$$\frac{dF_{ij}}{dK_{st}} = \widetilde{K}_{ij} \left(\frac{d\varphi_j}{dK_{st}} - \frac{d\varphi_i}{dK_{st}} \right)$$

$$\mathrm{sgn}\left(\frac{dF_{ij}}{dK_{st}} \right) = \mathrm{sgn}\left(\frac{d\varphi_j}{dK_{st}} - \frac{d\varphi_i}{dK_{st}} \right)$$

STEP 3: $\mathbb{E}_{\mathrm{BE}} = \left\{ \{i, j\} \in \mathbb{E} \quad |\mathrm{sgn}\left(\frac{dF_{ij}}{dK_{st}} \right) = \mathrm{sgn}\left(F_{ij} \right) \right\}.$

We demonstrate in Figure 6.2 that this algorithm indeed accurately predicts all Braessian edges (BE's) in a linear network.

Corollary 6.2.3. *In a linear flow network with a single dipole current injection, no edge is Braessian.*
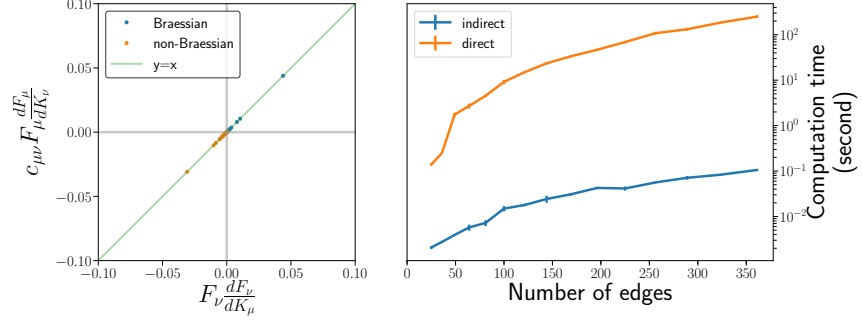
Figure 6.2: (left) Determining Braessian edges in a linear flow network by computing $F_\nu \frac{dF_\nu}{dK_\mu}$ by the efficient way Eq. (6.10) yields results identical to the brute force calculations. ν is the most heavily loaded edge. The x-axis shows direct computation and the y-axis the indirect one. Blue dots represent Braessian edges, green dots non-Braessian ones. Computation done on a 10×10 square lattice network, with 25 randomly chosen sources and 25 randomly chosen sinks. (right) The indirect method for computing Braessian edges is much faster than the direct brute force method. For each network size, 10 independent runs were made. Error bars depict standard deviations.

Proof. Suppose the current inputs are $+I$ and $-I$ at nodes s and t respectively, and zero otherwise. Then the steady state flows are given by Eq. (6.8),

$$
\begin{aligned}
L_{ij}\varphi_j &= I\left(\delta_{is} - \delta_{it}\right) \\
F_{ij} &= K_{ij}\left(\varphi_j - \varphi_i\right).
\end{aligned}
\tag{6.25}
$$

The maximum flow, obviously, will be along the edge $\{s, t\}$. Now,

$$
\begin{aligned}
\widetilde{L}_{ij}\frac{d\varphi_j}{dK_{st}} &= -\frac{F_{st}}{K_{st}}\left(\delta_{is} - \delta_{it}\right) \\
\frac{dF_{ij}}{dK_{st}} &= \widetilde{K_{ij}}\left(\frac{d\varphi_j}{dK_{st}} - \frac{d\varphi_i}{dK_{st}}\right) \\
&= -\frac{\widetilde{K_{ij}}}{K_{ij}}\frac{F_{st}}{K_{st}}F_{ij}
\end{aligned}
\tag{6.26}
$$

$$
\Rightarrow F_{ij}\frac{dF_{ij}}{dK_{st}} \geq 0
$$

$$
\Rightarrow F_{st}\frac{dF_{st}}{dK_{ij}} \geq 0 \quad \text{(using corollary 6.2.1)}.
$$

Comparing Eq. (6.26) with definition 6.2.2, the corollary follows. $\square$

6.3   TOPOLOGICAL FEATURES BEHIND BRAESS' PARADOX

So far, we have established that determining Braessian edges (BE's) on infinitesimally strengthening an edge in a conservative flow network

is equivalent to evaluating flows in a *linear* flow network with a single dipole source. Establishing this equivalence has enabled us to formulate an efficient algorithm that determines BE's in a network much faster than brute force computation, as illustrated in Figure 6.2. Now we will aim at understanding which *topological features* causes certain edges to be Braessian.
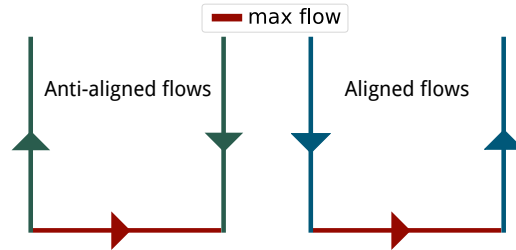

Figure 6.3: Notion of flow alignment in flow networks. (left) the vertical edges are anti-aligned to the maximally loaded (red) edge. (right) the vertical edges are aligned to the maximally loaded edge. We hypothesize that edges flow aligned to the maximally loaded edge are more likely to be Braessian.

We will presently introduce a notion of *flow alignment* between any two pairs of edges in a flow network, illustrated in Figure 6.3. We hypothesize that if the maximum flow is from node a to node b, then the edges $\{i,j\}$ which are *flow aligned* to the maximally loaded edge $\{a,b\}$ are more likely to be Braessian. We will presently motivate this hypothesis. Suppose the flow across an edge $\{a,b\}$ is directed from a to b. If the capacity of this edge is increased, keeping all other edge capacities constant, we expect that there will be *more flow* from a to b. This "excess" flow must come from and go to the neighbouring edges, to satisfy the flow conservation condition Eq. (2.15). If the edge $\{a,b\}$ is anti-aligned to the maximally loaded edge (e.g. the left panel in Figure 6.3), the excess flow across $\{a,b\}$ will *reduce* the flow at the maximally loaded edge. However, if the edge $\{a,b\}$ is aligned to the maximally loaded edge (e.g. the right panel in Figure 6.3), the excess flow across $\{a,b\}$ will *flow into* the maximally loaded edge, causing BP.

If our hypothesis is true, predicting Braessian edges in a network boils down to finding a suitable definition of flow alignment. We first provide a very intuitive definition of flow alignment in section 6.3.1, which turns out to be accurate at predicting Braessian edges close to the maximally loaded edge, but less accurate for edges further away. Then we propose two more advanced definitions in section 6.3.2 and 6.3.3 that overcome this shortcoming, but have disadvantages of their own.

6.3.1   *Classifier based on edge distance*

Definition 6.3.1 (Flow alignment by edge distance). *Consider a connected and simple flow network* $\mathbb{F} = (G, \mathbf{I}, \mathcal{F})$. *For each edge* $e := \{i, j\}$, *let's define* i *to be the "head" and* j *to be the "tail" if and only if* $F_{ij} > 0$. *Let* $d(s, t)$ *be the shortest path length between nodes* s *and* t. *Label the edge set so that for all edges* $\{i, j\}$, $F_{ij} > 0$.

Then $\{h_1, t_1\}$ *is defined to be aligned to the edge* $\{h_2, t_2\}$

$$\{h_1, t_1\} \rightrightarrows \{h_2, t_2\} \tag{6.27}$$

if

$$\min\{d(h_1, t_2), d(t_1, h_2)\} < \min\{d(h_1, h_2), d(t_1, t_2)\}. \tag{6.28}$$

Likewise, $\{h_1, t_1\}$ *is defined to be anti-aligned to the edge* $\{h_2, t_2\}$

$$\{h_1, t_1\} \rightleftarrows \{h_2, t_2\} \tag{6.29}$$

if

$$\min\{d(h_1, t_2), d(t_1, h_2)\} > \min\{d(h_1, h_2), d(t_1, t_2)\}. \tag{6.30}$$

We illustrate this definition in Figure 6.4.

We note that given two edges, one might neither be aligned nor be anti-aligned, according to this definition.
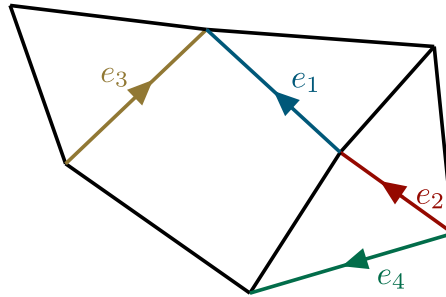

Figure 6.4: Aligned and non-aligned flows, as defined in definition 6.3.1. e_2 and e_3 are respectively aligned and anti-aligned to e_1. Flow alignment is undefined between e_4 and e_1.

Claim 6.3.1. *If an edge* $\{i, j\}$ *is aligned to the edge* $\{s, t\}$ *with maximum flow in a network, then* $\{i, j\}$ *is more likely to be a BE. If it is anti-aligned, then it is less likely to be a BE.*

We show the effectiveness of this classifier in Figure 6.5 in two network topologies: a 30×30 square lattice, and Voronoi tessellation of 20 uniformly randomly drawn points from a unit square. In both topologies, 1/4th of the nodes were chosen to have inputs 1 and an equal
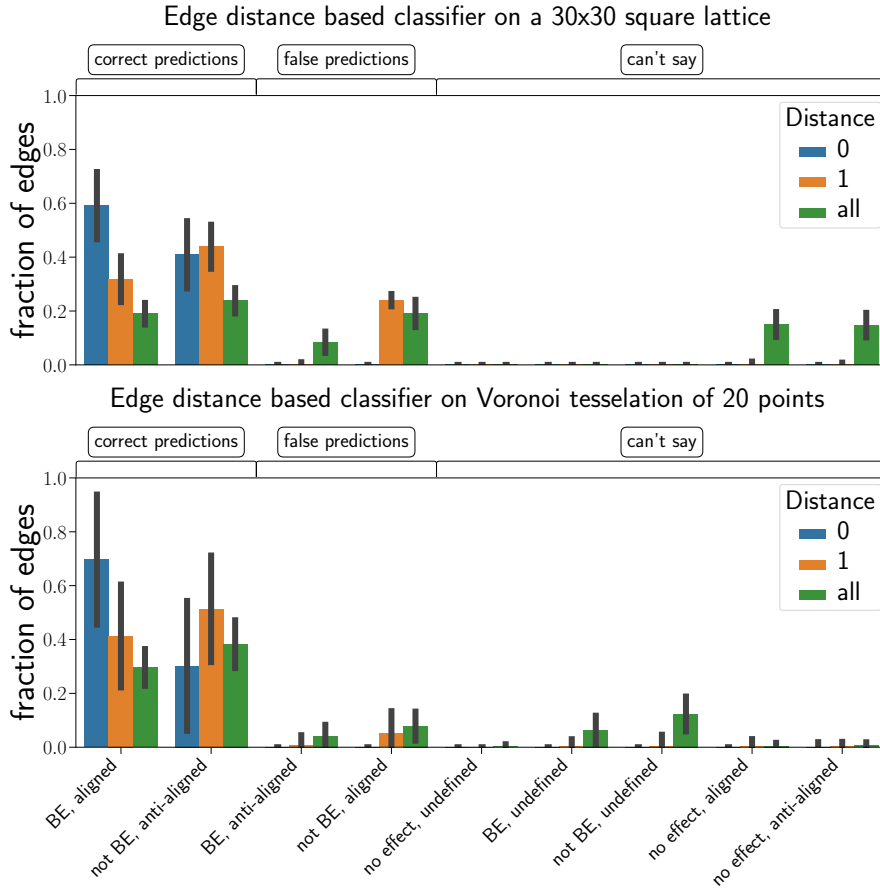
Figure 6.5: The flow alignment based classifier as per claim 6.3.1 works well for edges close to the edge with maximum flow, but worsens with distance. Classifier was tested in two network topologies: 15×15 square lattice and Voronoi tessellation of 20 uniformly randomly chosen points in the unit square. In each case 200 independent runs were made. Error bars display the standard deviations. Edges with susceptibilities $\leq 10^{-5}$ were assumed to have no effect on the maximally loaded edge.

number to have inputs -1. The rest of the nodes had inputs 0. In both topologies, 200 independent realizations were made. The edges with

$$\eta_{\mu \to \alpha} < \varepsilon = 10^{-5}, \tag{6.31}$$

we considered to have too little effect on the maximally loaded edge α to be called wither BE or not BE. We clearly see that for edges with distance < 2 from the maximally loaded edge, the classifier is quite accurate: there are very few edges that are not aligned, yet BE or aligned, yet not BE. The accuracy of this predictor worsens, however, for edges with distance ≥ 2 from the maximally loaded edge.

6.3.1.1 *Reason behind false predictions in Topological classifier*

We have seen that the edge distance based classifier fails for a significant fraction of edges. Now we investigate for which edges this classifier fails. In Figure 6.6, we illustrate the edges for which the classifier fails in a
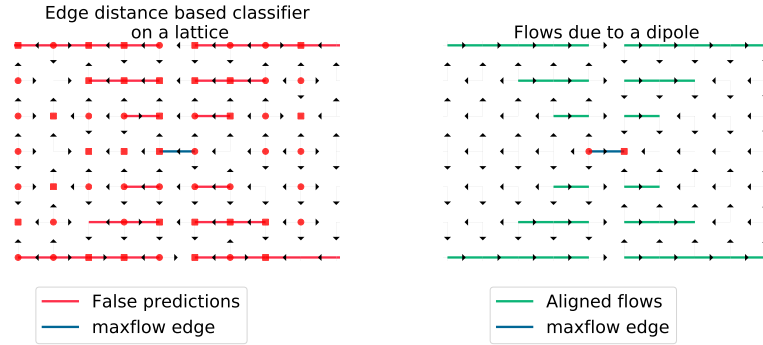

Figure 6.6: (left) Illustrating which edges are falsely classified by the edge distance based classifier (we set the threshold ε as per Eq. (6.31) to 0). A region centered around the maximally loaded edge is shown. (right) In purely dipole flows, the same edges happen to be aligned with the dipole.

square lattice network. We see that these edges have one property in common: they have *aligned flows due to a purely dipole source term.* Lemma 6.2.1 then explains why our classifier fails at those edges. Only those edges are Braessian, whose flows are in the same direction as the flow would have been, if all the inputs were set to zero and a single dipole were placed across the maximally loaded edge. The flow alignment based classifier assumes the wrong direction to this dipole flow on those edges, and consequently wrongly predicts Braessian edges.

6.3.2 *Classifier based on cycle distance*

Now that we know why our classifier performed poorly at certain edges, we can build a better one by defining another way of computing align-

ment of flows, according to which flows due to a single dipole are more likely to be anti-aligned. Now we will present one such way of computing alignments of flows by replacing edge distances in definition 6.3.1 by a certain "cycle distance". In order to do that, we must define a couple of graph theoretic quantities.
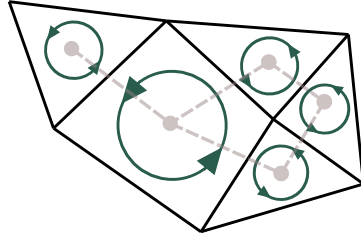

Figure 6.7: A planar graph (solid edges) and its dual (dashed edges, filled circular nodes) corresponding to this specific embedding.

Definition 6.3.2. *Dual graph*
Given a planar graph $G(V, E)$ and an embedding, we choose a cycle basis B_C consisting of the faces of the embedding. The dual graph G_D is a undirected multigraph whose vertex set is equal to B_C. Its edge set E' is as follows. For each edge $e \in E$, if it is shared between two cycles c_1 and c_2, then an edge between c and c' is added to E'. We illustrate this definition in Figure 6.7.

Definition 6.3.3 (Cycle distance). *Given two cycles c_1 and c_2 in the cycle basis B_C of a graph G, the* cycle distance *between them $d_{cycle}(c_1, c_2)$ is simply the shortest path length in the dual graph between the nodes c_1 and c_2.*
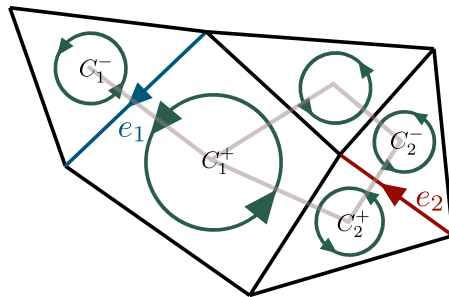

Figure 6.8: Defining alignment of flows, according to cycle distance. The cycles $C_{1/2}^+$ are flow-oriented to the flows in edges $e_{1/2}$, and cycles $C_{1/2}^+$ are anti flow-oriented to the flows in edges $e_{1/2}$. As a result, e_1 and e_2 are flow aligned by cycle distance, because C_2^+ and C_1^+ are only one hop away, less than all other pairs.

Definition 6.3.4 (Flow-cycle alignment). *Consider a connected, simple,* planar *flow network* $\mathbb{F} = (G, \boldsymbol{I}, \mathcal{F})$ *in a specific plane embedding.*

Let G_D be the dual graph for this embedding. For each edge $e := \{i, j\}$, let's define i to be the "head" and j to be the "tail" when $F_{ij} > 0$. The edge e is defined to be flow oriented *to a cycle c containing e if the cycle, when traversed in the anti-clockwise direction, encounters i before j. Otherwise, e is said to be* anti flow-oriented *to c.*

Definition 6.3.5 (Flow alignment by cycle distance). *Consider a connected, simple,* planar *flow network* $\mathbb{F} = (G, \boldsymbol{I}, \mathcal{F})$ *in a specific plane embedding and let G_D be the dual graph for this embedding. For each edge e, denote the cycle (if it exists) it is flow aligned to by C_e^+ and the cycle (if it exists) it is anti flow-oriented to by C_e^-.*

Then two edges e_1 and e_2 are said to be aligned(anti-aligned) by cycle distance if and only if

$$\min\{d_{cycle}\left(C_1^+, C_2^+\right), d_{cycle}\left(C_1^-, C_2^-\right)\} \\ \gtrless \min\{d_{cycle}\left(C_1^+, C_2^-\right), d_{cycle}\left(C_1^-, C_2^+\right)\}. \tag{6.32}$$

If either C_j^+ or C_j^- does not exist, then all terms in the min *function containing it is omitted. If both C_j^+ and C_j^- does not exist, flow alignment by cycle distance between them is undefined. We illustrate this definition in Figure 6.8.*

We evaluate the performance of this cycle-distance based classifier in Figure 6.9, again in two topologies: square lattice and Voronoi tessellations of uniformly randomly drawn points in $\mathbb{R}^2$, for the same flow network realizations we tested the edge distance based classifier at (see Figure 6.5). We see that for this classifier, the robustness of the classification does not drop as much with distance as the edge distance based classifier did. However, for Voronoi planar graphs, it fails to classify more number of edges than the edge distance based one.

A crucial disadvantage of the cycle distance based classifier is that it is applicable only to planar graphs. This is so because the notion of flow cycle alignment in definition 6.3.4 cannot be defined for non-planar graphs. We will now discuss yet another classifier, which overcomes this restriction, at the same time being no less accurate than the cycle distance based classifier for plane networks.

6.3.3   Flow rerouting classifier

Definition 6.3.6 (Rerouting alignment). *Given a flow network $(G(\mathbb{V}, \mathbb{E}), \boldsymbol{I}, \mathcal{F})$, consider two edges $e_1 := \{s, t\}$ and $e_2 := \{m, n\}$. Assume without loss of generality that $F_{st} > 0, F_{mn} > 0$. Then e_2 is defined to be aligned(anti-aligned) by flow rerouting to e_1 if and only if in the shortest simple path from s to t not containing $\{s, t\}$ but containing $\{m, n\}$, m appears before(after) n. This is illustrated in Figure 6.10.*

We evaluate the performance of this flow rerouting based classifier in Figure 6.11, the networks being identical to the ones considered for
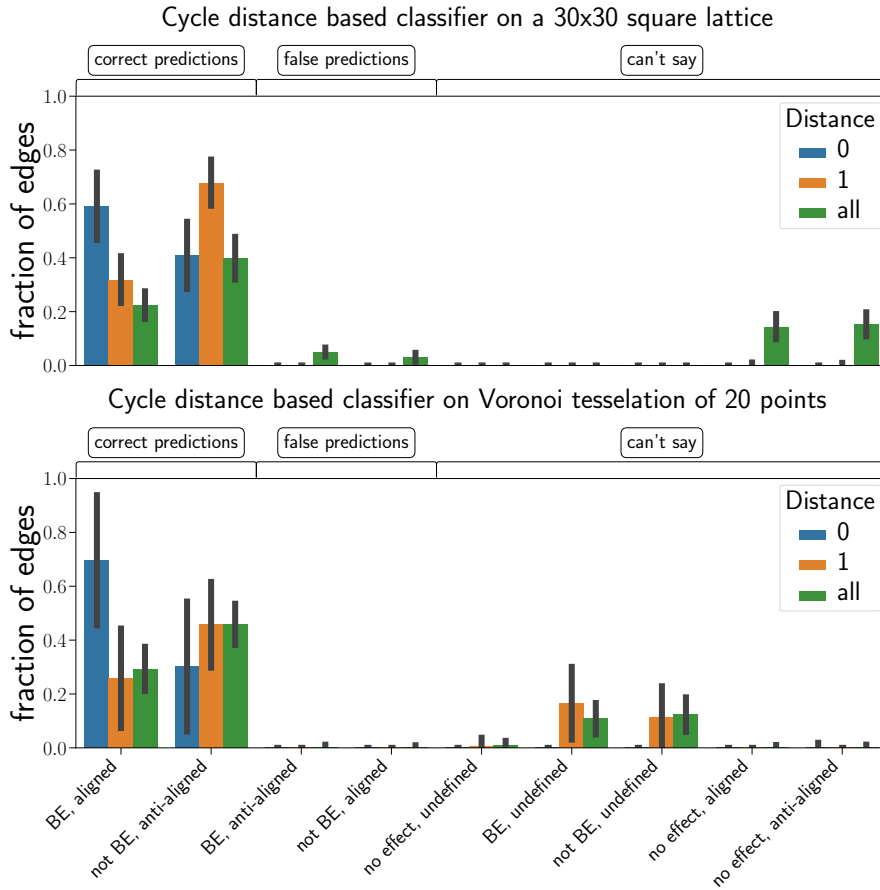
Figure 6.9: The cycle distance based flow alignment (see definition 6.3.5) classifies Braessian edges much better than the edge distance based classifier (see Figure 6.5), especially at distances larger than 1. Classifier was tested in two network topologies: 15×15 square lattice and Voronoi tessellation of 20 uniformly randomly chosen points in the unit square. In each case 200 independent runs were made.
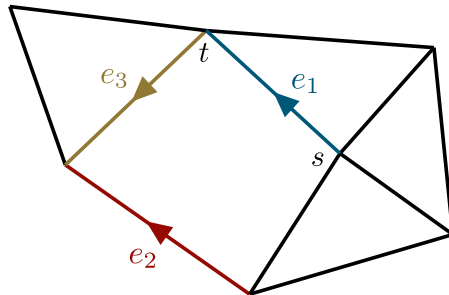
Figure 6.10: Defining alignment of flows, according to flow rerouting. Edge e_2 is flow aligned to e_1 because the shortest path from s to t involving e_2 traverses e_2 in the same direction as its flow. For the same reason, e_3 is anti-aligned to e_1.

Figure 6.11: Flow rerouting based alignment (see definition 6.3.6) classifies Braessian edges better than both the edge distance based one and the cycle distance based one. Classifier was tested in two network topologies: 15×15 square lattice and Voronoi tessellation of 20 uniformly randomly chosen points in the unit square. In each case 200 independent runs were made.
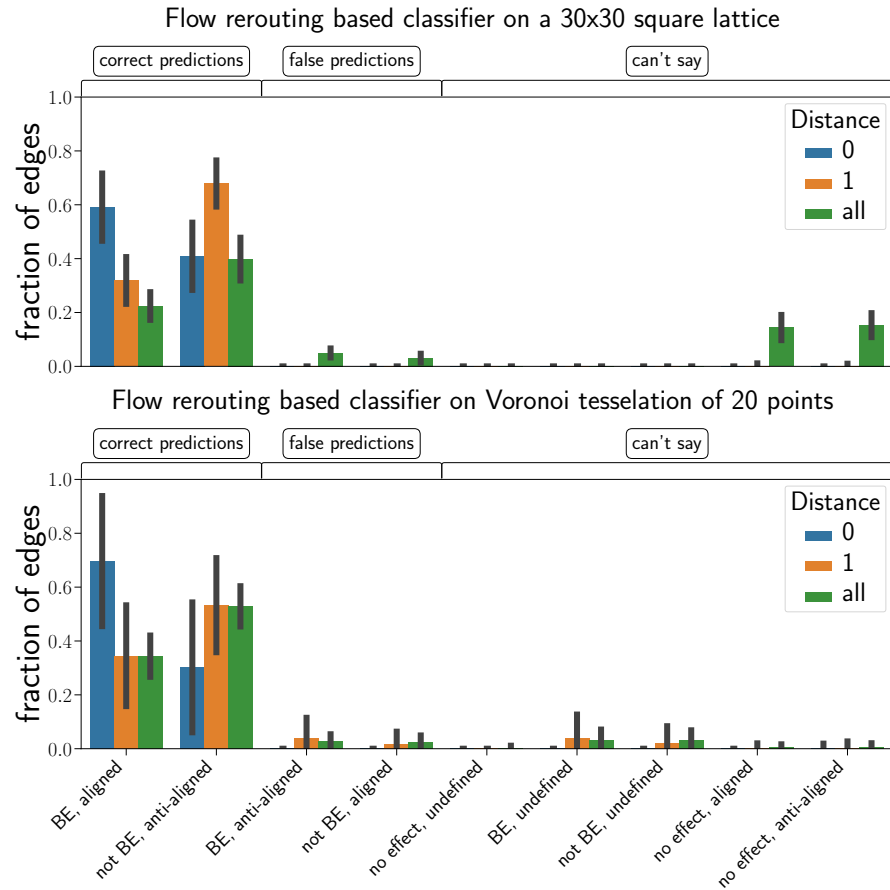
testing the other two classifiers in Figure 6.5 and Figure 6.9. We see that this classifier performs better than the edge distance based one in both lattice and Voronoi graph topologies. Compared to the cycle distance based one, it performs equally well.

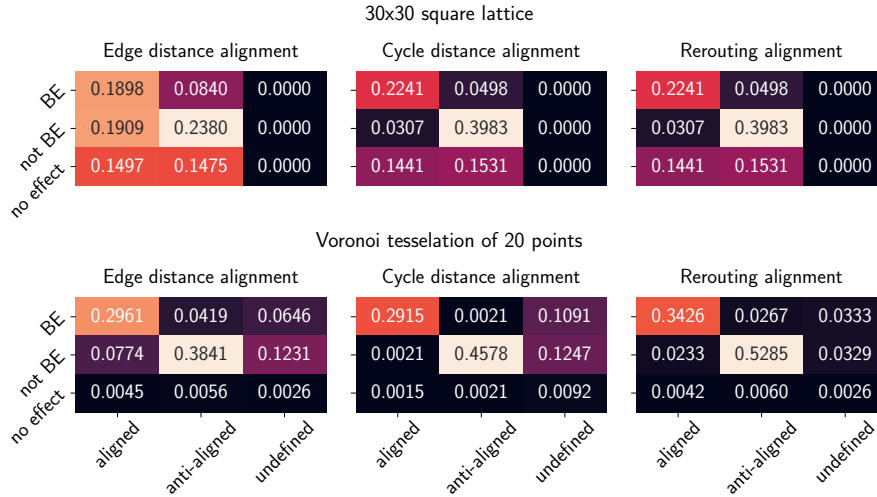### 6.3.4 *Comparison between classifiers*

Figure 6.12: Comparison of accuracies of three classifiers in predicting Braessian edges in two topologies, 15×15 square lattice and Voronoi tessellation of 20 uniformly randomly chosen points in the unit square. In each case 200 independent runs were made.

In Figure 6.12, we illustrate comparative performances of all the three classifiers in two different network topologies: square lattices and Voronoi planar graphs. We observe that for lattice topology, the edge distance classifier suffers from significant false predictions. The cycle distance classifier and the rerouting classifier works equally well, with very little false predictions.

For Voronoi tessellations, the performances are more even across classifiers. The edge distance based classifier fares almost on par with the other two, however the cycle distance classifier and rerouting classifier both perform slightly better still. The cycle distance based classifier has slightly less false predictions than the rerouting based one, but it fails to classify (due to alignment being undefined) more edges than the rerouting based one.

6.3.5 *Effect of distance on classifier accuracy*

We have already seen in Figures 6.5, 6.9 and 6.11 that all three classifiers work well for edges at distances < 2 from the maximally loaded edge, and their accuracies decrease for edges that are further away. Now
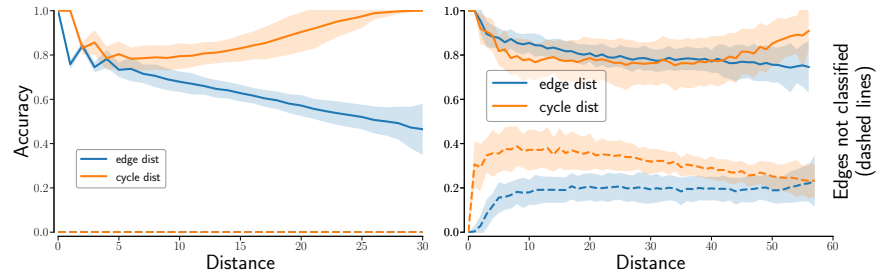
Figure 6.13: (solid lines) Classification accuracy $= \frac{\text{Number of correct predictions}}{\text{number of all predicted edges}}$ for edge and cycle distance based classifiers. Threshold $\varepsilon = 10^{-5}$, as before. Simulation done on (left) a 30×30 square lattice, with 200 independent runs; and (right) Voronoi tessellations of 2000 randomly chosen points, with 50 independent runs. Cycle distance is much better than edge distance in lattices, especially at large distances. In Voronoi tessellations, both classifiers work well, edge distance based one slightly more so. But the gap between them decreases with distance. (dashed lines) Fraction of edges that cannot be classified. For lattice networks, close to 0 for both classifiers. For Voronoi, cycle distance based one fails to classify more edges than the edge distance based one, but the gap decreases with distance. All error bands depict standard deviations.

we systematically study how accurate the classifiers are at identifying Braessian edges at different distances from the maximally loaded edge. For our simulations, we choose as before, two network topologies. As an accuracy measure, we choose the probability of correct prediction $= \frac{\text{Number of correct predictions}}{\text{Number of all predicted edges}}$. Due to the high runtime of the flow rerouting based classifier for large networks, we omitted it from this study. We present our findings in Figure 6.13. In square lattice topology, the cycle distance based classifier is seen to be vastly superior to the edge distance based one: the accuracy of it, after a slight drop till distance < 6, actually *increases* with distance afterwards. It remains better in accuracy than the edge distance based one at all distances. The accuracy of the edge distance based one steadily decreases with distance.

The situation, however, is quite different for Voronoi planar graphs. The cycle distance based classifier is slightly *less accurate* than the edge distance based one for distances < 40, after which it gets better. Both classifiers manage accuracy ≈ 0.8 at all distances. Unlike in square lattices, both classifiers *fail* to predict certain fraction of edges due to alignment being undefined. The fraction of such unclassified edges is also higher for cycle distance classifier, but the gap steadily declines with distance.

6.4 USING BRAESSIAN EDGES TO MITIGATE A DAMAGE

Braessian edges, by their very definition, lessen the flow on the maximally loaded edge in the network, when they are infinitesimally damaged. Utilizing this property, we will now show, that one can *mitigate* overload in a network caused by damage at an edge by *damaging a second,* Braessian edge. We note that a similar phenomenon was reported in [59]. In Figure 6.14, we illustrate this for a 15×15 square lattice,
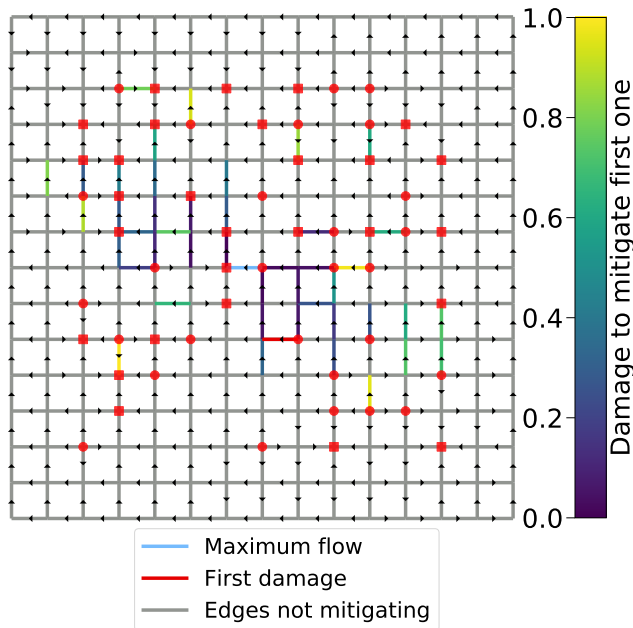

Figure 6.14: Braessian edges can be *intentionally damaged* to prevent overload caused by damaging another edge. In a lattice network, on reducing weight of one edge (coloured red) by 10%, the maximally loaded edge (coloured sky blue) overloads. Among the Braessian edges, some, when damaged by an extent (depicted in colourmap) reverses this overload. Edges that cannot reverse the overload even when completely removed are coloured grey.

with each edge having weight $= 1$. We damaged the red coloured edge by reducing its capacity by 0.1, thereby causing an overload in the maximally loaded edge coloured sky blue. Along the remaining edges, many, when damaged by a suitable degree (i.e. reducing their capacities), mitigated the overload. The colourmap in the figure illustrates the amount by which the weight of an edge must be reduced to bring the maximum flow in the network back to its original value. Not coincidentally, all non-Braessian edges failed to mitigate the overload by this strategy of weight reduction. However, not *all* Braessian edges could do the mitigation either. This was due to one of two reasons. Firstly, there were edges that, even when damaged to the maximum degree (i.e.

completely taken out), could not completely reverse the overload. Secondly, there were some edges, which when damaged suitably, although reversed the overload in the previously maximally loaded edge, ended up overloading *another edge* so much that the maximum flow in the network increased.
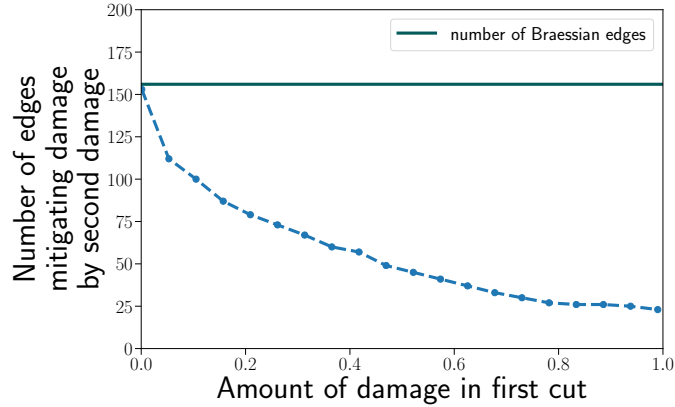

Figure 6.15: Overload due to damaging one edge can be mitigated by damaging a Braessian edge. But as the amount of damage inflicted increases, less and less edges are able to mitigate the damage. The network and the inputs are identical to Figure 6.14.

The second effect becomes more and more pronounced as the *amount* of the first damage increases. This is so, because more damage is then needed to reverse the first damage, which increases the amount of the "side effects" on other edges as well, thereby increasing the probability that some other edge becomes the maximally loaded one. We illustrate this in Figure 6.15, where we compute, if an edge is damaged by a certain degree, how many edges can mitigate the overload by a second damage. We see that for very small amount of (first) damage, almost all Braessian edges can do the mitigation, but with more damage, less and less such edges can do so.

6.5   CONCLUSION

In a flow network, adding an edge is not always beneficial: this fact, first discovered in the context of traffic flows in road networks [32], has been demonstrated in various continuous flow networks [102, 103, 37, 36, 38]. It has been shown in [38] that in a phase oscillator network with chain topology, based on steady state phases alone, it is possible to determine which two nodes, if connected by a new edge, will show Braess' paradox. However, neither in the original setting of traffic flow networks, nor in continuous flow networks, it is well understood which (if any) topological features cause some edges to exhibit Braess' paradox.

In complex network topologies, we earlier introduced a concept called "network susceptibility" [106] to quantify the effect of an infinitesimal

increase in an edge capacity on the flows in other edges. In this article, we have used the tools of network susceptibility to study the question: which edges in a network, when their capacities are infinitesimally increased, cause an increase in the maximal load in the network? Under a specific class of network dynamics, that we call conservative flow networks, we have shown that to answer to this question it is sufficient to compute the flows in the same network due to a single dipole source placed along the maximally loaded edge.

Utilizing this equivalence, we proceeded to define a topological notion of flow alignment between two edges in a network and proposed that such flow alignment will determine if an edge is Braessian. Our first definition of flow alignment, based on edge distances, proved promising but classified significant amount of edges wrongly as Braessian or non-Braessian. We demonstrated that this classifier is improved significantly if one replaces edge distances with cycle distances. However, our definition of cycle distance is not valid for non-planar networks. To overcome this shortcoming, we defined yet another flow alignment, based on flow reroutings, that works as well as the cycle distance based one for predicting Braessian edges, and is applicable for non-planar networks as well.

We also showed that Braess' paradox has a useful side effect: it is possible to *mitigate* the overload caused by damaging an edge by making an *additional damage* at one of the Braessian edges.

APPENDIX

6.A MOORE-PENROSE PSEUDOINVERSE OF SYMMETRIC MATRICES

Lemma 6.A.1. *If A is a symmetric matrix, then its Moore-Penrose pseudoinverse A^+ is also symmetric.*

Proof. By definition, A^+ is the unique Moore-Penrose pseudoinverse of A if and only if

$$AA^+A = A \tag{6.33}$$
$$A^+AA^+ = A^+ \tag{6.34}$$
$$(AA^+)^T = AA^+ \tag{6.35}$$
$$(A^+A)^T = A^+A \tag{6.36}$$

Taking transpose of all these equations and exploiting $A = A^T$ yields:

$$A\left(A^+\right)^T A = A \tag{6.37}$$
$$\left(A^+\right)^T A \left(A^+\right)^T = A^+ \tag{6.38}$$
$$(A\left(A^+\right)^T)^T = A\left(A^+\right)^T \tag{6.39}$$
$$(\left(A^+\right)^T A)^T = \left(A^+\right)^T A. \tag{6.40}$$

Therefore, A^T is a valid Moore-Penrose pseudoinverse of A as well. By uniqueness of A^+, the lemma follows.

$\square$

FINAL CONCLUSION AND OUTLOOK

In this thesis we have studied three different ways in which topology influences the flows in a network: Firstly, which topological conditions guarantee the stability of flows in phase oscillator networks; secondly, which topological features result in more *coexisting steady flows* in the same system; thirdly, which topological features cause certain edges in a network to exhibit Braess paradox (i.e. the maximum flow in the network *increases* when any of these edges are infinitesimally strengthened). In this Chapter we will summarize our key results, put them in the context of existing research, and outline future research directions.

7.1 TOPOLOGY DEPENDENCE OF STEADY FLOWS AND THEIR STABILITY

In Chapter 4, we studied how topology influences loss of stability in a phase oscillator network whose dynamics follows the swing equation (defined in Eq. (4.20)). This equation is frequently used to model the high voltage AC power grid [19]. Loss of steady states in such systems results in power outages, and hence establishing criteria for loss of stability in this system is an important problem.

We first derived an exact mapping between the fixed points and their bifurcation structure of this model and that of the well studied Kuramoto oscillators [1, 2]. It has been known for more than 40 years that Kuramoto networks have a unique globally attracting steady state if the coupling is stronger than a certain critical value, and no steady state otherwise; for infinite *and* all-to-all coupled networks. But power grids are far from all-to-all coupled: In fact, they are almost planar, with very few long distance edges [20, 21]. For arbitrary topologies, necessary and sufficient conditions for steady states in Kuramoto networks are still not known.

One necessary condition for steady states (or steady flows) was presented using a purely graph theoretic approach in [45]: they considered any cut or 2-partition of the network (i.e. a partition of the network into two non-overlapping subnetworks, see Definition 2.1.5) and showed that the power generated in one partition but not consumed there must be able to flow to the other partition. This means coupling has to be strong enough so that the edges in the cutset have enough capacity to deliver this excess power. This leads to a necessary condition for the existence of steady flows but not to a sufficient one, since steady states in such networks must fulfill some geometric criteria [108] in addition to the topological ones considered in this approach.

We improved upon this purely graph theoretic condition by connecting two known results from literature: the fact that the Jacobian for linear stability for such system has the form of a graph Laplacian [49] and the fact that the multiplicity of the zero eigenvalue of a graph Laplacian equals its number of connected components [52]. We showed that stability of steady flows is lost precisely when a cut of the graph emerges with the property that all the edges in the cutset carry maximum possible flows.

While deriving this result, we noticed that it holds only when the phase differences along each edge is less than $\frac{\pi}{2}$, since otherwise the graph theoretic relation between Laplacian eigenvalues and connectivity of a graph no longer holds. This gives rise to the curious phenomenon where a network loses stability without overload on any line. We showed using the network topology of the British power grid that this is not an esoteric scenario, but may take place in practice. This leads to the insight that determining vulnerable edges in a power grid by looking at the loads may not be the best choice. This topic was subsequently studied by our colleagues in [27].

7.2 MULTISTABILITY AND TOPOLOGY

In Chapter 5, we demonstrated that certain topological features result in more coexisting steady flows in networks of Kuramoto oscillators. Existence of a unique steady flow is typically desired for power grids, as it guarantees same power flows along the edges for all initial conditions. It is well known that the completely coupled Kuramoto networks can have only unique fixed points (or none at all) [29]. In very sparse networks (trees), this uniqueness is also guaranteed.

There exist conflicting claims in the literature about multistability in Kuramoto networks with arbitrary topology. A well cited paper [28] presented an analytical argument that one can always find a sufficiently high coupling strength guaranteeing unique steady flows in any topology. However, multistability has been demonstrated in ring networks [30, 53] multiple times.

We found out that the claim in [28] is flawed, due to a flaw in the application of Banach's contraction principle in its proof. So, there is no guarantee of unique steady states in Kuramoto networks of arbitrary topologies. We determined the number of steady flows in planar networks, extending already existing works [30, 54] and complementing independent and parallel research published during this thesis work [109, 31, 55]. We showed that three topological features favour more fixed points: long loops in the minimal cycle basis, high coupling strengths and geographically homogeneous distribution of power generators and consumers. In the limit of large loop lengths and high coupling strength, we derived a scaling law for the number of fixed points, that we numerically showed to be accurate even for loop sizes as small as 50. Curiously,

all these results were applicable only to *planar* networks, because our method depended on the guarantee that no more than two cycles share an edge. It remains an open question if our results can be generalized to non-planar networks.

7.3 TOPOLOGICAL PERTURBATIONS AND STEADY FLOWS: BRAESS' PARADOX

In Chapter 6, we investigated the intriguing phenomenon of Braess' paradox (BP), where strengthening an edge of a flow network *worsens* the performance of the network. Despite significant research in traffic engineering [60, 35, 61], BP has only recently been studied for continuous flow networks and oscillator networks such as power grids [36, 37, 38]. Which topological features cause certain edges to exhibit BP still remains an unanswered question.

We demonstrated that the edges with a certain topological property of being "flow aligned" to the maximally loaded edge are more likely to exhibit BP (for a suitable definition of flow alignment). To establish this result, we studied Braess' paradox using the *network susceptibility* formalism we introduced in [106]. Taking a differential view, we defined BP as the *maximum load* in the network increasing on *infinitesimally* strengthening an edge. This reformulation allowed us to reduce the problem of identifying edges exhibiting BP to a much simpler problem of determining the flows in a *linear flow* network (e.g. DC resistor networks) with a single dipole input. This equivalence allowed us to utilize a certain symmetry of the dipole flow problem, resulting in the insight that edges with flows aligned to the maximum flow are more likely to exhibit BP.

In addition, we established an efficient algorithm to detect BP in arbitrary conservative flow networks; utilizing our reduction of the problem of detecting Braessian edges to the problem of computing flows due to a single dipole.

7.4 OUTLOOK

In this thesis, we set out to understand the broad question: *"How does topology influence the flows in a network?"*.

Our work shed light on a few aspects of this broad question. We showed that existence of steady flows in Kuramoto oscillator networks is intimately related to the *connectedness* of the *residual capacity graph* of the network. The concept of residual capacities has been further utilized by our colleagues [27] to *identify weak links* in the same network model. Residual capacities are readily generalizable to almost all flow networks where the edges have a upper bound on the flow they can carry. This leads to the question: Can residual capacities be used to

understand dynamical properties of other flow networks as well (such as the third order model of power grids [70])?

We found an answer to the puzzle of conflicting claims in the literature regarding uniqueness of steady flows in phase oscillator networks. Building upon and extending existing knowledge [30, 31, 55] on the number of coexisting steady flows, we demonstrated that the number of steady flows increase with three topological features: cycle lengths, edge capacities and input heterogeneities. Our findings indicate that power grids may cease to have unique steady flows if the distribution of generators and consumers get more *decentral*. This may be problematic, since our power grids *are* gradually getting more decentral; due to big coal and nuclear power plants being phased out in favour of smaller and more distributed wind or solar power based generators to reduce CO_2 emissions [62]. In addition, decentral grids have been shown to be more *robust* against topological perturbations [71]. Strategies to design decentral power grids, while maintaining unique steady flows would be interesting to study.

Knowing the number of steady flows in a network is important for understanding its dynamics. The next question of interest is measuring the basin volumes of those steady flows, i.e. answering "*how likely* is the network to end up with one specific steady flow, if it is started from many random initial conditions?". This topic was first raised for Kuramoto networks in [53], and aspects of it has been presented in a recent preprint [110].

While we have made substantial progress into predicting which edges cause Braess paradox in linear flow networks, it remains to be seen if our works hold for *nonlinear* flow networks, e.g. models of AC power grid. Analytical insights motivating our predictor of Braessian edges remains valid for a broad class of *nonlinear* flow networks, including the swing equation model of power grids.

in many real networks, it is more important to know whether Braess paradox would occur on *adding* an edge, rather than on *infinitesimally* strengthening an edge. We studied the second question because it was analytically tractable by using edge-to-edge susceptibilities that we introduced in [106]. However, we hope that our findings can be extended to find out Braessian edges on adding an edge as well, because there exists a concept called "line outage distribution factor" (LODF) in power engineering, that quantifies the flow changes in a network on complete removal of an edge. LODF's happen to be related to edge-to-edge susceptibilities by a prefactor [107].

Much remains to be answered of the question we posed at the beginning of this thesis: "How does topology influence the flows in a network?" This question will arise in additional contexts in future, as the tools of network science are introduced to study new systems, e.g. the flow of information in the world wide web, or the flow of cars in road networks. While approaches specific to the system at hand are indispensable for

understanding them, a generalized approach of establishing causal relationships between topology and dynamics may give rise to new insights by uncovering unifying features across different systems.

BIBLIOGRAPHY

[1]   Y. Kuramoto. "Self-entrainment of a population of coupled non-linear oscillators." In: *International Symposium on on Mathematical Problems in Theoretical Physics.* Ed. by H. Araki. Lecture Notes in Physics Vol. 39. New York: Springer, 1975, p. 420.

[2]   Juan A Acebrón et al. "The Kuramoto model: A simple paradigm for synchronization phenomena." In: *Reviews of modern physics* 77.1 (2005), p. 137.

[3]   H. Hildenbrandt, C. Carere, and C.K. Hemelrijk. "Self-organized aerial displays of thousands of starlings: a model." In: *Behavioral Ecology* 21.6 (2010), pp. 1349–1359.

[4]   Steven H. Strogatz. "From Kuramoto to Crawford: Exploring the onset of synchronization in populations of coupled oscillators." In: *Physica D: Nonlinear Phenomena* 143 (2000), p. 1.

[5]   Jesús Gómez-Gardeñes et al. "Explosive synchronization transitions in scale-free networks." In: *Physical review letters* 106.12 (2011), p. 128701.

[6]   Fumiko Yonezawa, Shoichi Sakamoto, and Motoo Hori. "Percolation in two-dimensional lattices. II. The extent of universality." In: *Physical Review B* 40.1 (1989), p. 650.

[7]   Fumiko Yonezawa, Shoichi Sakamoto, and Motoo Hori. "Percolation in two-dimensional lattices. I. A technique for the estimation of thresholds." In: *Physical Review B* 40.1 (1989), p. 636.

[8]   Reinhard Diestel. *Graph Theory (Graduate Texts in Mathematics).* Springer, 2000. ISBN: 0387989765.

[9]   Donald E Knuth. "A generalization of Dijkstra's algorithm." In: *Information Processing Letters* 6.1 (1977), pp. 1–5.

[10] Otakar Borůvka. "O jistém problému minimálním." In: *Práce moravské přírodovědecké společnosti v Brne* 111.3 (1926), pp. 37–58.

[11] Duncan J Watts and Steven H Strogatz. "Collective dynamics of 'small-world'networks." In: *nature* 393.6684 (1998), pp. 440–442.

[12] A. L. Barabási and R. Albert. "Emergence of scaling in random networks." In: *science* 286.5439 (1999), pp. 509–512.

[13] Carsten Matke et al. "Structure Analysis of the German Transmission Network Using the Open Source Model SciGRID." In: (2017), pp. 177–188.

[14] Eleni Katifori, Gergely J Szöllősi, and Marcelo O Magnasco. "Damage and fluctuations induce loops in optimal transport networks." In: *Physical Review Letters* 104.4 (2010), p. 048704.

[15] Kurt Wiesenfeld, Pere Colet, and Steven H Strogatz. "Synchronization transitions in a disordered Josephson series array." In: *Physical review letters* 76.3 (1996), p. 404.

[16] Francisco Varela et al. "The brainweb: phase synchronization and large-scale integration." In: *Nature reviews neuroscience* 2.4 (2001), pp. 229–239.

[17] István Z Kiss, Yumei Zhai, and John L Hudson. "Emerging coherence in a population of chemical oscillators." In: *Science* 296.5573 (2002), pp. 1676–1678.

[18] Brian Stott, Jorge Jardim, and Ongun Alsaç. "DC power flow revisited." In: *IEEE Transactions on Power Systems* 24.3 (2009), pp. 1290–1300.

[19] Giovanni Filatrella, Arne Hejde Nielsen, and Niels Falsig Pedersen. "Analysis of a power grid using a Kuramoto-like model." In: *The European Physical Journal B - Condensed Matter and Complex Systems* 61.4 (2008), pp. 485–491.

[20] Saleh Soltan and Gil Zussman. "Generation of synthetic spatially embedded power grid networks." In: *Power and Energy Society General Meeting (PESGM), 2016.* IEEE. 2016, pp. 1–5.

[21] Paul Schultz, Jobst Heitzig, and Jürgen Kurths. "A random growth model for power grids and other spatially embedded infrastructure networks." In: *The European Physical Journal Special Topics* 223.12 (2014), pp. 2593–2610.

[22] Jesús Gómez-Gardeñes, Yamir Moreno, and Alex Arenas. "Synchronizability determined by coupling strengths and topology on complex networks." In: *Physical Review E* 75.6 (2007), p. 066106.

[23] Hyunsuk Hong, Moo-Young Choi, and Beom Jun Kim. "Synchronization on small-world networks." In: *Physical Review E* 65.2 (2002), p. 026139.

[24] Patrick N McGraw and Michael Menzinger. "Clustering and the synchronization of oscillator networks." In: *Physical Review E* 72.1 (2005), p. 015101.

[25] Motoki Nagata et al. "Smoothing effect for spatially distributed renewable resources and its impact on power grid robustness." In: *Chaos: An Interdisciplinary Journal of Nonlinear Science* 27.3 (2017), p. 033104.

[26] Martin Rohden et al. "Self-organized synchronization in decentralized power grids." In: *Physical review letters* 109.6 (2012), p. 064101.

[27]   Dirk Witthaut et al. "Critical links and nonlocal rerouting in complex supply networks." In: *Physical review letters* 116.13 (2016), p. 138701.

[28]   Ali Jadbabaie, Nader Motee, and Mauricio Barahona. "On the stability of the Kuramoto model of coupled nonlinear oscillators." In: *Proceedings of the 2004 American Control Conference.* Vol. 5. IEEE. 2004, pp. 4296–4301.

[29]   Richard Taylor. "There is no non-zero stable fixed point for dense networks in the homogeneous Kuramoto model." In: *Journal of Physics A: Mathematical and Theoretical* 45.5 (2012), p. 055102.

[30]   J Ochab and PF Gora. "Synchronization of coupled oscillators in a local one-dimensional Kuramoto model." In: *Acta Physica Polonica. Series B, Proceedings Supplement* 3.2 (2010), pp. 453–462.

[31]   Robin Delabays, Tommaso Coletta, and Philippe Jacquod. "Multistability of phase-locking and topological winding numbers in locally coupled Kuramoto models on single-loop networks." In: *Journal of Mathematical Physics* 57.3 (2016), p. 032701.

[32]   Dietrich Braess. "Über ein Paradoxon aus der Verkehrsplanung." In: *Unternehmensforschung* 12.1 (1968), pp. 258–268.

[33]   Richard Steinberg and Willard I. Zangwill. "The Prevalence of Braess' Paradox." In: *Transportation Science* 17.3 (1983), pp. 301–318.

[34]   Stella Dafermos and Anna Nagurney. "On some traffic equilibrium theory paradoxes." In: *Transportation Research Part B: Methodological* 18.2 (1984), pp. 101–110.

[35]   Eric I. Pas and Shari L. Principio. "Braess' paradox: Some new insights." In: *Transportation Research Part B: Methodological* 31.3 (1997), pp. 265–276.

[36]   Dirk Witthaut and Marc Timme. "Braess's paradox in oscillator networks, desynchronization and power outage." In: *New journal of physics* 14.8 (2012), p. 083036.

[37]   Dirk Witthaut and Marc Timme. "Nonlocal failures in complex supply networks by single link additions." In: *The European Physical Journal B* 86.9 (2013), p. 377.

[38]   Tommaso Coletta and Philippe Jacquod. "Linear stability and the Braess paradox in coupled-oscillator networks and electric power grids." In: *Physical Review E* 93.3 (2016), p. 032222.

[39]   Chris Godsil and Gordon F Royle. *Algebraic graph theory.* Vol. 207. Springer Science & Business Media, 2013.

[40]   Alex Arenas et al. "Synchronization in complex networks." In: *Physics reports* 469.3 (2008), pp. 93–153.

[41]   Dirk Witthaut and Marc Timme. "Kuramoto dynamics in Hamiltonian systems." In: *Physical Review E* 90.3 (2014), p. 032917.

[42]   Marc Durand. "Structure of optimal transport networks subject to a global constraint." In: *Physical Review Letters* 98.8 (2007), p. 088701.

[43]   Dean Karnopp. *Bond graph models for fluid dynamic systems.* American Society of Mechanical Engineers, 1972.

[44]   Clayton R Paul. *Fundamentals of electric circuit analysis.* Wiley, 2001.

[45]   Sergi Lozano, Lubos Buzna, and Albert Díaz-Guilera. "Role of network topology in the synchronization of power systems." In: *The European Physical Journal B-Condensed Matter and Complex Systems* 85.7 (2012), pp. 1–8.

[46]   Mauricio Barahona and Louis M Pecora. "Synchronization in small-world systems." In: *Physical review letters* 89.5 (2002), p. 054101.

[47]   Nikhil Chopra and Mark W Spong. "On synchronization of Kuramoto oscillators." In: *Decision and Control, 2005 and 2005 European Control Conference. CDC-ECC'05. 44th IEEE Conference on.* IEEE. 2005, pp. 3916–3922.

[48]   Alexander C Kalloniatis. "From incoherence to synchronicity in the network Kuramoto model." In: *Physical Review E* 82.6 (2010), p. 066202.

[49]   Florian Dörfler, Michael Chertkov, and Francesco Bullo. "Synchronization in complex oscillator networks and smart grids." In: *Proceedings of the National Academy of Sciences* 110.6 (2013), pp. 2005–2010.

[50]   Per Sebastian Skardal, Dane Taylor, and Jie Sun. "Optimal synchronization of complex networks." In: *Physical review letters* 113.14 (2014), p. 144101.

[51]   Florian Dörfler and Francesco Bullo. "Synchronization in complex networks of phase oscillators: A survey." In: *Automatica* 50.6 (2014), pp. 1539–1564.

[52]   M. E. J. Newman. *Networks – An introduction.* Oxford: Oxford University Press, 2010. ISBN: 978-0-19-920665-0.

[53]   Daniel A Wiley, Steven H Strogatz, and Michelle Girvan. "The size of the sync basin." In: *Chaos: An Interdisciplinary Journal of Nonlinear Science* 16.1 (2006), p. 015103.

[54]   Dhagash Mehta et al. "Algebraic geometrization of the Kuramoto model: Equilibria and stability analysis." In: *Chaos: An Interdisciplinary Journal of Nonlinear Science* 25.5 (2015), p. 053103.

[55]   Robin Delabays, Tommaso Coletta, and Philippe Jacquod. "Multistability of phase-locking in equal-frequency Kuramoto models on planar graphs." In: *Journal of Mathematical Physics* 58.3 (2017), p. 032703.

[56]   U.S.-Canada Power System Outage Task Force. https://reports.energy.gov/BlackoutFinal-Web.pdf. 2004.

[57]   Union for the Coordination of Transmission of Electricity. *Final report on the system disturbance on 4 November 2006.* http://www.entsoe.eu/~library/publications/ce/otherreports/Final-Report-20070130.pdf. 2007.

[58]   Åke J Holmgren. "Using graph models to analyze the vulnerability of electric power networks." In: *Risk analysis* 26.4 (2006), pp. 955–969.

[59]   Adilson E Motter. "Cascade control and defense in complex networks." In: *Physical Review Letters* 93.9 (2004), p. 098701.

[60]   Marguerite Frank. "The Braess paradox." In: *Mathematical Programming* 20.1 (1981), pp. 283–302.

[61]   Gregory Valiant and Tim Roughgarden. "Braess's Paradox in large random graphs." In: *Random Structures & Algorithms* 37.4 (2010), pp. 495–515.

[62]   Emma Marris. "Energy: Upgrading the grid." In: *Nature News* 454.7204 (2008), pp. 570–573.

[63]   John A Turner. "A realizable renewable energy future." In: *Science* 285.5428 (1999), pp. 687–689.

[64]   Thiemo Pesch, H-J Allelein, and J-F Hake. "Impacts of the transformation of the German energy system on the transmission grid." In: *The European Physical Journal Special Topics* 223.12 (2014), pp. 2561–2575.

[65]   Dominik Heide et al. "Seasonal optimal mix of wind and solar power in a future, highly renewable Europe." In: *Renewable Energy* 35.11 (2010), pp. 2483–2489.

[66]   Frank Böttcher, Joachim Peinke, et al. "Small and large scale fluctuations in atmospheric wind speeds." In: *Stochastic environmental research and risk assessment* 21.3 (2007), pp. 299–308.

[67]   Patrick Milan, Matthias Wächter, and Joachim Peinke. "Turbulent character of wind energy." In: *Physical review letters* 110.13 (2013), p. 138701.

[68]   Arthur R Bergen and David J Hill. "A structure preserving model for power system stability analysis." In: *IEEE Transactions on Power Apparatus and Systems* 1 (1981), pp. 25–35.

[69]   David J Hill and Guanrong Chen. "Power systems as dynamic networks." In: *Circuits and Systems, 2006. ISCAS 2006. Proceedings. 2006 IEEE International Symposium on*. IEEE. 2006, 4–pp.

[70]   Jan Machowski, Janusz W Bialek, and James Richard Bumby. *Power system dynamics, stability and control*. New York: John Wiley & Sons, 2008.

[71]   Martin Rohden et al. "Impact of network topology on synchrony of oscillatory power grids." In: *Chaos: An Interdisciplinary Journal of Nonlinear Science* 24.1 (2014), p. 013123.

[72]   Adilson E Motter et al. "Spontaneous synchrony in power-grid networks." In: *Nature Physics* 9.3 (2013), pp. 191–197.

[73]   Peter J Menck et al. "How dead ends undermine power grid stability." In: *Nature communications* 5 (2014).

[74]   Prabha Kundur, Neal J Balu, and Mark G Lauby. *Power system stability and control*. Vol. 7. McGraw-hill New York, 1994.

[75]   Yoshihiko Susuki, Igor Mezic, and Takashi Hikihara. "Global swing instability of multimachine power systems." In: *Decision and Control, 2008. CDC 2008. 47th IEEE Conference on*. IEEE. 2008, pp. 2487–2492.

[76]   Yoshihiko Susuki, Igor Mezić, and Takashi Hikihara. "Coherent swing instability of power grids." In: *Journal of nonlinear science* 21.3 (2011), pp. 403–439.

[77]   Florian Dorfler and Francesco Bullo. "Kron reduction of graphs with applications to electrical networks." In: *IEEE Transactions on Circuits and Systems I: Regular Papers* 60.1 (2013), pp. 150–163.

[78]   Katrin Schmietendorf et al. "Self-organized synchronization and voltage stability in networks of synchronous machines." In: *The European Physical Journal Special Topics* 223.12 (2014), pp. 2577–2592.

[79]   Hsiao-Dong Chiang, Felix Wu, and P Varaiya. "Foundations of direct methods for power system transient stability analysis." In: *IEEE Transactions on Circuits and systems* 34.2 (1987), pp. 160–173.

[80]   CJ Perez and F Ritort. "A moment-based approach to the dynamical solution of the Kuramoto model." In: *Journal of Physics A: Mathematical and General* 30.23 (1997), p. 8095.

[81]   James Howard. "Stability of Hamiltonian equilibria." In: *Scholarpedia* 8 (2013), p. 3627. DOI: 10.4249/scholarpedia.3627.

[82]   Hassan K Khalil and JW Grizzle. *Nonlinear systems*. Vol. 3. Prentice hall Upper Saddle River, 2002.

[83]   M Levi, Frank C Hoppensteadt, and WL Miranker. "Dynamics of the Josephson junction." In: *Quarterly of Applied Mathematics* 36.2 (1978), pp. 167–198.

[84]   Hannes Risken. *Fokker-planck equation.* Springer, 1996, pp. 63–95.

[85]   Peter J Menck et al. "How basin stability complements the linear-stability paradigm." In: *Nature Physics* 9.2 (2013), pp. 89–92.

[86]   Yuri A Kuznetsov. *Elements of applied bifurcation theory.* Vol. 112. Springer Science & Business Media, 2013.

[87]   Patrick C Parks. "AM Lyapunov's stability theory - 100 years on." In: *IMA journal of Mathematical Control and Information* 9.4 (1992), pp. 275–303.

[88]   Union for the Coordination of Transmission of Electricity. *Continental Europe Operation Handbook.* https://www.entsoe.eu/publications/system-operations-reports/operation-handbook/Pages/default.aspx. 2014.

[89]   Peter Fairley. "The unruly power grid." In: *IEEE Spectrum* 41.8 (2004), pp. 22–27.

[90]   Ingve Simonsen et al. "Transient dynamics increasing network vulnerability to cascading failures." In: *Physical review letters* 100.21 (2008), p. 218701.

[91]   William N Anderson Jr and Thomas D Morley. "Eigenvalues of the Laplacian of a graph." In: *Linear and multilinear algebra* 18.2 (1985), pp. 141–145.

[92]   Bojan Mohar et al. "The Laplacian spectrum of graphs." In: *Graph theory, combinatorics, and applications* 2.871-898 (1991), p. 12.

[93]   Miroslav Fiedler. "Algebraic connectivity of graphs." In: *Czechoslovak mathematical journal* 23.2 (1973), pp. 298–305.

[94]   Santo Fortunato. "Community detection in graphs." In: *Physics reports* 486.3 (2010), pp. 75–174.

[95]   Surya D Pathak et al. "Complexity and adaptivity in supply networks: Building supply network theory using a complex adaptive systems perspective." In: *Decision sciences* 38.4 (2007), pp. 547–580.

[96]   Antônio MT Ramos and Carmen PC Prado. "Role of hysteresis in stomatal aperture dynamics." In: *Physical Review E* 87.1 (2013), p. 012719.

[97]   Kåre Hartvig Jensen et al. "Optimality of the Münch mechanism for translocation of sugars in plants." In: *Journal of the Royal Society Interface* 8.61 (2011), pp. 1155–1165.

[98]   JW Patrick. "Phloem unloading: sieve element unloading and post-sieve element transport." In: *Annual review of plant biology* 48.1 (1997), pp. 191–222.

[99]   Yannis A. Korilis, Aurel A. Lazar, and Ariel Orda. "Avoiding the Braess paradox in non-cooperative networks." In: *Journal of Applied Probability* 36.1 (1999), pp. 211–222.

[100]   R.E. Azouzi, E. Altman, and O. Pourtallier. "Properties of equilibria in competitive routing with several user types." In: vol. 4. IEEE, 2002, pp. 3646–3651.

[101]   Rinaldo M. Colombo and Helge Holden. "On the Braess Paradox with Nonlinear Dynamics and Control Theory." In: *Journal of Optimization Theory and Applications* 168.1 (2016), pp. 216–230.

[102]   Joel E. Cohen and Paul Horowitz. "Paradoxical behaviour of mechanical and electrical networks." In: *Nature* 352.6337 (1991), pp. 699–701.

[103]   Ladimer S Nagurney and Anna Nagurney. "Physical proof of the occurrence of the Braess Paradox in electrical circuits." In: *EPL (Europhysics Letters)* 115.2 (2016), p. 28004.

[104]   S Toussaint et al. "Counterintuitive behavior of simulated network's conductance analogous to the Braess paradox." In: *Bulletin of the American Physical Society* 61 (2016).

[105]   Ian Dobson et al. "Complex systems analysis of series of blackouts: Cascading failure, critical points, and self-organization." In: *Chaos: An Interdisciplinary Journal of Nonlinear Science* 17.2 (2007), p. 026103.

[106]   Debsankha Manik et al. "Network susceptibilities: Theory and applications." In: *Physical Review E* 95.1 (2017), p. 012319.

[107]   Henrik Ronellenfitsch et al. "Dual theory of transmission line outages." In: *IEEE Transactions on Power Systems* (2017).

[108]   Debsankha Manik et al. "Supply networks: Instabilities without overload." In: *The European Physical Journal Special Topics* 223.12 (2014), pp. 2527–2547.

[109]   Kaihua Xi, Johan LA Dubbeldam, and Hai Xiang Lin. "Synchronization of cyclic power grids: Equilibria and stability of the synchronous state." In: *Chaos: An Interdisciplinary Journal of Nonlinear Science* 27.1 (2017), p. 013109.

[110]   Robin Delabays, Melvyn Tyloo, and Philippe Jacquod. "The Size of the Sync Basin Revisited." In: *arXiv preprint arXiv:1706.00344* (2017).

ACKNOWLEDGMENTS

Firstly, I would like to thank Marc: for letting me dabble in all those network related projects: powergrids, ecobus, law evolution, and more. Some of them produced less scientific results then others, but you were never anything but encouraging. I learnt something from each of these projects, and am happy that I tried.

I would like to thank Dirk (my unofficial co-supervisor): I never cease to be amazed at how effortlessly you converted ideas and notes coming from brainstorming sessions into working drafts of manuscripts.

Thank you Eleni, for introducing me to networks in biological systems, and showing that one can have fun with cool mathematical tools, and at the same time understand real stuff in nature.

Thank you Andreas, Harold, Jana, Tariq, Sebastian, Alexander and everybody in the Python teaching gang: due to you, I never stopped learning programming and other computer related stuff, and it made my PhD so much more fun.

Special thanks go to Nora, Tariq, and Andreas, for proofreading my thesis and giving me so many constructive criticisms.

Warm thanks to everybody in the network dynamics group, and the rest of you in the now gone Bunsenstrasse building, for leaving me with so many fond memories of my PhD life: coffee breaks at the red kitchen, cooking evenings at the yellow kitchen, barbecue on the terrace in summer, one day trips, ruthless grilling at the test talks and so much more.

I thank the whole CoNDyNet crowd: Martin, Frank, Sabine, Paul, Carsten, Tom (and the rest) for the amazing time at all the conferences.

I thank my family in India, for always being supportive, and trusting that I knew what I was doing. Last but not the least, thank you Fenna: for making sure that my math is not too sloppy, and making me come home at a sensible hour in the last few crazy weeks before the thesis submission.

So long, and thanks for all the fish!